DISSERTATION

UNDERSTANDING THE MOLECULAR AND HOST DETERMINANTS OF POWASSAN VIRUS PATHOGENESIS ACROSS CELLULAR AND ANIMAL MODELS

Submitted by

Samantha J. Courtney

Department of Microbiology, Immunology, and Pathology

In partial fulfillment of the requirements

For the Degree of Doctor of Philosophy

Colorado State University

Fort Collins, Colorado

Fall 2025

Doctoral Committee:

Advisor: Gregory D. Ebel

Angela Bosco-Lauth
Elizabeth Hemming-Schroeder
Dan Sloan

ABSTRACT

UNDERSTANDING THE MOLECULAR AND HOST DETERMINANTS OF POWASSAN VIRUS PATHOGENESIS ACROSS CELLULAR AND ANIMAL MODELS

Powassan virus (POWV) is a tick-borne flavivirus that affects the United States, Canada, and parts of Russia. Despite its capacity to cause severe and sometimes fatal neurologic disease, POWV remains poorly understood. Here, we use both cellular and animal models to investigate the molecular and host determinants of POWV evolution and pathogenesis, with a focus on recombination patterns, strain-specific disease phenotypes, and mechanisms of neurotropism.

While prior studies have examined viral diversity arising from single nucleotide polymorphisms, little is known about POWV recombination, defective RNAs (D-RNAs), or functional structural variants (SVs). Understanding POWV recombination in its natural vector could offer important insights into its replication and evolution. To address this, we analyzed POWV sequence data from 53 ticks collected in the Northeastern United States to characterize and quantify recombination patterns in naturally infected ticks. We then compared these patterns to single cell culture passage isolates. Deletions were common in tick-derived POWV RNA, with several genome regions enriched for recombination junctions, which were often associated with areas of microhomology. While most deletions were unique to individual samples, two prominent deletion archetypes emerged across multiple ticks. The first involved small 19-50 base deletions in the NS5 methyltransferase domain, resulting in a mixture of putative SVs

and D-RNAs. The second involved larger ~1600 base deletions spanning the NS2A-NS3 coding regions, generating putative D-RNAs that likely lack viral protease function. Interestingly, these protease deletions became significantly enriched after a single passage in baby hamster kidney cells, despite an overall decrease in deletion frequency. Together, these results demonstrate that POWV RNA recombines frequently, with particular variants more common than others. These findings may carry implications for virus immune evasion and persistence in ticks.

POWV also exhibits considerable genetic and phenotypic diversity, including highly variable pathogenesis in mice. To better understand this, we investigated the genotypic and phenotypic variability of lineage II strains in C57BL/6 mice. Two New York isolates, NY.19.12 and NY.19.32, caused earlier clinical signs in mice and earlier detection of viral RNA (vRNA) in both spleen and brain compared to infections with a lineage II infectious clone (WI.97.ic). Notably, NY.19.12 and NY.19.32 share three amino acid mutations in the envelope, NS1, and NS5 proteins. These mutations were engineered into an infectious clone (NY.19.12.ic) to evaluate their contribution to pathogenesis. At six days post-infection, clinical scores, vRNA detection in the cerebellum, and viral distribution in the brain were comparable between NY.19.12 and NY.19.12.ic, suggesting these mutations may play a role in early neuroinvasion and faster disease progression. However, vRNA levels in the spleen were significantly higher in NY.19.12-infected mice compared to WI.97.ic and NY.19.12.ic, indicating that factors beyond these three mutations likely contribute to increased peripheral viral burden. Importantly, this study highlights the complexity of POWV pathogenesis and

suggests that POWV lineage II strains have varying disease phenotypes likely driven by multiple genetic differences.

The mechanisms by which host immune responses shape flavivirus neurotropism remain poorly understood. To address this, we used both wild-type (C57BL/6) and mitochondrial antiviral-signaling protein (MAVS) knockout mice to compare disease progression and neurotropism of POWV (lineages I and II) and West Nile virus (WNV) in the context of type I interferon signaling. We also developed and validated a comprehensive mouse model workflow for studying flavivirus CNS infection, integrating diverse inoculation routes (subcutaneous, intraperitoneal, and intracranial) with imaging techniques such as immunofluorescence assays and whole-brain imaging to map viral distribution and immune responses. MAVS knockout mice showed enhanced susceptibility, faster disease progression, and greater weight loss compared to wild-type controls, highlighting the essential role of type I interferon signaling in controlling neurotropic flavivirus infection. Additionally, a chimeric Kunjin virus displayed lower pathogenicity than WNV, supporting its use as a lower-containment model for neurotropic flavivirus research. Overall, this work provides a valuable platform for future studies on POWV pathogenesis and neurotropism, as well as for guiding therapeutic and vaccine development.

ACKNOWLEDGEMENTS

I'd first like to thank Josh, for without him I would have literally survived (maybe) on frozen meals and sadness. Instead, this PhD experience was full of support, warm homemade meals, and wonderful adventures when we found the time. And of course, I'd like to thank Finley, our labrador, who let me snuggle her (on her terms, of course) when I needed it and kept me sane throughout all of this.

To all the science mentors who truly trained me to be a scientist, a mentor, a writer, a critical reader, a public speaker, the list could go on. My one soap box I will stand on is to find good mentors and hold on to them – I would have not made it this far without them.

To those who trained me to be ready for this PhD, and who encouraged me to pursue my career in research – Kris White, Sneha Murthy, Ann Williams (who I quote, "being a doctor would be too boring for you, you should get a PhD"), and Jess Kubicek-Sutherland. All of whom, might I add, are powerful, inspiring women in science.

Emily Gallichotte – without her I would be completely lost. We started weekly meetings maybe a year and a half ago to get manuscripts written and it has been one of the best things for me. Thank you so much for continuing to check in, add deadlines to beat my procrastinator attitude, "kick me in my butt" (when I requested it), making things "really clear," and being the most profound mentor I've ever had.

Greg – your no BS attitude is exactly what I needed to excel in this PhD, and I always looked forward to our weekly meetings where we mostly talked about science but would also usually rant about something else (paperwork, quitting and working on a

farm, different ways to make coffee, smoking meats, etc). You provided feedback when I needed it, put out every fire that came up, and you were always in my corner. They always say your PI can make or break your PhD, and I can safely say we made it.

My committee members – Angela Bosco-Lauth, Liz Hemming-Schroeder, and Dan Sloan for always having way more confidence in me than I had in myself!

Anna Overby – little did I know that you visiting for your sabbatical would be one of the most challenging yet transformational things in my PhD. Your passion for research, your driven attitude, and your friendly manner are all together inspiring and I hope to pave my career with the same attributes. And I can't wait to work more with you one week after my defense. (Ha!)

To Ebel lab members. Bekah – I am eternally grateful that you passed the POWV torch to me and taught me so many lessons about BSL-3 work, tick work, animal work, and how to navigate working with difficult people in the first year of my PhD. Fitz – I have literally bugged you so much throughout this whole thing that I genuinely feel bad, but you were always so happy to help and I'm so thankful for that! And you kept Ebel lab vibes high which is also a crucial role and a high honor. Emma Harris – thank you for training me on ISE6 tick cells, listening to me rant, and talking to me about how to be a woman in science and have a family. August Luc – I have to give you a shoutout because you brought a literal sledgehammer to threaten the Illumina sequencing machine. That was the most difficult (failed) project in my PhD and you made it bearable. I'd also like to thank other Ebel lab members past and present and for all those that helped me with these POWV projects (Chasity Trammell, Kate Kimball, Anna Fagre, Michelle Savran, Kaitlynn Williams, Marina Fuji, Bri Marsico, Toby Koch). I'd also

like to thank Allison Vilander for teaching me how to slice brains, as well as everyone in CVID in general for building a collaborative scientific community.

Lastly, and most importantly, I'd like to thank my entire support system, which is a huge, wonderful group of people that always checked in, cheered me on, and got me where I am today: Mom, Dad, Amanda, Josh, Grammy, PawPaw, Tracie, Butch, Jacob, Jenny, Katie, Holly, Emily, Kelsey, Austin, Taylor, Sean, Christa, Emilee, Kylee, and several fantasy book series (these count as people with how much time I spent with them). My PhD people – Shelby, Lauren, Maggie, JP, Eric and Sarah, Jesse, and Christian. To y'all, I cannot thank you enough. The countless hours spent studying together, talking about our research, talking about things that people not in the program just don't understand (I'm pretty sure all of our non-science partners can attest to this!), drinking whiskey together, just going through *all of it* together. Thank you thank you thank you and I hope these bonds last a lifetime.

Thank you all!

TABLE OF CONTENTS

LIST OF TABLES

LIST OF FIGURES

CHAPTER 1: INTRODUCTION

1.1 POWV tick transmission cycle and evolution.

POWV disease burden and spread. Powassan virus (POWV) is an emerging tick-borne neuroinvasive flavivirus in North America with a 10% fatality rate, where 50% of survivors experience long-term neurological sequelae.[1,2] POWV cases have been rising in the last 20 years, although this is partly due to better detection methods.[3] Interestingly, phylogeographic studies estimate a relatively slow expansion rate (~3 km/year) of POWV lineage II driven by *Ixodes scapularis* range growth, consistent with underlying ecological shifts.[4] These trends of neurological severity, a rise in human cases, and geographic expansion highlight POWV as an increasing public health importance.

POWV genome and replication. POWV consists of a single-stranded, positive-sense RNA genome of approximately 10.8 kilobases, encoding one polyprotein that is cleaved into 10 structural and nonstructural proteins. The genome encodes three structural proteins–capsid (C), premembrane/membrane (prM/M), and envelope (E)–which are essential for viral entry, assembly, and packaging. Seven nonstructural proteins (NS1-NS5) are also encoded: NS1 is involved in genome replication and virion maturation, NS2A and NS2B contribute to replication and assembly, NS3 has protease and helicase activities necessary for polyprotein processing and RNA unwinding, NS4A and NS4B modulate host responses and support replication complex formation, and NS5 encode for the RNA-dependent RNA polymerase (RDRP) and methyltransferase, crucial for RNA synthesis and capping.[1,5,6]

Viral recombination is a critical evolutionary process in positive-sense RNA viruses, primarily facilitated by template switching of the error-prone replicase complex during replication.[7] This mechanism can yield full-length structural variants (SVs), which are genomes with point mutations or minor rearrangements that retain function, as well as defective RNAs (D-RNAs) (also known as defective interfering RNAs or defective genomes), which contain large deletions or frame-shift mutations that are non-functional.[7–9] Although recombination is well-studied in alphaviruses, there are limited studies for flaviviruses. However, both tick-borne encephalitis virus (TBEV) and dengue virus (DENV) show evidence of homologous recombination in nonstructural gene regions.[10,11]

ClickSeq is a sequencing method that preserves the integrity of RNA molecules and prevents artificial chimeras, which are essential for accurate detection of SVs and D-RNAs at low abundance. ClickSeq uses “click” chemistry to generate RNA-seq libraries free of enzymatic fragmentation artifacts: reverse transcription terminates at randomly incorporated 3′-azido-nucleotides, followed by ligation of adapters through copper-mediated azide-alkyne cycloaddition.[12,13] Originally demonstrated in Flock House virus, a positive-sense RNA virus, ClickSeq revealed naturally occurring D-RNAs across replication time points.[14] In addition, Viral Recombination Mapper (ViReMa) is a computational pipeline specialized for mapping recombination junctions from next-generation sequencing data, offering single-nucleotide resolution of structural rearrangements such as deletions, duplications, and template-switch junctions.[15] Taken together, ClickSeq and ViReMa provide an unparalleled platform for quantifying recombination rates and characterizing POWV recombination patterns. Our group has

previously used this method to uncover several deletions and recombination junctions in tick-derived POWV RNA, indicating the generation of defective RNAs and the potential for recombination.[16] While full-length homologous recombinants of POWV have yet to be confirmed, these findings underscore the need to determine the evolutionary and functional roles of recombination within the POWV transmission cycle between ticks, mammals, and humans.

1.2 Mouse models of Powassan virus disease

Animal models are valuable tools for studying flaviviruses, offering insights into viral pathogenesis, host immune responses, transmission dynamics, and therapeutic interventions. Animals have been extensively used to study mosquito-borne flaviviruses such as DENV, Zika virus (ZIKV), and West Nile virus (WNV) to uncover mechanisms of disease progression and to support the development of vaccines and antiviral therapies .[17–20] Similarly, the pathogenesis of some tick-borne flaviviruses (TBFVs) such as TBEV and Omsk hemorrhagic fever virus have been extensively characterized using mice.[21,22] In the decades immediately following the discovery of POWV in 1957, studies utilized a range of animals, including rabbits, hamsters, and non-human primates.[23–25] However, mouse models have also become central to POWV research, where recent research has shifted toward laboratory mouse strains, particularly BALB/c and C57BL/6 mice.[26–29] These mice exhibit severe neurological disease upon POWV infection, showing clinical signs that closely resemble human encephalitis such as rapid onset of neurological symptoms (i.e., weakness, paralysis), viral RNA and infectious virus in the central nervous system (CNS), and histological findings such as lymphocytic perivascular

cuffing and microgliosis in the brain and spinal cord.[26,30,31] In addition, C57BL/6 mice experience chronic neurological disease, similar to long-term neurological sequelae seen in many human survivors of POWV encephalitis.[32] These models have been

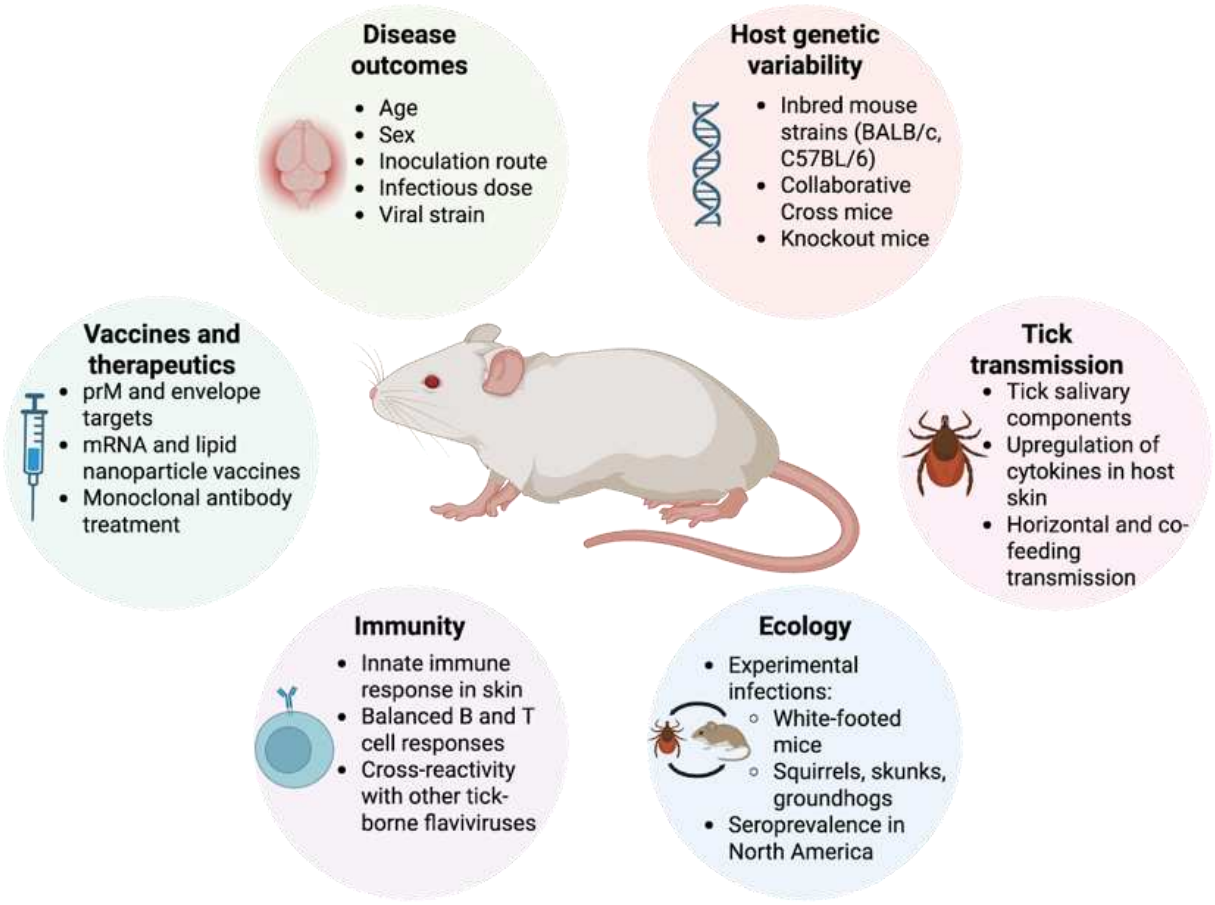

Figure 1.1. Using mouse models to characterize POWV. POWV disease outcomes, host-genetic variability, tick transmission dynamics, ecology, immunity, and vaccine and therapeutic strategies can all be investigated using mouse models.

critical for studying the impacts of host genetic variability[33], age-related susceptibility[34], and tick-host interactions (including the tick-skin interface[35]) and help guide the development of vaccines and antiviral therapies[36,37] (**Figure 1.1).** In this minireview, we explore the following facets of POWV: virus lineage, mouse genetics, disease

outcomes, sex differences, age, inoculation route, infection dose, immune response, development of vaccines and therapeutics, and non-model organisms.

POWV strain-dependent phenotypes. POWV comprises two genetically and mostly ecologically distinct lineages that are indistinguishable serologically.[38,39] These are termed lineage I and lineage II (also known as deer tick virus (DTV)).[40] POWV Lineage I was first reported in 1958 by Mclean and Donahue from a fatal case of encephalitis in a five-year old boy from Powassan, Ontario.[41] The virus was isolated from the postmortem brain tissue and subsequently characterized as a tick-borne flavivirus.[42,43] The resulting isolate, referred to as “LB” after the initials of the fatal case, is frequently used in POWV research because it is widely available, constitutes the prototype POWV strain, and produces well-formed plaques in convenient culture systems.[39] POWV lineage II was first identified in New England in 1997 in *Ixodes dammini* (*scapularis*), and in 1999 in Spooner, Wisconsin, also in *Ixodes scapularis*, which has since become the prototype lineage II strain.[44]

Early field studies indicated that lineage I is now known to circulate in nature in transmission cycles involving groundhogs and squirrels and the ticks that feed on these hosts (e.g., in *Ixodes cookei* and *Ixodes marxi*). However, lineage I POWV has been isolated in *Dermacentor andersoni* in 1952[41], *Dermacentor variabilis* in 2021[45], and *Ixodes scapularis* in 2019[46], suggesting that alternate, albeit rare, enzootic cycles exist in nature. In addition, early work showed that snowshoe hares in Canada were seropositive for POWV and showed viremia when experimentally inoculated.[47] Interestingly, when tested for seroprevalence in Canada in 2015, only one groundhog

out of 265 samples from a wide array of wild animals (squirrel, raccoon, fox, etc.) was seropositive for POWV.[48]

Lineage II reservoir hosts are less clear, where a broader range of small mammals, including red squirrels, striped skunks, raccoons, opossums, and porcupines are implicated as hosts for *Ixodes* spp. ticks. This is typical of *I. scapularis* biting behavior, where their broad host range could represent low host specificity.[4] However, the range of potential reservoir hosts could also be attributed to multiple tick species and enzootic transmission cycles in POWV maintenance in any given landscape.[49,50] Notably, Goethert et al. conducted bloodmeal analysis of *I. scapularis* ticks using a novel host-specific retrotransposon-targeted real time PCR and found a positive correlation between POWV positivity and having fed on shrews (with no infected ticks having fed on mice).[51] Additionally, of three shrews collected, they detected POWV RNA in brain tissue from one shrew but were unable to isolate virus. These results suggest a possible shrew reservoir role in specific habitat niches like Nantucket or Martha's Vineyard.[51] However, there are no established shrew models or generally available shrew-derived cell lines, and live trapping is notoriously difficult, thus limiting investigation. To further understand the absence of a clearly defined reservoir host, co-feeding has been shown to be a likely determinant of POWV circulating in nature; for example, Hermance et al demonstrated that POWV lineage II can be transmitted from infected *I. scapularis* females to uninfected *Haemaphysalis longicornis* larvae and nymphs by feeding them next to each other on an uninfected BALB/c mouse.[50] For a more comprehensive review of POWV ecology, extensive overviews are provided by Hassett and Thangamani[52] as well as Brackney and Vogels.[53]

POWV disease prevalence in humans is quite lower than the number of infected ticks in North America, raising questions about phenotypic variance among strains.[54,55] Lineage II has emerged as the more common cause of human infections in North America compared to lineage I.[56] Viral genomics studies have demonstrated extensive genetic diversity within POWV lineage II, but most studies of POWV lineage II use the Spooner isolate. Far fewer studies have used more recently collected, genetically diverse lineage II isolates.[32,33,57,58] This results in critical knowledge gaps about the range of phenotypes within POWV, including transmission, replication, tissue tropism, pathogenesis, neuroinvasion, and antiviral immune responses. Controlled studies comparing different virus strains are crucial because clear phenotypic differences between lineages I and II have been demonstrated in mice, with notable differences in clinical presentation and the areas in which the two lineages infected the brain, where lineage II caused more weight loss and seizures as well as increased inflammation in the hippocampus infection compared to lineage I.[59] In addition, it has been shown that there is phenotypic variability even within lineage II, where one lineage II isolate from New York caused increased mortality in mice compared to another lineage II isolate from Minnesota.[58] These findings emphasize the need for expanded use of genetically and temporally diverse isolates within both lineages in experimental systems to better understand how viral genetics contributes to various disease phenotypes.

Studies of POWV lineage II have utilized the ‘Spooner’ strain due to the availability of a reverse genetics system.[60] Virus derived from an infectious clone of the Spooner lineage II strain has been used in mouse studies and produces disease similar to the original virus isolated in 1997.[31] Tractable reverse genetics for lineage II POWV

allow for targeted studies of the role of specific viral determinants of pathogenesis and immune evasion in mice. In addition, an infectious clone generated from a passage-attenuated lineage II strain, LI9, revealed that a single mutation in the envelope protein abolished lethality and neuroinvasion in older mice.[34] No published infectious clone currently exists for lineage I, limiting the ability to perform reverse genetics or comparative, side-by-side mutational analyses between lineages. Expanding the repertoire of reverse genetics systems for POWV strains with distinct phenotypes will significantly accelerate research into viral genetic determinants of key phenotypes, including pathogenesis.

Mouse genetics. A wide array of distinct mouse models has been used to understand various aspects of POWV biology and pathogenesis. These include standard commercially available inbred lines, gene-specific knockout mice, deliberately outbred lines, and colonized wild, non-*Mus musculus* animals. Inbred mouse strains such as BALB/c and C57BL/6 have been instrumental in POWV research due to their well-characterized genomes and consistent clinical signs that closely resemble human encephalitis. BALB/c are highly inbred mice and are considered a general multipurpose model; in addition, they have a robust B and T cell response, making them an ideal mouse model for vaccination studies.[32,61] Similarly, C57BL/6 is a widely used inbred mouse strain with a permissive genetic background. Both mouse strains are susceptible to POWV[26,28] and exhibit similar clinical signs with C57BL/6 having a slightly longer survival time.[30] Moreover, these standard, commercially available inbred mouse strains have demonstrated that they are adequate models to represent POWV disease in humans.

Mice that have had key genes either specifically removed from or inserted into their genomes have similarly facilitated an advanced understanding of the key vertebrate immune genes and pathways required for POWV pathogenesis. For example, immunodeficient recombination-activating gene 1-deficient ($RAG^{-/-}$) and NOD SCID gamma (NSG) knockout mice lack the ability to trigger B and T cell responses. Interestingly, following POWV infection both $RAG^{-/-}$ and NSG mice had extended survival and delayed weight loss compared to wildtype mice, suggesting that the adaptive immune response can drive morbidity and mortality.[62] When *Oas1g* knockout (*Oas1g* $^{-/-}$) mice on a C57BL/6 background were infected with POWV lineage I, they exhibited similar disease outcomes to wild-type C57BL/6 mice. While *Oas1b* has been shown to restrict flavivirus pathogenesis, C57BL/6 mice carry a nonfunctional *Oas1b* allele and remain highly susceptible to infection. This suggests that, in the absence of functional *Oas1b*, the loss of *Oas1g* does not further alter susceptibility to POWV.[33] There are many other knockout mouse strains (e.g., IFNAR, MAVS, IRF3/5/7) that have been used with other flaviviruses (e.g., WNV, DENV, TBEV) to answer specific questions about neurotropic flavivirus pathogenesis that could be applied to POWV.[63,64] Although one study investigated the T cell response to POWV lineage I using RAG and NSG knockout mice[62], gene knockout models in general have yet to be leveraged to explore POWV pathogenesis in detail.

The genetic uniformity of inbred mice, including knockout/knock in lines, limits the exploration of host genetic factors that influence pathogenesis. To address this, researchers have employed Collaborative Cross (CC) mice.[65] Based on eight founder mouse strains, CC mice were created to introduce genetic diversity from well-

characterized inbred strains, thus improving genetic analyses and better reflecting the genetic variation within the human population.[66] This genetic tractability is extremely useful to understand viral infections, identify viral genes that impact pathogenesis, and map host traits that contribute to disease phenotypes. A recent study used CC mice to identify host factors that restrict neuroinvasive flavivirus pathogenesis. They showed that knocking out *Oas1b* on a CC mice line caused the mice to be extremely susceptible rather than highly resistant to disease.[33] Thus, to identify host restriction factors outside of *Oas1b*, they used a panel of *Oas1*^{null} CC lines and found varying susceptibility to POWV infection with certain lines exhibiting complete resistance and others demonstrating high susceptibility. In these resistant lines, mice had rapid viral clearance from peripheral infection and limited brain infection. These findings underscore the role of host genetics in POWV pathogenesis and highlight the utility of CC mice in identifying genetic factors that modulate disease outcomes.

The white-footed mouse (*Peromyscus leucopus*) is frequently cited as a potential vertebrate host for POWV lineage II[67] and offers critical insights into natural virus maintenance and host resistance mechanisms as an experimental model. While *P. leucopus* is a common bloodmeal source for *I. scapularis* ticks (vectors of POWV), and serological studies have detected antibodies against POWV in wild-caught *P. leucopus*, virus has never been isolated from these mice in nature.[52,68] Notably, *P. leucopus* mice infected with POWV had very low viremia, and virus in the brain without overt clinical disease.[30] This resistance to severe neuropathogenesis was linked to a robust type I interferon (IFN-I) response, characterized by the upregulation of IFN-stimulated genes (signal transducer and activator of transcription 1 (STAT1), IFN-induced protein with

tetratricopeptide repeats 2 and 3 (IFIT2 and IFIT3).[69] In contrast, C57BL/6 mice exhibit severe disease and high mortality upon POWV infection, highlighting differences in immune responses between these models. However, using *P. leucopus* in research presents challenges due to the limited availability of genetic, immunological, and molecular tools compared to well-characterized laboratory strains of mice. Despite these limitations, incorporating *P. leucopus* into POWV research has the potential to enhance our understanding of transmission dynamics in natural hosts and is essential for uncovering key host-pathogen interactions and improving our understanding of virus persistence and transmission in nature.

Disease outcomes. Different mouse models exhibit distinct patterns of disease following POWV infection, highlighting the importance of host genetic background in shaping disease outcomes (**Table 1.1**). Notably, inbred mouse strains such as C57BL/6 and BALB/c mice show relatively consistent but distinct disease outcomes upon infection. BALB/c mice are highly susceptible, with clinical signs such as weakness, seizures, ataxia, and paralysis reflecting robust viral neuroinvasion.[26,30,70] In contrast, C57BL/6 mice display a "poliomyelitis-like" presentation characterized by flaccid paralysis and spinal cord involvement, which has been attributed to motor neuron infection and inflammation.[27,30] Both strains show weight loss and variable survival depending on age, viral dose, and infection route which are discussed in detail below. Mortality often begins around 6–8 days post-infection (dpi), with most sick mice succumbing by 10–12 dpi. In addition, age plays a critical role in disease severity, where older mice (e.g., 50-week-old C57BL/6) exhibit prolonged viral persistence in the CNS and more severe or chronic neurological outcomes, such as sustained motor deficits,

compared to younger cohorts.[32] Interestingly, one study showed evidence of transplacental infection in C57BL/6 mice, where pregnant dams were inoculated with POWV and caused fetal demise in 50% of mice.[71] In comparison, *P. leucopus* exhibit little to no clinical disease, minimal weight loss, and very low or undetectable viremia when subcutaneously inoculated.[30] These comparative findings emphasize that both age and species-specific immune responses play a role in modulating POWV pathogenesis and highlight key limitations and advantages of various mouse models for studying disease.

Table 1.1 Animal models used in POWV research.

Species	Age	Sex	POWV Strain	Dose	Route	Reference
Pathogenesis models						
C57BL/6J	10 weeks, 50 weeks	Not specified	Lineage II - Attenuated LI9P	2×10^3 FFU	Footpad	Himmler et al, 2025
C57BL/6J	10 to 50 weeks	Male and female	Lineage II - LI9	2×10^3 FFU	Footpad	Mladinich et al, 2024
BALB/cJ	6 weeks	Male and female	Lineage I - LB Lineage II - Spooner	10^3 FFU	Footpad	Reynolds et al, 2024
BALB/c	15 weeks	Female	Lineage II - NJ56, ME1051	10^3 PFU	I.P.	McMinn et al, 2024
C57BL/6J	6 weeks	Male and female	Lineage II - Spooner	10^3 FFU	I.P.	Scroggs et al, 2023
Collaborative Cross (*Oas1b*^{null})	5 weeks, 9-12 weeks	Male and female	Lineage I - LB Lineage II - Spooner, MB5/12	10^2 FFU	Footpad, I.C.	Jasperse et al, 2023

			MBFV - WNV, JEV, SLEV			
BALB/cJ	6 weeks	Male and female	Lineage II - Spooner	10^1-10^5 FFU	Footpad	Hermance et al, 2020
C57BL/6J	Not specified	Female	Lineage II - Spooner	10^3 FFU	Footpad	Platt et al, 2018
Peromyscus leucopus, C57BL/6J, BALB/cAnNHSd	4 weeks	Not specified	Lineage I - LB	10^2-10^8 PFU, 10^3 PFU	I.P., I.C	Mlera et al, 2017
Peromyscus leucopus	4 weeks	Not specified	Lineage I - LB	10^3 PFU	I.C.	Mlera et al, 2017
C57BL/6	4 weeks	Male	Lineage I - LB	5×10^6 PFU, 5×10^3 PFU	Footpad	Santos et al, 2016
BALB/c	3-5 weeks	Female	Lineage I - LB	1.25×10^4 PFU	I.P.	Holbrook et al, 2005
Swiss inbred mice	Not specified	Not specified	Lineage I - LB	N/A	I.C., I.P., I.D.	Weiner et al, 1970
Suckling mice	Not specified	Not specified	Basal ganglia of infected human patient	N/A	I.C.	Mclean and Donohue, 1959
Immunity models						
C57BL/6	8-10 weeks	Male and female	Lineage II - Spooner (infectious clone)	2.5×10^4 PFU	S.C. or I.P. immunization, S.C. inoculation	Cheung et al, 2023
C57BL/6J, Nod SCID gamma (NSG), Recombination activating	10-12 weeks	Male and female	Lineage I - LB, Lineage II - Spooner	10^2 FFU	I.M. immunization, footpad inoculation	Stone et al, 2022

genes 1 (Rag –/-)						
C57BL/6J	7 weeks	Not specified	Lineage I - LB, Lineage II - Spooner, LGTV	10^2 FFU	I.P. administration, footpad inoculation	VanBlargan et al, 2021
C57BL/6	6-8 wks	Female	Lineage I - LB	10^4 FFU	I.M. immunization, footpad inoculation	Choi et al, 2020
C57BL/6	7-14 weeks	Male and female	Lineage I - LB Lineage II - Spooner	10^2 FFU	I.M. immunization, I.P. administration, footpad inoculation	VanBlargan et al, 2018
Other animal models and seroprevalence studies						
Groundhogs, skunks, and fox squirrels	Live trapped adults and juveniles	Male and female	Lineage I - LB Lineage II - Spooner	$10^{2.8}$-10^6 PFU	S.C.	Nemeth et al, 2021
Shrews	Not specified	Not specified	Lineage II - Spooner	N/A	N/A	Goethert et al, 2021
Wild mammals (squirrel, skunk, groundhog, raccoon, chipmunk, beaver, deer mice, possum, rabbit, porcupine, fox)	Not specified	Not specified	Lineage I - LB Lineage II - Spooner	N/A	N/A	Smith et al, 2018

Rabbits, horses	Not specified	Not specified	Lineage I - M794	~10^6 MICL D_{50}	I.C	Little et al, 1985
Monkeys	Not specified	Not specified	P40 (USSR) Lineage I - LB	N/A	I.C.	Frovola et al, 1985
Goat	Kid	Female	Lineage I	10^3 LD_{50}	I.M.	Woodall and Roz, 1977
Spider monkeys, Swiss mice	Not specified	Not specified	Lineage I	10^3 LD_{50}	S.C. inoculation and immunization	Price and Thind, 1973
Hamsters	Not specified	Not specified	Lineage I - LB	10^1-10^5 mouse LD_{50}	S.C.	Chernesky et al, 1972
Guinea pigs, Swiss mice	Not specified	Not specified	Lineage I - LB	N/A	N/A	Casals 1960
Tick models						
BALB/c	6 weeks	Male and female	Lineage II - Spooner	10^3 FFU	Tick infestation	Obelliane et al, 2024
BALB/c	6 weeks	Female	Lineage I - LB	10^3 PFU or 10^6 PFU with SGE	Footpad	Santos et al, 2021
BALB/c	7 weeks	Female	Lineage II - P0375	10^4 PFU	I.P.	Grubaugh et al, 2016
BALB/c	6 weeks	Female	Lineage I - LB	N/A	Tick infestation	Hermance et al, 2016
BALB/c	6 weeks	Female	Lineage I - LB	10^3 PFU or 10^6 PFU with SGE	Footpad	Hermance and Thangamani, 2015
BALB/c	6 weeks	Female	Lineage II - Spooner	~10^3 PFU/tick	Tick infestation	Ebel et al, 2004

FFU, focus forming units; I.C., intracranial; I.D., intradermal; I.M., intramuscular; I.P., intraperitoneal; JEV, Japanese encephalitis virus; LD_{50}, lethal dose 50%; LGTV, Langat virus; MBFV, mosquito-borne flavivirus;

$MICLD_{50}$, mouse intracerebral lethal dose 50%; PFU, plaque forming units; S.C., subcutaneous; SGE, salivary gland extract; SLEV, St. Louis encephalitis virus; TBEV, tick-borne encephalitis virus; WNV, West Nile virus

Comprehensive analysis of POWV infection in animal models relies on detecting viral dissemination and host responses in both peripheral and CNS tissues. POWV RNA and antigen have been detected in peripheral tissues of BALB/c and C57BL/6 mice such as the spleen, kidney, and liver, particularly during early stages of infection prior to neuroinvasion.[30] Quantification of viral burden in these tissues is typically achieved using RT-qPCR for viral RNA, and plaque or focus-forming assays to quantify infectious virus. To evaluate tissue-specific virus localization, immunofluorescence assays (IFA), immunohistochemistry (IHC), and *in situ* hybridization are commonly used, providing spatial resolution of viral antigen and insights into tissue and cellular tropism.[26,27,30,59] In addition to viral detection, histopathological analyses are used to assess tissue damage and immune cell infiltration, often alongside cytokine profiling, such as ELISA or multiplex assays, to characterize the inflammatory response. These methods parallel clinical approaches in human studies, where viral RNA can be detected in blood or cerebrospinal fluid, and histopathology from fatal cases reveals CNS inflammation, neuronal necrosis, and microglial activation[72,73], thus providing translational value to these mouse models.

Sex differences. Sex differences in immune responses are well established in both humans and animal models, and they can shape disease outcomes across a wide range of viral infections.[74] In particular, male and female laboratory mice show distinct immune responses that influence disease susceptibility and pathology following viral infections such as influenza and SARS-CoV-2, where females often mount stronger

IFN-I responses and exhibit more robust inflammatory signaling.[75,76] Despite this, sex differences during flavivirus infections in mice remain surprisingly unclear. While some studies document varying trends in mortality and IFN responses across sexes following Japanese encephalitis virus (JEV) and WNV infection[77,78], there is limited evidence for sex-based differences in disease outcomes across other viruses. Although female C57BL/6 mice exhibit stronger type I IFN responses than males, this has not been consistently observed for flaviviruses[79,80] even though many of these viruses antagonize type I IFN signaling.[81]

In the case of POWV, findings for sex differences are mixed. Many studies contain mice of only one sex or fail to report sex. When studies include both male and female mice, they often do not see differences between sexes. However, one study that compared results by sex did suggest dose-dependent sex differences in survival. Following POWV infection, 75% of female mice survived compared to only 25% of males, and at higher doses, 25% of females survived and no males survived, however, these trends were not statistically significant.[26] Another study noted sex differences in clinical signs at day seven post-infection, where males infected with POWV lineage II had more severe disease compared to females.[59] However, this was not observed with mice infected with POWV lineage I, and neither lineage caused differences in weight loss between sexes. The lack of consistent sex-based differences in POWV disease outcomes highlights a gap in our understanding and suggests a need for further studies to investigate the impact of sex-dependent immune modulation, such as the IFN pathway, on POWV infection.

Age. Age is a critical determinant of disease severity in POWV infection, influencing both immune responses and clinical outcomes in murine models. Although there are no significant differences in survival time between younger POWV-infected mice (8-14 weeks)[29,31], studies investigating age-related differences in POWV infection in mice have shown that older mice (50 weeks) experience more severe outcomes compared to younger mice (10 weeks).[32] While viral loads in the CNS are similar across age groups, older mice exhibit higher lethality and persistent viral RNA, alongside a pro-inflammatory Th1 cytokine response linked to neuroinflammation and impaired viral clearance. In contrast, younger mice display a more protective Th2 response. These findings highlight the role of age in POWV pathogenesis, where older mice show chronic viral persistence and long-term neurological damage. Importantly, this mirrors clinical observations in humans, where older adults face a higher risk of severe POWV-related encephalitis and lasting neurological effects.[73,82]

Inoculation route. Modeling POWV transmission in laboratory settings requires careful consideration of infection routes to accurately reflect natural exposure and disease progression. In nature, POWV transmission occurs when an infected tick (typically *Ixodes* spp.) attaches to a host, such as a rodent, medium-sized mammal, or human, and feeds for several days (although POWV transmission can occur within 15 minutes).[49,83,84] To replicate this natural infection route in experimental settings, studies commonly use peripheral routes such as footpad, subcutaneous (S.C.), intradermal (I.D.), or intraperitoneal (I.P.) inoculations.[26,28,30,57] These are valuable for pathogenesis studies in mice, as they mimic the general disease progression observed in humans: initial viral entry into the skin, followed by infection of peripheral tissues like the spleen

and lymph nodes before reaching the CNS.[27,35] In addition, these routes are useful for understanding POWV peripheral tissue infection, immune recruitment, and neuroinvasion. Many studies use live, infected ticks and allow them to feed on mice, guinea pigs, and rabbits to study POWV infection and transmission dynamics.[49,50,57,85] Lastly, I.P. inoculation is often employed in vaccine and therapeutic development studies, making these varied routes essential tools for dissecting POWV pathogenesis and intervention strategies.

Conversely, intracranial (I.C.) inoculation directly targets the CNS and bypasses the blood-brain barrier (BBB), making it an ideal method for investigating neurotropism and immune responses within the brain. For example, a study by Mlera et al. used I.C. inoculation in *P. leucopus* and sequenced the brain transcriptome to gain insights into neuroinvasion and the host immune response to POWV independent from the peripheral infection.[30]

While peripheral inoculation methods are instrumental in studying POWV pathogenesis, they may not fully replicate the immunological complexity of natural tick-mediated transmission that is crucial for natural infection. During their prolonged feeding, ticks inoculate not only the virus but also a complex mixture of salivary proteins, metabolites, and other immune modulators into the host skin at the site of attachment.[86] This process, known as saliva-activated transmission (SAT), is crucial for efficient viral dissemination and immune evasion.[87] For example, *Ixodes ricinus* ticks, the vector for TBEV, secrete IrSPI, a salivary protein that inhibits $CD4^+$ T cell proliferation and proinflammatory cytokine secretion to subvert the host immune response and promote tick feeding.[88] Tick saliva suppresses pro-inflammatory cytokine

production, including IL-8 and TNF-α, while promoting anti-inflammatory factors such as IL-10.[84] It can also inhibit dendritic cell maturation and migration, impairing antigen presentation and subsequent T cell activation.[89] Prostaglandin E2 (PGE2) in tick saliva inhibits the secretion of the pro-inflammatory cytokines TNF-α, IL-6, IL-1β, and IL-12 after stimulation of mouse and human dendritic cells.[84] Additionally, tick saliva increases the permeability of the BBB, making it easier for pathogens to invade the CNS.[90]

Recent studies have started to explore the effects of tick saliva in the context of POWV. Notably, tick transmission of POWV induces a rapid proinflammatory response in the skin of BALB/c mice, with increased expression of IL-1β, IL-6, IL-36A, TLR4, and CCR3.[35] However, obtaining tick saliva is laborious and not always feasible; to avoid this, some studies have used salivary gland extracts (SGE) with virus to inoculate mice. When POWV is administered with SGE, particularly in low-dose inoculations, the SGE appears to enhance viral establishment in the skin and dissemination from this site of tick attachment[91,92], suggesting that it may be a critical factor in POWV transmission if titers in the saliva are low. These findings highlight the immunomodulatory role of tick saliva in shaping early host responses and facilitating viral dissemination during natural POWV transmission. The extent to which immunomodulation during tick feeding shapes downstream protection and pathogenesis is not fully understood at present.

POWV infection dose. The amount of infectious virus inoculated by ticks during the feeding process is not well defined. Experiments that use peripheral inoculation typically use doses around 10^3 plaque/focus forming units (PFU/FFU), although both lower (below 10^2 PFU) and higher (up to 10^6 PFU) have been used.[36,59,93] Hermance et al tested a range of inoculation doses (10^1-10^6 FFU) and reported that morbidity,

mortality and levels of vRNA in tissues were dose-independent[26], in contrast to some literature on the flaviviruses. Overall, there has been no significant impact in morbidity, mortality, or tissue tropism noted about infection dose in the POWV literature.

Immune response. Several studies have characterized both innate and adaptive immune responses to POWV. Innate immune mechanisms have been particularly well explored, especially at the site of tick bite and within the CNS. Early targets of POWV infection at the skin interface include macrophages and fibroblasts[35,94], which are critical initiators of IFN-I responses. Within the CNS, resident glial cells such as microglia and astrocytes contribute to the antiviral response during POWV infection.[94] In *Peromyscus leucopus*, I.C. inoculation with POWV leads to robust upregulation of interferon-stimulated genes (ISGs), suggesting that the brain establishes an early restrictive environment to limit viral replication.[95] Like other TBFVs, POWV may also utilize mechanisms such as cell-to-cell spread or "Trojan horse" entry via migratory immune cells to access the CNS.[96] These findings highlight the critical role of both peripheral and CNS innate immune responses in restricting early POWV replication, while also suggesting that the virus may exploit immune cells to facilitate neuroinvasion.

IFN-mediated innate immunity is a critical first line of defense against TBFVs. For example, mice lacking IFN-I signaling ($IFNAR^{-/-}$) infected with TBEV or Langat virus (LGTV) exhibit dramatically elevated viral loads and severe neurological disease.[97] Similarly, glial activation and IFN-mediated responses have been well documented in the CNS during TBEV and LGTV infection, highlighting conserved antiviral mechanisms across TBFVs.[98] Although the pathogenesis of POWV is not yet fully established to parallel that of TBEV or LGTV, findings from these related viruses provide valuable

context. Taken together, these studies underscore the role of IFN-mediated innate immunity in controlling viral replication and limiting CNS invasion across TBFVs, including POWV.

However, studies investigating adaptive immune responses to POWV in mice remain limited. It was demonstrated that C57BL/6 mice generate POWV-specific B cells producing IgG and IgM antibodies during acute POWV infection.[62] In addition, POWV immune sera was partially protective against POWV challenge when passively transferred to naïve mice.[62] In a different study, Van Blargan et al. generated and characterized monoclonal antibodies (mAbs) from POWV-infected C57BL/6 mice, finding they primarily generate IgG2c isotype antibodies that target the envelope protein, with many binding domain III (DIII).[37] Most were strongly neutralizing against both lineage I and II, with some mAbs cross-neutralizing other TBFVs (e.g., TBEV, LGTV).

Regarding T cell immunity, there are limited studies. One study showed that POWV-infected mice generate a detectable POWV-specific $CD8^+$ T cell response at 7 dpi and $CD4^+$ T cell responses at 10 dpi.[62] Another study demonstrated that different cytokines were induced based on mouse age, indicating that 1) older mice (50 weeks) had a strong Th1 response to POWV infection, suggesting that POWV induces a neurodegenerative M1 microglial response, and 2) younger mice (10 weeks) had a strong Th2 response, suggesting that POWV induces a neuroprotective M2 microglial response.[32] Therefore, studies show that IFN-mediated innate immunity is critical for controlling POWV replication at the site of infection and within the CNS, while adaptive

immune responses, though less explored, include the production of neutralizing antibodies and age-dependent T cell responses that affect neuroinflammation.

Development of vaccines and therapeutics. Although there are no vaccines available for human use or specific treatment for POWV, vaccines and therapeutics for POWV are being actively explored using mice (**Table 1.2**). Current vaccine platforms utilize the prM and envelope proteins as immunogenic targets.[29,31,36,61,62,99,100] A POWV prM and envelope VLP-based vaccine induced neutralizing antibodies, resulting in 100% seroconversion in mice.[61] This vaccine elicited both IgG1 and IgG2 subclasses, suggesting a balanced Th1/Th2 immune response. A different VLP vaccine, also targeting prM and envelope, activated both $CD4^+$ and $CD8^+$ T cells following immunization, generated neutralizing antibodies, and was protective against weight loss and mortality following lethal POWV challenge, indicating that cellular immunity contributes to protection.[62] Another study demonstrated that a prM-envelope mRNA vaccine in C57BL/6 mice produced potently neutralizing antibodies that were protective

Table 1.2 POWV vaccine platforms.

Vaccine Platform	Immunogen Targets	Protection in Mice (with POWV Lineage)	Immune Response & Findings	Reference
VLP	prM and envelope proteins	100% seroconversion; high neutralizing antibody titers following challenge with POWV lineage I (LB)	Induced robust neutralizing antibodies; elicited IgG1 and IgG2 subclasses, suggesting a balanced Th1/Th2 response. Hybridomas expressing monoclonal antibodies were	Cimica et al., 2021

			produced following immunization.	
VLP	prM and envelope proteins	Protection against weight loss and mortality after lethal challenge with POWV lineage I (LB)	Activated both $CD4^+$ and $CD8^+$ T cells; generated neutralizing antibodies. Robust B and T cell responses correlated with protection.	Stone et al., 2022
mRNA	prM and envelope proteins	Sterilizing immunity against lethal challenge with POWV lineage I (LB); cross-protection against lineage II (Spooner)	Induced potently neutralizing antibodies; cross-neutralized TBEV, LGTV, and Gadgets Gully virus. Protected against disease following LGTV challenge.	VanBlargan et al., 2018
DNA	prM and envelope proteins	Single dose protected mice from lethal challenge with lineage I (LB)	Elicited broad T and B cell immunity with minimal cross-reactivity to other flaviviruses; antibody epitope mapping showed similarity to natural infection; protection confirmed in lethal challenge experiments.	Choi et al., 2020
Live-attenuated	prM and envelope proteins	70% survival with two-dose regimen; 100% survival with heterologous prime-boost (live virus prime + EDIII protein boost)	Live virus prime followed by EDIII protein boost conferred complete protection without morbidity; recoded CpG/UpA virus	Cheung et al, 2023

		against lineage II (Spooner)	showed minimal attenuation and was not pursued further.	
Nanoparticle-based immunogen	envelope domain III (EDIII)	Protection against POWV lineage I (LB) challenge; reduced viremia and weight loss	Generated neutralizing polyclonal antibodies; passive serum transfer conferred protection; high-affinity monoclonal antibodies recognized multiple EDIII epitopes.	Malonis et al., 2022

LGTV, Langat virus; prM, premembrane; TBEV, tick-borne encephalitis virus; VLP, virus-like particle

against lineage I and II lethal challenge and provided sterilizing immunity.[29] Importantly, sera from POWV-vaccinated mice cross-neutralized TBEV, LGTV and Gadgets Gully virus, a distantly related TBFV, and vaccination was protective against disease following LGTV challenge.[29] Another recent study developed a nanoparticle-based immunogen displaying DIII of the envelope protein.[36]

Vaccinated mice generated neutralizing, polyclonal antibodies, and passive transfer of immune sera to naïve mice reduced viremia, weight loss, and provided protection against challenge with POWV lineage I. This vaccine immunogen elicited high affinity mAbs that recognized multiple distinct epitopes within DIII. These VLP, mRNA and nanoparticle-based vaccine platforms have proven successful in eliciting protective immunity in mice, but their mechanisms of action and application to humans remain an area of active investigation. Lastly, a promising immunoinformatics-based approach has predicted B-cell and T-cell epitopes from the POWV capsid, envelope,

and membrane proteins as potential vaccine candidates; however, these predictions have not yet been validated *in vivo*.[101] Together, these studies demonstrate that multiple vaccine platforms targeting POWV can elicit robust and protective immune responses in mice, providing a strong foundation for future translational research aimed at developing effective vaccines for human use.

In addition to vaccine development, mAbs have also been explored as a potential therapeutic for POWV. One study evaluated mAbs that target domain II and III of the envelope protein and showed that they provided protection against POWV lineage II in mice when administered as prophylaxis or post-exposure therapy.[37]

Moreover, there has been interest in exploring cross-reactive immunity with other flaviviruses, such as TBEV, which may provide broader protection against related viruses. Some studies have demonstrated that human antibodies against TBEV neutralize POWV in cell culture, suggesting the potential for broad therapeutics between these related flaviviruses, but protection from viral challenge with related TBFVs has not been well characterized.[102] Together, these studies emphasize both the promising potential of diverse vaccine and mAb platforms against POWV and the essential role of well-defined mouse models, such as C57BL/6 and knockout strains, in uncovering immune mechanisms, evaluating cross-protective responses, and supporting the preclinical advancement of targeted strategies against this emerging tick-borne virus.

1.3 POWV infection in non-model organisms

Before the widespread use of standardized mouse models, early POWV research relied on a variety of non-model mammals to investigate disease pathogenesis

and neuroinvasion. These included Swiss mice, rabbits, horses, hamsters, and non-human primates, which were selected for their physiological similarities to humans or practical accessibility.[23,25,103,104] These studies demonstrated that POWV could cause neuroinvasive disease across diverse species: inoculated animals developed neurological symptoms such as ataxia, lethargy, and encephalitis, with histopathological findings including neuronal necrosis, gliosis, and perivascular inflammation. For example, following I.C. inoculation with either the P-40 strain from the USSR or the prototypic lineage I LB strain, rhesus macaques exhibited signs of degenerative neurological disease.[24] In addition, rabbits and horses also developed encephalitis following I.C. POWV infection, similar to what is seen in mice.[23] Surprisingly, a study in 1977 showed that lactating goats can secrete POWV into their milk following experimental inoculation, although this was not explored further.[105] Collectively, these early animal studies provided foundational evidence that POWV can cause neurological disease across a range of mammalian hosts, reinforcing its broad neurotropic potential. However, mice offer a more cost-effective and versatile model for studying POWV pathogenesis as discussed in this minireview.

To better approximate natural transmission dynamics, recent studies have turned to wild-caught mammals to evaluate their potential as reservoir hosts for POWV. A recent study experimentally infected wild-caught mammals to better mirror transmission cycles in nature and evaluate potential reservoir hosts. Groundhogs, striped skunks, and fox squirrels were infected with POWV lineage I and II strains, where no overt disease was observed and viremia was minimal or undetectable.[93] However, all species seroconverted by 21 dpi, and viral RNA was occasionally detected in brain tissues.

These findings suggest that while groundhogs, skunks, and squirrels can mount an immune response to POWV, their low or undetectable viremia and absence of clinical disease make it unlikely that they play a major role in maintaining viral transmission, though their seroconversion highlights the complexity of identifying true reservoir hosts in nature.

1.4 Conclusions on animal models

This minireview highlights the decades of work using animal models, particularly mice, to advance our understanding of POWV pathogenesis, immunity, and transmission. These models have provided key insights into age and sex differences in disease outcomes, innate and adaptive immune responses, and viral neuroinvasion, while also serving as essential platforms for evaluating vaccine candidates and mAb therapies. While traditional inbred strains such as C57BL/6 and BALB/c have laid the groundwork for much of this research, the use of genetically diverse models like Collaborative Cross mice and natural reservoir species such as *Peromyscus leucopus* is expanding our understanding of how host factors influence disease. In addition, studies involving non-model mammals and field-based surveillance elucidate the ecological complexity of POWV transmission.

Despite significant advancements in our understanding of POWV biology, host immune interactions, and transmission dynamics, several critical gaps remain. Most experimental models rely on historic, laboratory-adapted virus strains, which may not reflect the genetic diversity observed in circulating field isolates, thus highlighting the need for studies using contemporary and geographically diverse strains. Additionally, most of the current work utilizes inbred laboratory mouse strains, which do not fully

recapitulate the complexity of human disease. The use of humanized mouse models may help bridge this gap and better characterize tissue-specific viral tropism and long-term sequelae.[106] Furthermore, while tick saliva gland extracts are known to enhance POWV infection at low doses and modulate host immunity, the effects of natural tick saliva are not fully understood.[91,92] The relationship between tick salivary factors and viral transmission, particularly at site of infection in the skin, warrants further investigation using techniques such as single-cell RNA sequencing, which have been applied in mosquito-borne virus research but remain underutilized in tick-virus models.[107] Lastly, discrepancies surrounding the role of inoculation dose, route, and host-specific variables such as age, sex, and mouse genetic background continue to complicate interpretation across studies. Nonetheless, mouse models remain indispensable, providing a foundational platform for determining viral mechanisms, elucidating host-pathogen interactions, and evaluating vaccine and therapeutic efficacy.

1.5 Neurotropic flaviviruses: a broad overview of viral distribution in the brain

TBEV and LGTV are closely related flaviviruses with distinct neuropathology. TBEV, first isolated in 1937, causes neurologic disease in humans with symptoms ranging from meningitis to severe encephalitis. Approximately 33–60% of patients develop post-encephalitis syndrome, characterized by long-term cognitive and motor deficits.[108] LGTV, sharing ~85% nucleotide homology with TBEV, exhibits lower human pathogenicity but retains neurovirulence in rodent models. Both viruses invade the CNS, targeting neurons and triggering neuroinflammation, though their mechanisms differ. In humans, TBEV preferentially infects cortical neurons, basal ganglia, thalamus, and

cerebellum, leading to neuronal necrosis and microgliosis.[108] LGTV infection in mice induces hippocampal neuron damage, reduced dendritic spine density in the CA1 region, and microglia activation, correlating with anxiety-like behavior and memory deficits.[109] In addition, LGTV had strain-dependent immune responses, with wildtype mice showing subclinical hippocampal infections and Irf-7$^{-/-}$ mice developing encephalitis.

Imaging is a powerful tool to understand viral distribution within the brain. Anna Överby's team combined optical projection tomography (OPT) and MRI to map LGTV distribution in whole mouse brains. Their whole-brain imaging technique demonstrated that IFN-I signaling restricts LGTV to sensory grey matter regions (e.g., entorhinal cortex, primary somatosensory cortex) in wildtype mice. In contrast, Ifnar$^{-/-}$ mice showed expanded tropism into white matter and ventricular systems, including the rostral migratory stream and choroid plexus.[110] Confocal and electron microscopy confirmed that IFN plays a role in limiting viral spread, protecting neuronal regions, and shifting cellular tropism from neurons in wildtype mice to astrocytes and microglia in IFN-I-deficient models.[109,110] Immunofluorescence assays in LGTV-infected hippocampus cultures revealed viral protein colocalization with Fox3-positive neurons, particularly in the dentate gyrus and cornu ammonis.[109] These imaging approaches provide a holistic view of neurotropic flavivirus dynamics, linking immune responses to spatial infection patterns, which will ultimately lead to developing better therapeutic and vaccine strategies.

1.6 Goals of dissertation

The overarching goals of this dissertation were to characterize POWV at both the molecular and host levels. First, we investigated the potential for POWV recombination within its enzootic transmission cycle, which is characterized by focal and slow evolution among ticks, mammalian reservoirs (e.g., rodents, deer), and human hosts. To assess whether recombination occurs in ticks, 53 POWV-positive ticks (collected in the Northeast U.S. in 2019) were sequenced with Nextera and ClickSeq, where rare recombinant variants were detected via Viral Recombination Mapper (ViReMa).

Next, we characterized the phenotypic diversity of POWV disease in mice. Focusing on lineage II, we chose POWV strains isolated from *I. scapularis* ticks in the Northeast U.S. in 2019, as well as the widely used Spooner strain (as an infectious clone), and older isolates such as NFS9601 (1996). These strains were evaluated for morbidity and mortality in mice, as well as for viral replication kinetics in the blood, spleen, and brain throughout the course of infection. To further explore genotype-phenotype relationships, we developed an infectious clone of a New York strain (NY.19.12) isolated from *I. scapularis* in 2019 that had three unique amino acid mutations compared to the other strains used in this study. This clone was used to determine that these mutations were partially sufficient to recapitulate the *in vivo* disease phenotype observed for the natural NY.19.12 isolate.

Finally, we examined how host antiviral responses influence neurotropism in POWV and related neurotropic flaviviruses such as WNV. We developed a streamlined workflow to study viral dissemination and immune responses in both C57BL/6 mice and MAVS knockout mice. By employing multiple inoculation routes, we assessed differences in morbidity and mortality between POWV lineage I and II in MAVS knockout

mice. In addition, we will be determining how innate immune signaling impacts viral distribution within the CNS, providing new insight into the determinants of flavivirus neuropathology.

CHAPTER 2: EVIDENCE FOR POWASSAN VIRUS DELETIONS AND DEFECTIVE RNA IN FIELD COLLECTED TICKS

2.1 Introduction

Powassan virus (POWV) is a flavivirus within the tick-borne encephalitis virus (TBEV) serogroup that affects the US, Canada, and the Russian Far East.[41,111–113] POWV is an emerging pathogen of concern[114], given the increase in disease incidence over the past two decades and the propensity of the virus to cause severe and frequently fatal viral encephalitis. While analysis of POWV genome sequences has yielded critical data for understanding POWV genomic epidemiology, spatial population structure, and evolution, few studies have considered the diversity of POWV populations within individual hosts. Still fewer have considered the recombinant components of intrahost populations. Viral RNA recombination can have a profound influence on viral evolution, as well as produce defective virus that can impact viral replication, persistence, and disease severity. Thus, by characterizing viral recombination in relevant POWV hosts, we can determine potential sources of genetic variation and identify novel research avenues for identifying determinants of persistence and virulence.

Recombination is a key driver of RNA virus evolution[115], including mosquito-borne flaviviruses.[116,117] This process involves template switching between distinct RNA strands or within the same strand and can generate deletions and duplications[118] that result in RNA structural variants (SVs) or defective RNAs (D-RNAs; also known as defective viral genomes, DVGs, or defective-interfering RNAs, DI-RNAs).[119,120] SVs and D-RNAs differ functionally: SVs remain autonomously functional, while D-RNAs cannot replicate and/or transmit in the absence of functional complementation by intact co-infecting viral

genomes.[7,121,122] Although SVs and D-RNAs were initially thought to be artifacts of *in vitro* passaging, subsequent studies detected and characterized them in animal models of mosquito-borne flaviviruses[120,123] and alphaviruses[124–126] and natural infection of respiratory viruses.[127–129]

D-RNAs in tissue culture can disrupt viral replication and induce host pro-inflammatory responses.[130] However, in natural infection, D-RNAs may have variable roles in pathogenesis[130], with some studies showing antiviral effects for SARS-CoV-2 and Zika virus[125,131], others demonstrating a role in persistent infection for Usutu and Langat viruses[124,132], and still others suggesting differential roles for transmitted versus *de novo* produced alphavirus D-RNAs.[126] Despite the significant global health impact of tick-borne flaviviruses (TBFVs), our understanding of recombination in these viruses remains limited[133–135], especially the formation of D-RNAs in natural tick vectors. In addition, while recombination has been documented in other flaviviruses[117,133,136], few studies have mapped specific regions of microhomology or performed genome-wide deletion analyses, limiting direct comparisons.[137]

Ixodes ticks transmit POWV via bloodmeal exchange with mammalian hosts (e.g. shrews, deer mice, groundhogs, squirrels) and humans.[111] Relatively little is known about the maintenance of POWV and other TBFVs in mammalian reservoirs, and experimental and modeling studies suggest that TBFVs also can be effectively maintained in tick populations.[138,139] Ticks are unique among arthropod vectors due to their multi-stage, blood-meal dependent life cycle: between each of three active life stages (larva, nymph, and adult), ticks take a single bloodmeal from a single host before molting into the next stage. POWV has been identified in field-collected ticks of multiple life stages[111,140] and is

maintained through all life stages through transstadial[49,141,142] and vertical transmission [139,143], as well as through infected ticks transmitting virus through an animal's bloodstream to an uninfected tick via co-feeding.[138] Because the tick vector may act as an important reservoir for POWV, it is a critical host in which to study POWV replication and recombination. Accordingly, we sought to expand our knowledge of POWV recombination in ticks naturally infected with POWV lineage II virus to gain insight into viral population dynamics within critical hosts. We performed detailed recombination analyses to: 1) characterize POWV deletions in naturally infected ticks; 2) determine potential factors that influence recombination leading to deletions; and 3) determine whether tissue culture passage affects POWV deletion content.

2.2 Results

Deletions occur throughout the POWV genome, and most are predicted to result in defective RNAs. We analyzed POWV reads generated by RNA metagenomic short-read sequencing from 53 individual POWV-positive ticks collected from the Northeastern U.S. between 2018 and 2020 [29] (**Table 2.1**, **Table S2.1**). Most of the samples (n=33)

Table 2.1. Naturally infected ticks included in study, by year and location.

State	2018	2019	2020	Total
ME	3	14	16	33
MA	2	0	6	8
NY	0	9	0	9
NJ	0	3	0	3

were collected from Maine in 2018 (n=3), 2019 (n=14), and 2020 (n=16). The remaining samples were collected in either Massachusetts (2018, n=2; 2020, n=6), New York state

(2019, n=9), or New Jersey (2019, n=3). All ticks in this study were positive for POWV lineage II.

Across all samples, we identified 330 deletions with unique nucleotide positions at each recombination junction (**Figure 2.1**). Most samples contained between 1 and 10

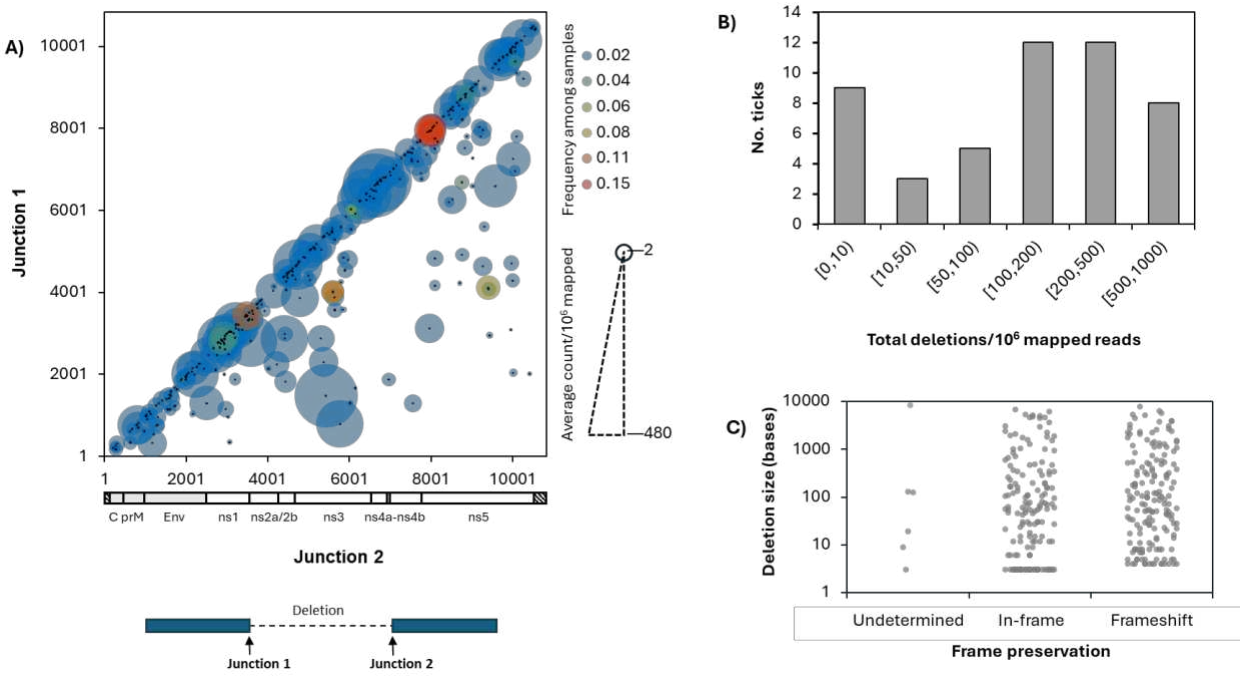

Figure 2.1. Characteristics of POWV recombination breakpoint junctions and deletions. POWV RNA derived from 53 naturally infected tick samples underwent random-primer cDNA synthesis, Nextera XT tagmentation, and sequencing on an Illumina platform, and recombination events were mapped using Viral Recombination Mapper (ViReMa). Deletions were extracted, and recombination breakpoint junction nucleotide positions (Junction 1, Junction 2) were indexed to the POWV reference HM440559.1. Unique deletions were defined as having a unique combination of J1 and J2 nucleotide positions. **A)** Nucleotide positions of Junction 1 (y-axis) and Junction 2 (X-axis) for each unique deletion, colored by its frequency among samples and sized by its average read count per million mapped reads within each sample; **B)** Distribution of the total number of deletions per 10^6 mapped reads across 53 tick samples; **C)** Distribution of deletion size (Y-axis) by coding frame (undetermined are deletions occurring between non-coding and coding regions of the genome; in-frame are deletions with a base size divisible by 3, and frameshift are deletions predicted to result in a shift to the coding frame).

unique deletions (**Figure S2.1**). Most unique deletions were specific to a single sample and ranged in expression from 2 to 480 deletions per 10^6 mapped reads (**Figure 2.1A**),

corresponding to between 0.004% - 35% of the number of reads at a given position (**Figure S2.1**). The observation that most deletions were specific to a single sample suggests *de novo* production within each tick, rather than accumulation over multiple transmission cycles between vector and host, as has been suggested for some mosquito-borne viruses.[144] Among all samples, the number of deletions ranged between 0 and 1,986 per 10^6 mapped reads, with a median of 119 deletions per 10^6 mapped reads (**Figure 2.1B**). There were a large number of deletions with a 5' recombination breakpoint junction (Junction 1, J1) in the envelope (E) coding region, as well as deletions with a 3' recombination breakpoint junction (Junction 2, J2) in the ns3 coding region (**Figure 2.1B**), suggesting that there could be junction enrichment in specific genomic regions.

Some specific deletions were observed across multiple samples. The most common included deletions in the methyltransferase (MTase) region of the ns5 RNA-dependent RNA-polymerase (RdRp) coding region; deletions spanning the viral protease (ns2a-ns3); small deletions in ns1; and deletions spanning the majority of the non-structural region between ns2A and ns5 (**Figure 2.1A**). Interestingly, a common deletion archetype previously described for flaviviruses–deletions spanning envelope (E) and ending at the beginning of ns1[120,145,146] were rare among these samples, with only one such deletion identified in one sample.

Deletions can result in autonomously functional SVs or D-RNAs, which require helper virus to replicate and/or transmit. To evaluate whether the deletions we observed might represent SVs or D-RNAs, we considered their size and coding frame preservation (**Figure 2.1C**). Over half of all deletions found in the POWV single open reading frame (ORF) resulted in a frameshift, suggesting they would result in D-RNAs (**Figure 2.1C**). A

further 23% of all deletions were over 500 nucleotides in length (**Figure 2.1C**), and would be expected to disrupt necessary viral proteins, also resulting in D-RNAs. On the other hand, 10% of all deletions observed were only 3 nucleotides in length, resulting in a single amino acid deletion (**Figure 2.1C**), which would largely be predicted to result in SVs. In addition to deletions, single nucleotide variants may occasionally result in D-RNAs if they result in an early stop codon. As this is a common type of D-RNA for other flaviviruses such as dengue virus, we analyzed intra-sample single nucleotide variants (iSNVs) in our samples and found 4 iSNVs that would result in a premature stop codon, out of 334 total iSNVs identified. The position of these did not seem to correspond to peaks in breakpoint junction usage and thus seem to occur more or less at random (**Figure S2.2**).

Common deletion archetypes occur in the ns2A-ns3 protease regions and in the methyltransferase domain of the ns5 RNA-dependent RNA-polymerase. Comparing POWV deletions positions between samples, we identified specific recombination patterns that were present in multiple ticks (**Figure 2.2**). One common archetype shared similar breakpoint junctions in the ns2A gene between nucleotides 3889-4259 (J1) and in the ns3 gene between nucleotides 5597-5793 (J2). Two specific deletions occurred frequently among samples with this archetype: one with J1^J2 junctions at 4020^5599 and the other with J1^J2 junctions at 4010^5597 (**Figure 2.2 top,** inset I). These two deletions were collectively present in almost 20% of all tick samples at frequencies between 0.0007-0.034 and also corresponded to a region of the genome that had overall higher deletion frequency (**Figure 2.2 bottom,** inset I). All deletions of this archetype (J1

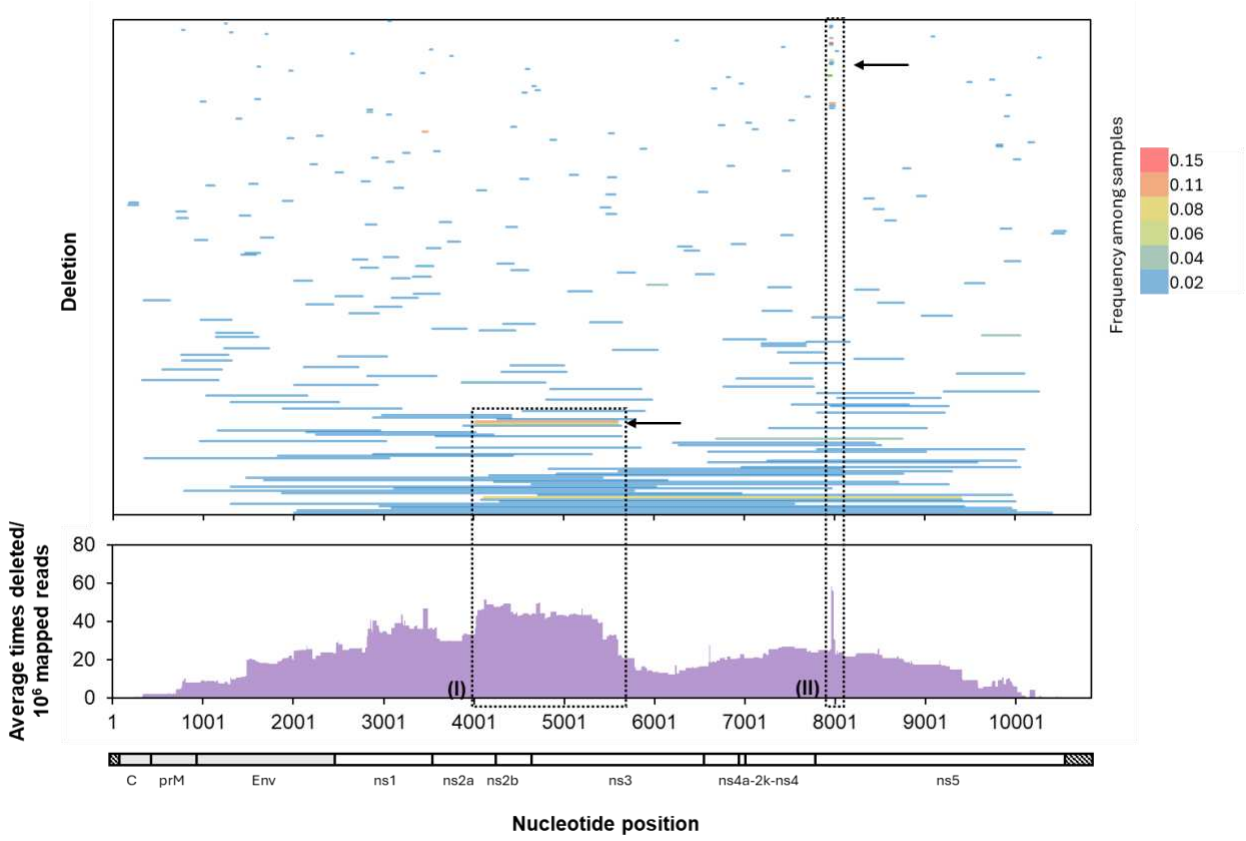

Figure 2.2. POWV deletion archetypes in naturally infected ticks correspond to peaks in cumulative nucleotide deletion. Individual deletions identified in naturally infected ticks were mapped and colored by frequency among 53 samples (**top**). For each nucleotide position, the number of times it was deleted in each sample was calculated and averaged across all 53 samples (**bottom**). **Inset (I)** highlights a peak in nucleotide deletion frequency across the ns2a-ns3 coding regions that corresponds to two highly represented deletion archetype with similar boundaries (arrow), and **inset (II)** highlights a peak in nucleotide deletion frequency driven by small deletions in the methyltransferase region of the ns5 coding region (arrow).

in ns2a and J2 in ns3) are expected to result in the partial removal of the ns3 viral protease as well as the complete removal of its viral cofactor ns2B, and are therefore referred to as “protease deletions” and are predicted to function as D-RNAs. However, the potential functions of these D-RNAs and their potential impact on viral replication have not been assessed.

The most common single deletion, which was identified in 15% of all samples, had J1^J2 nucleotide junctions at 7953^7981 in the methyltransferase (MTase) region of the

ns5 coding region (**Figure 2.2 top,** inset II), resulted in a 9 amino acid in-frame deletion, and occurred at frequencies between 0.002-0.08. In addition, we detected eleven other deletions with similar junctions, all with J1 between nucleotides 7932-7954 and J2 between nucleotides 7968-8004. Because they all occur in the same area of the MTase coding region, we refer to this deletion archetype as "MTase deletions." At least one MTase deletion between 19 and 50 bases in length was identified in over 30% of samples (**Figure 2.2 top**). These MTase deletions corresponded to a peak in overall deletion frequency across all samples (**Figure 2.2 bottom,** inset II). Interestingly, while five MTase deletions are predicted to result in an SV with an in-frame 9 amino acid deletion, including the most common MTase deletion with J1^J2 nucleotide junctions at 7953^7981, seven others result in 22-49 nucleotide frameshifts and therefore are predicted to result in D-RNAs. In-frame and frameshift deletions occurred at similar frequencies, between 0.0004-0.08 and 0.0003-0.07, respectively. The deletions occur in a region of the MTase domain that is believed to interact with the RNA-dependent polymerase (RDP) domain in a predicted model of the POWV RdRp (**Figure 2.3**). Deleting amino acids at the MTase-RDP interface in Japanese encephalitis virus (JEV) results in significantly decreased, though intact, replication[147], so it is possible that in-frame deletions here would have a similar impact.

POWV deletions occur at sites of microhomologies between nucleotide junctions. To assess the role of nucleotide sequence in POWV recombination, we evaluated the nucleotide composition and sequence identity at recombination junctions for deletions ≥100 bases in length (**Figure 2.4**). Smaller deletions were excluded in order to avoid biases from differential mechanisms regulating small, local deletions such as polymerase

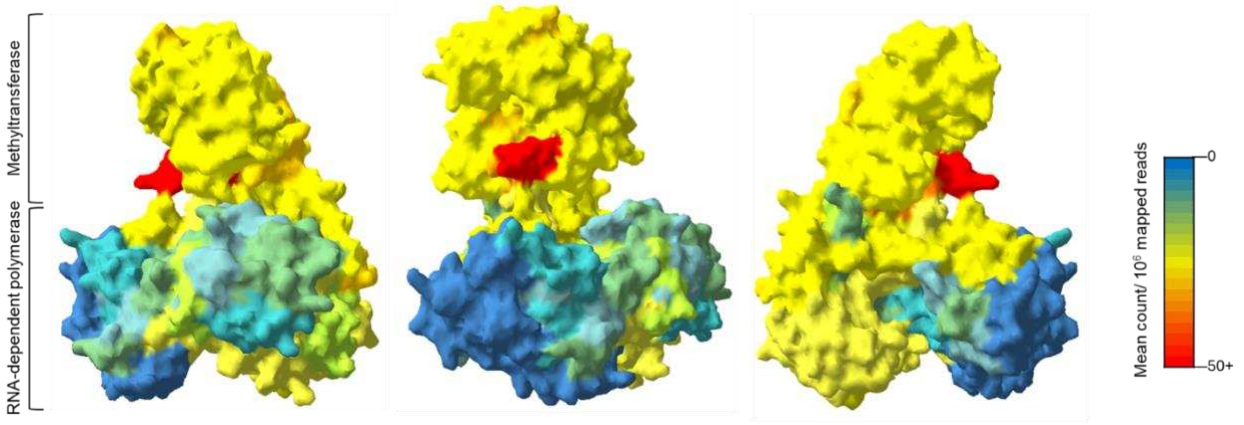

Figure 2.3. Frequency of amino acid deletion within the POWV ns5 RNA-Dependent RNA-polymerase (RdRp). The POWV ns5 RdRp protein was modeled based on the complete PDB structure for the Japanese encephalitis virus RdRp (PDB 4MTP; Lu G and Gong P 2013 *PLoS Path*) using the ExPasy/SWISS-MODEL tool (Schwede et al 2003 Nucleic Acids Res). Each amino acid was colored by the average number of times it was deleted across all 53 naturally infected ticks. Lysine108 is indicated as a reference point.

slippage. While a slight enrichment of uracils were observed immediately downstream of J1 (**Figure 2.4A, top**) and a slight enrichment of guanines were observed upstream of both junctions (**Figure 2.4A, bottom**), no specific nucleotide sequence or motif was associated with either junction. However, we found evidence for high nucleotide sequence identity between the 5 nucleotides upstream of J1 and the 5 nucleotides upstream of J2 in most deletions (**Figure 2.4B/C**). This suggests that microhomologies between breakpoint junctions play a role in template selection during POWV RNA recombination for many but not all deletions. This is consistent with previous studies, which found that dengue virus (DENV) deletions were frequently associated with small microhomologies.[148]

POWV protease deletions are enriched after one passage in tissue culture. Because tissue culture passaging has been reported to increase D-RNAs in other viruses[140], we compared deletions between viruses from 13 naturally infected ticks and

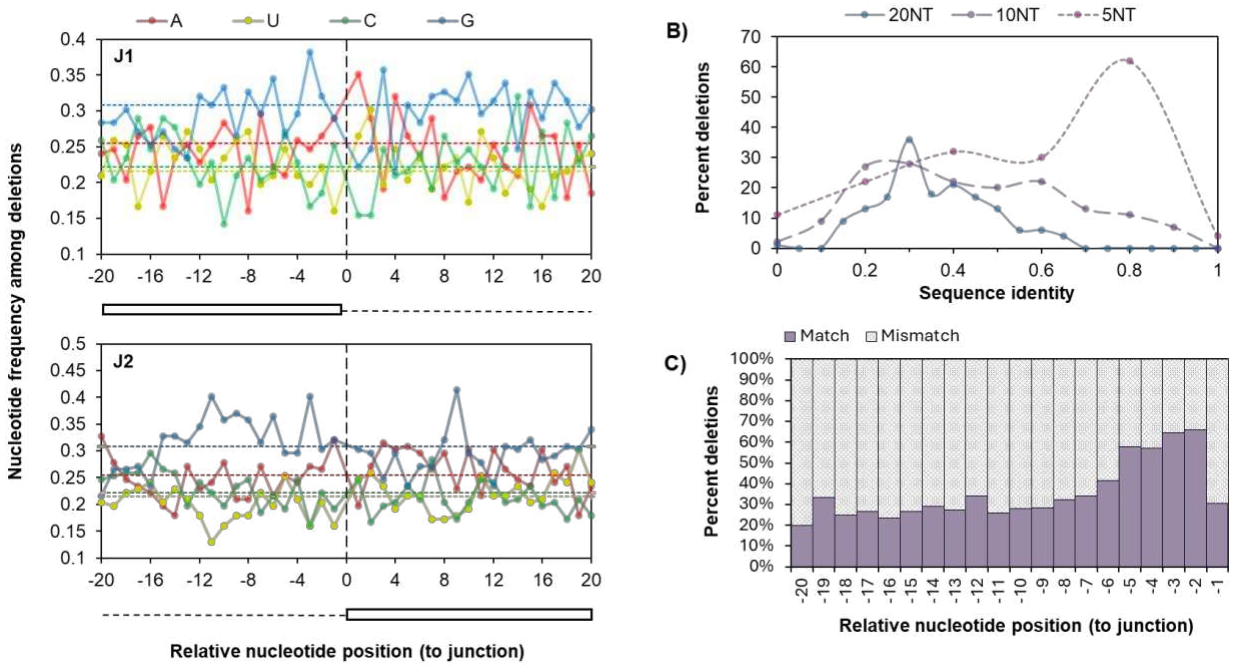

Figure 2.4. Sequence characteristics at recombination breakpoint junctions identified in naturally infected POWV ticks. A) The distribution of bases (solid lines) within 20 bases up- and -downstream of recombination junctions 1 (J1; top) and 2 (J2; bottom) compared to the relative distribution of each base across the POWV genome (dashed lines). **B)** Percent of deletions (Y-axis) with nucleotide sequence identities (X-axis) between junction 1 (the sequence observed upstream of J1 present in the read) and J2 (observed upstream of junction 2 present in the reference) within 5 (pink), 10 (purple), and 20 (blue) nucleotides of the recombination junction. **C)** Percent of deletions with a match (purple) or mismatch (grey) at each nucleotide position relative to the recombination junction.

their corresponding culture supernatants after one passage in baby hamster kidney (BHK) cells. We did not observe a statistically significant difference in the number of unique deletions (Wilcoxon rank test, p=0.064; **Figure 2.5A**) or the total number of deletions (Wilcoxon rank test, p=0.11; **Figure 2.5B**), though both tended to decrease after a single passage. Although there was no difference in expression of MTase deletions (Wilcoxon rank test, p=0.6; **Figure 2.5D**), there was a trend towards higher expression of protease deletions after passage (Paired-Sample Sign Test, p=0.077, **Figure 2.5E**). Sequencing depth was not correlated with normalized deletion counts

(Kendall test, tau=0.006, p=0.96; **Figure 2.5F**), so we do not expect this to be a confounding variable.

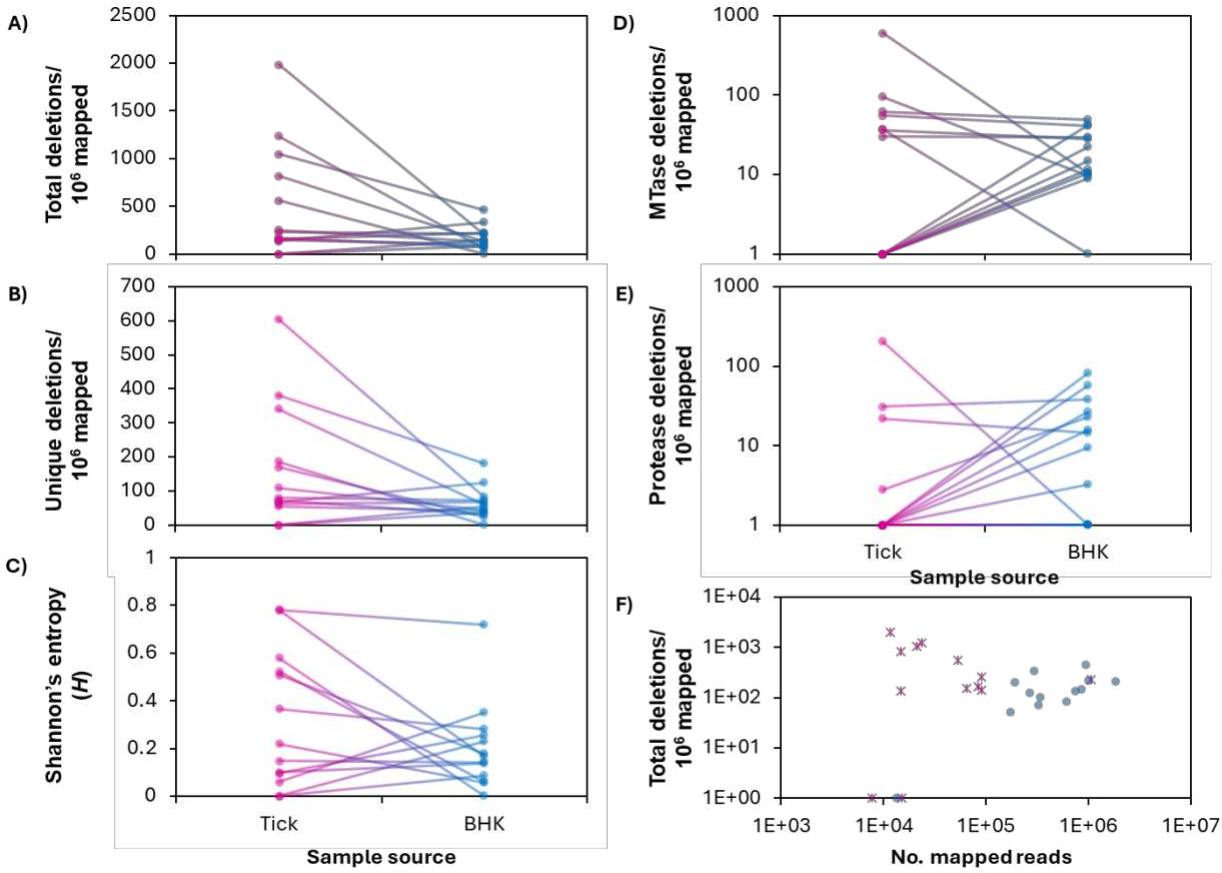

Figure 2.5. Comparison of POWV deletions between naturally infected ticks and single passage tissue culture supernatants. POWV RNA from 13 naturally infected ticks (**tick**) and RNA derived from the same virus after one passage in baby hamster kidney cells (**BHK**) was sequenced, and deletion content was determined by recombination mapping. **A)** Total number of deletions per million mapped reads; **B)** Number of unique deletion species per million mapped reads; **C)** Diversity of deletion species, as determined by Shanon's entropy (*H*); **D)** Total number of MTase deletions (small deletions between 19 and 50 bases in length between nucleotide positions 7932 and 8004) per million mapped reads; **E)** Total number of protease deletions (approximately 1600 base deletions occurring between the ns2a and ns3 genes) per million mapped reads. The total number of deletions per million mapped reads was also compared to the total number of reads per sample **(F**), and the two were not significantly correlated (Kendall test, tau=0.006, p=0.96)

To determine if specific deletions were differentially expressed between naturally infected ticks and single-passage isolates, differential gene (deletion) expression analysis

was performed in DESeq2 (**Figure 2.6**). Principal component analysis (PCA) revealed that 12/13 tick samples clustered closely together based on deletion expression, while 5/13 BHK samples clustered closely with tick samples and the remaining 8/13 BHK samples showed little to no clustering pattern (**Figure 2.6A**). Additionally, very few tick/BHK sample pairs clustered closely with one another. This suggests that, when excluding deletions specific to a single sample, tick samples are more similar to each other than they are to BHK samples. Hierarchical clustering analysis supported this result, with two naturally infected tick sample groups clustering closely together and multiple BHK groups clustering more distantly (**Figure 2.6B**). Finally, when evaluating differential expression of specific deletions, two deletions had higher expression in BHK cells than tick samples: an in-frame 1578 base deletion between nucleotides 4020 and 5599 (fold change=-2.8, padj=0.03; **Figure 2.6B** inset *, **Figure 2.6C** inset I) and a 1582 base frameshift deletion between nucleotides 4020 and 5603 (fold change=-3, padj=0.04; **Figure 2.6B** inset *, **Figure 2.6C** inset I). Both are protease deletions and are predicted to be D-RNAs. Three other deletions—two MTase deletions (**Figure 2.B** inset #, **Figure 2.6C** inset II) and one protease deletion (**Figure 2.6B** inset #, **Figure 2.6C** inset I)—were more highly expressed in BHK cells, though this difference was not statistically significant (-1<log2foldchange<-1.4; 0.05<p<0.38; **Figure 2.6C**). No specific deletions were significantly more highly expressed in tick samples than BHK samples.

ClickSeq confirms ns2A-ns3 deletions in POWV from tick samples. The above analyses used data from RNA metagenomic sequencing libraries, which were generated through random primer cDNA synthesis and Nextera XT tagmentation (Illumina). To assess the reliability of this technique for recombination detection, we made additional

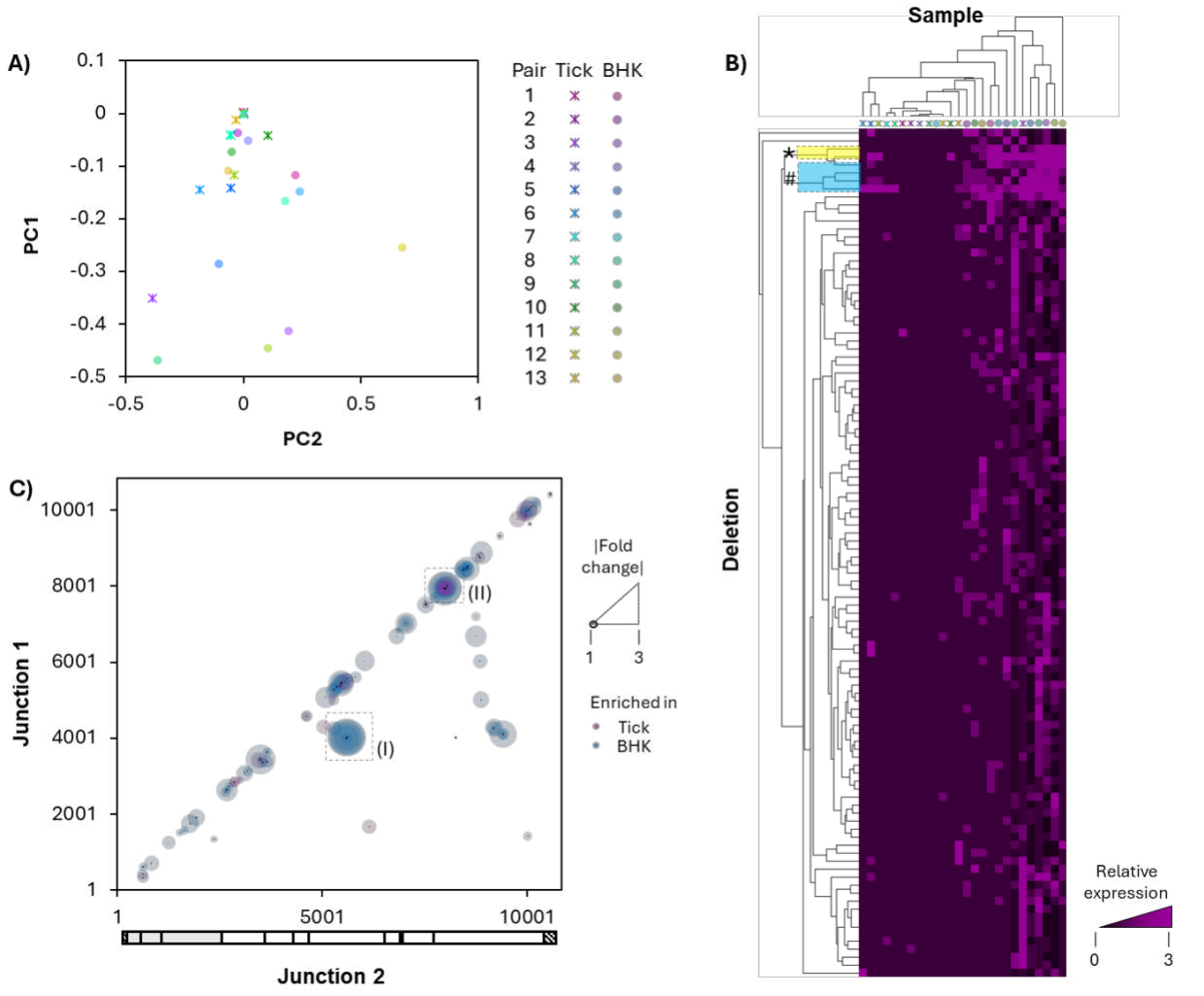

Figure 2.6. Differential expression of POWV deletions between 13 naturally infected ticks and the same virus after one passage in tissue culture. Differential gene expression of individual deletion species was evaluated using DESeq2 software. **A)** Principal component analysis (PCA) was performed, and eigenvalues for components 1 (Y-axis) and 2 (X-axis) were plotted for both tick (stars) and BHK (circles) samples and colored by tick/BHK sample pair. **B)** Hierarchical clustering was performed with clustering by sample (X-axis) and deletion (Y-axis). **C)** Each deletion species included in DESeq2 analysis was plotted by recombination junction (Junction 1, Y-axis; Junction 2, X-axis), colored by enrichment by compartment (pink, tick; blue, BHK), and sized by log2 fold change; inset (I) highlights protease deletions, while inset (II) highlights MTase deletions.

libraries from 16 of the samples (those with available RNA remaining) using ClickSeq, a library preparation method specifically designed to reduce artifactual recombination events.[12,149] Analysis of ClickSeq libraries confirmed the presence of ns2B-ns3 protease

deletions with J1 between nucleotides 3889-4259 and J2 between nucleotides 5597-5793, including the 4020^5599 deletion, the 4010^5597 deletion, and one other previously identified deletion, as well as 5 additional unique protease deletions (**Figure 2.7A-B**; insets A.I and B.I); these protease deletions occurred at frequencies between 0.0002-0.02.

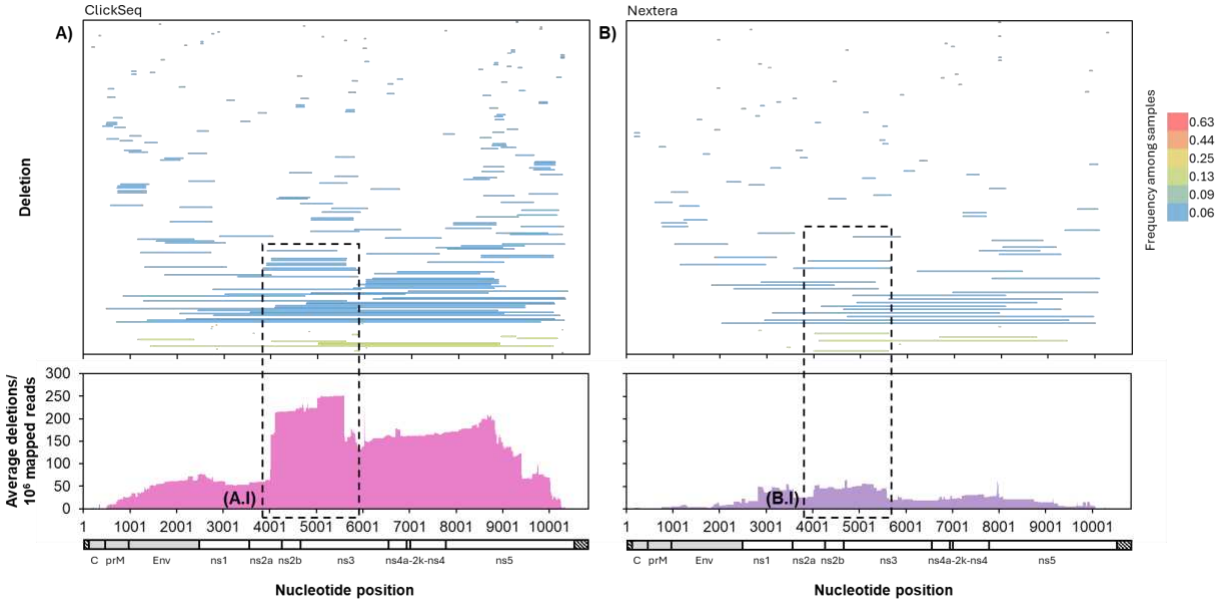

Figure 2.7. Comparison of POWV deletion expression using two different library preparation methods. POWV RNA from 16 naturally infected tick samples was sequenced using ClickSeq (**A**) and a metagenomic approach (**B**). Individual deletion species were mapped by genome position and colored by frequency across samples (**top**). For each nucleotide position, the number of times it was deleted in each sample was calculated and averaged across all 16 samples (**bottom**). Insets A.1. and B.1. indicate bases deleted by "protease deletions" with a junction 1 breakpoint position between nucleotides 3889-4259 and junction 2 breakpoint position between nucleotides 5597-5793.

We were not able to confirm the presence of MTase deletions because RNA was not available from the samples with high levels of MTase deletion expression, however 4 of the 16 samples that were analyzed using ClickSeq had MTase deletions at low levels (**Figure 2.7**).

2.3 Discussion

Deletions are common in RNA viruses and are thought to be the result of copy-choice non-homologous RNA recombination; they can result in D-RNAs, dysfunctional RNAs that can affect wild-type virus replication, as well as autonomously functional SVs. Despite the importance of characterizing deletions in RNA viruses, little work has been done to characterize intrahost recombinant RNAs of TBFVs, especially in the natural tick vector. Here, we found that POWV, a TBFV, produces frequent deletions with a range of sizes throughout the genome, leading to both putative D-RNAs and SVs. We found evidence for small 2-5 base homologies between recombination junctions, suggesting that microhomologies may impact template selection during recombination. Importantly, we found several deletion archetypes that were present in multiple samples, including deletions in the ns2-ns3 regions spanning the viral protease and its cofactors, as well as small deletions in the MTase region of the ns5 coding region. Deletion expression did not increase after a single passage in tissue culture and rather tended to decrease, except for protease deletions, which tended to increase after a single tissue culture passage. Finally, we validated the presence of deletions using a recombination-specific sequencing method. In all, we provide compelling evidence that POWV produces SVs and D-RNAs during replication in its natural tick vector, and that some deletions arise repeatedly across multiple samples.

While RNA virus recombination and deletions have been described in mammalian hosts, little work has been done to characterize recombinant populations in arthropods; still fewer studies have considered recombinant RNAs in tick hosts. Phylogenetic studies of tick-borne encephalitis virus (TBEV) and louping ill virus (LIV), both close relatives of

POWV, have indicated potential recombination events in the evolutionary history of these viruses[10,133,135,150], although it is not known in which host they may have occurred. Mosquito-borne flaviviruses have shown different proclivities for RNA recombination and deletion both *in vitro* and *in vivo*. D-RNAs consisting of deletions between the prM and ns1 genes have been described for WNV in lorikeets and JEV and Murray Valley fever virus in tissue culture, where they have been associated with inhibition of wild-type virus replication[120] and establishment of persistent infections.[145,146] Although the function of the POWV deletions identified in this study remains unclear, our identification of deletions in POWV from naturally infected ticks recommends further exploration of the role of recombination in TBFV evolution and pathogenesis.

We also show that POWV deletion archetypes arise independently in different tick samples. Prominent among these were deletions spanning the ns2A and ns3 regions, which would delete the viral protease and its cofactors and be predicted to function as D-RNAs. Our results additionally suggest that expression of protease deletions increases after one passage in mammalian cells. It is thus interesting to consider whether these POWV protease deletions may play a host-specific role during POWV replication or are simply by-products of processes critical to replication, such as RNA-RNA and/or protein-RNA interactions. For example, previous studies have shown that the TBFV protease triggers cellular antiviral responses through its interaction with human TRIM-5α for TBEV and Langat virus (LGTV), but not POWV.[151] While specific TRIM-family proteins and their functions are highly host- and virus-specific[152], it is possible that deleting this region may aid POWV in evading mammalian TRIM-mediated immunity. This recommends the

comparison of D-RNA populations between TBEV, LGTV, and POWV to determine potential roles for protease deletions during viral replication.

Our provisional results suggested that isolating POWV on BHK cells (i.e. a single passage from ticks to these cells) resulted in lower overall deletion content in isolated virus compared to virus in ticks. The current paradigm is that D-RNAs accumulate over high-multiplicity of infection (MOI) tissue culture passage. It is possible that a low MOI enriched the wild-type population in this case, but the MOI is unknown as whole tick homogenate was used for isolation in the absence of quantitative assessment of infectious titer. There are also several potential hypotheses for this result. The first is that tick homogenates include both intracellular and extracellular viruses, and the decrease in deletions in cell culture is driven by a lack of non-packaged virus in supernatant. Previous work with influenza virus[153] and multiple alphavirus species has shown that intracellular viral populations are more recombination-rich than extracellular populations in low-passage tissue culture experiments, as well as in a mouse-model of chikungunya virus infection.[126] Recombinant POWV populations may likewise be enriched intracellularly; this hypothesis can be explicitly tested experimentally by comparing intracellular and extracellular recombinant POWV RNA populations in similarly designed passaging studies or in carefully designed *in vivo* models of infection. Our group is currently conducting experiments in human and tick cell lines to understand the intracellular and extracellular RNA populations after multiple passages of POWV with a low MOI.

The second potential hypothesis for the observed overall enrichment of deletion expression in ticks, although less supported by current studies, is that POWV D-RNA expression may be associated with persistent replication in the tick vector. Ticks only take

bloodmeals preceding transitions from larval, nymphal, and adult life stages, necessitating persistent infection by TBFVs across life stages for effective transmission to a new host. TBEV has been shown to establish persistent infection in both ticks[141] and tick cells[154], with little evidence of significant genetic variation at the consensus level between parental virus and virus after up to 120 days persistence in *Ixodes* ticks. While previous work has not evaluated the relationship between D-RNA expression and persistence in tick hosts, persistence of LGTV in human embryonic kidney cell culture has been positively associated with the accumulation of defective particles.[132] Thus, D-RNA expression among POWV populations in ticks may be associated with persistent infection of the tick vector, either as a regulator of persistent infection or a byproduct thereof. Although speculative, this hypothesis could be expressly tested by characterizing D-RNA expression over the course of persistent POWV infection in laboratory-infected ticks.

The primary limitation of our study is the use of POWV sequencing data from prior studies not explicitly designed to detect recombination events. We therefore used ClickSeq, a library preparation method designed for accurate and specific detection of recombination, to validate our findings for a subset of samples with residual RNA available. To ensure a rigorous analysis, we only used data from samples that had a minimum average sequencing depth of 100X; above this threshold, we did not observe a relationship between higher sequencing depth and an improved ability to detect recombination. Further, deletions with only one read were removed in order to remove potential artifacts generated through either the library preparation process or the Illumina platform. An additional limitation is that our analyses were performed with short-read

sequencing data; further work is needed to evaluate whether the deletions we detected are present in full-length virus genomes, whether deletions can co-occur on the same RNA molecule, and whether they may be packaged and released as defective particles. Finally, the role and origin of small deletions such as single-amino acid deletions may differ from other deletions, and ultimately functional studies would be required to confirm their role in the viral population; these small deletions were included here for their potential impact on RNA function, particularly frameshift deletions that would result in defective transcripts, but small in-frame deletions may represent typical variance in the population.

In all, the data presented here offer foundational insight into recombination and deletion within POWV, with possible relevance to other TBFVs. Future studies are needed to understand the potential role of D-RNAs during infection and transmission in both *in vitro* and *in vivo* models of ticks and mammalian hosts. Through continued study of POWV recombination and deletion generation, we can gain further insights into evolution and pathogenesis.

2.4 Methods

Samples and metagenomic sequencing. RNA from POWV-positive tick homogenates and single-passage isolates underwent full POWV genome sequencing as part of previous studies.[57,140,155] Briefly, *Ixodes scapularis* ticks were collected between 2018 and 2020 from multiple survey sites in the Northeastern United States. Whole ticks were bead homogenized and screened for POWV as previously described.[140] For some samples, individual tick homogenate was placed onto a monolayer of BHK cells and supernatant was harvested at 50% cytopathic effect. RNA extracted from these samples

was sequenced using random primer cDNA synthesis followed by Nextera XT (Illumina) library preparation and Illumina sequencing. Recombination analysis was limited to data from samples with a minimum average sequencing depth of 100X across the POWV genome.

ClickSeq library preparation. Samples for ClickSeq were selected based on availability of residual total nucleic acid (TNA). TNA from tick homogenates was treated with DNase (ArcticZymes) according to manufacturer's instructions, and ClickSeq libraries were generated as previously described.[12,126] Briefly, RNA was primed with 1uL 100uM primer consisting of random hexamer and partial Illumina p7 adapter sequence, plus 1uL 1:35 azidoNTP: dNTP mix (ClickSeq Technologies), followed by first-strand synthesis with superscript III enzyme (Invitrogen). Template RNA was removed using RNase H (Invitrogen), first-strand cDNA was bead-purified (Ampure XP, Beckman Coulter), and the full p5 sequencing adapter with a 12 nucleotide unique molecular identifier was added to the first-strand cDNA via Click reaction. Click reaction proceeded at room temperature for two hours, with 2uL 5uM p5 oligo, "ClickMix" (ClickSeq Technologies), and ClickCatalyst (ClickSeq Technologies) prepped with 10mM vitamin C (Biotechne). "Clicked" cDNA was PCR amplified for a total of 21-24 cycles using OneTaq (New England Biolabs), a universal p5 primer, and an i7 indexing primer. Final libraries were run on a 2% agarose E-gel (Invitrogen) and gel-extracted from the 250-650bp range using the Zymo Gel DNA Recovery kit (Zymo Research). Libraries were quantified by QuantIt picogreen assay (Invitrogen), pooled, and sequenced on a NextSeq2000 (Illumina).

Bioinformatics and recombination analysis. Adapters were removed from reads by Illumina's BaseSpace software. Raw fastq files were processed using fastp version 0.23.2[156] to: 1) ensure complete adapter removal; 2) quality filter, deduplicate, filter reads less than 50 bases in length; and 3) merge overlapping reads and write non-overlapping reads to separate read1 and read2 files. For ClickSeq libraries, fastp was additionally utilized to trim and append UMI sequences to read names. Because paired-end sequencing was performed and recombination mapping tools were designed for single-end data, read names in overlapping read, non-overlapping read 1, and non-overlapping read 2 files were tagged with "/3","/1", and "/2", respectively, and all read files were concatenated into one fastq file for analysis. Reads from tick samples were first mapped to the *Ixodes scapularis* genome using hisat2 v 2.2.1[157] to remove tick reads. Then, for each sample, a sample-specific POWV consensus sequence was generated by mapping POWV reads to reference sequence HM440559.1 and using pilon[158] to generate a reference-based consensus sequence. POWV reads from each sample were aligned to the sample-specific consensus sequence, and recombination events were identified using ViReMa version 0.25.[159] Deletions were extracted from resulting BED files, and recombination breakpoint junctions were indexed to the HM440559.1 genome. To assess for any biases present in the mapping of ClickSeq reads, the length of each read split (5' end to recombination junction, and recombination junction to 3' end) were enumerated and compared; the distribution of read lengths between splits was similar (**Figure S2.3**). Single nucleotide variants were called by mapping reads to the pilon-generated consensus from the sample using bowtie2 with default local settings, followed by variant calling using LoFreq 2.1.5. Additionally, the relative read position of each variant was

determined using a pileup generated by bam-readcount, and variants with a relative read position less than 0.4 were removed from the final dataset. Variants were annotated using a custom annotator specific to each respective viral genome.

Protein modeling. The amino acid sequence of the POWV strain NFS001 (Genbank HM440559.1) nonstructural protein 5 was submitted to Expasy/SWISS-MODEL[160] to identify closely-matching amino acid sequences available in the Protein Data Bank (PDB) using the HHblits tool.[161] The structure for the Japanese encephalitis virus (JEV) ns5 was identified as a template (4K6M.1.A)[147], with 57% sequence identity and 99% sequence coverage. A model was subsequently built in ProMod3 v3.2.1[162] via SWISS-MODEL with a resulting QMGE score of 0.84 and a QMEANDisCo of 0.80±0.05. The molecular surface for the resulting model was calculated in Swiss PDB Viewer v4.1[160], and amino acids were colored by associated nucleotide deletion data.

Statistics. For analyses comparing total and unique deletions counts, deletions with only one read count were removed and raw counts were normalized to count/10^6 mapped reads. All statistical analyses were performed in RStudio version 2023.6.2.561 using R version 4.3.1. Normality was assessed using Q-Q plots in ggpubr version 0.6.0. The relationship between total read count and either Shannon's diversity index (H) or total deletion expression was assessed by Kendall correlation analysis. Analysis of variance for multiple groups was performed using the Kruskall-Wallis test, and paired sample analysis was performed using the Wilcoxon rank-sum test. For data that did not fit one or more assumptions of the Wilcoxon rank-sum test, a two-sided paired sample sign test was employed using the EnvStats package for R with mu=0 and confidence interval of 95%. Differential gene expression was assessed using DESeq2 v1.40.2[163]: for this, all

deletions were pooled across samples, and only deletions with at least two counts in at least two samples were included. Raw read counts were used for analysis, without normalization to total mapped reads as DESeq employs an internal normalization method. The program was run using paired data structure and a local regression fit. DESeq2 output was used to perform principal component analysis (PCA) using the prcomp() function and for hierarchical clustering analysis in Cluster 3.0[164]; clustering using average linkage is shown here, although all linkage algorithms resulted in highly similar results. Hierarchical clustering results were visualized in TreeView.

CHAPTER 3: IDENTIFYING POWASSAN VIRUS AMINO ACIDS THAT CONTRIBUTE TO DISEASE PHENOTYPES IN MICE

3.1 Introduction

Powassan virus (POWV, Flaviviridae, *Flavivirus*) is a tick-borne flavivirus that causes severe neuroinvasive disease in humans.[165] POWV is most frequently detected in the upper Midwest and Northeastern United States, Canada and the Russian Far East.[114] The virus is transmitted by Ixodid ticks that predominantly inhabit the Northeast and Midwest United States.[3] POWV is classified into two distinct lineages. Lineage I appears to mainly be associated with *Ixodes cookei* and *I. marxi*. Lineage II is mostly associated with *I. scapularis*, which frequently feed on humans.[166] POWV transmission in nature is highly focal, with genetically similar strains deriving from the same geographic region.[140] However, there is little understanding of how genetic diversity within POWV strains impacts transmission by ticks and disease outcomes in humans.

Following the bite of an infected tick, symptom onset often begins with flu-like illness including fever and vomiting. Ten percent of cases are fatal and neurologic sequelae persist in up to 50% of symptomatic cases. In severe cases, symptoms progress to encephalitis characterized by headaches, confusion, loss of coordination, and speech difficulties.[114] There is an urgent need to better understand this emerging tick-borne virus because the number of reported human cases has been increasing over the last 20 years.[111]

Mice are widely used to investigate POWV infection, where peripheral inoculation routes such as subcutaneous, intradermal, or footpad injections are designed to mimic natural tick-bite transmission. The virus replicates to high levels in the central nervous

system (CNS), leading to significant neuropathology and a high mortality rate in C57BL/6 mice.[26] In addition, there is evidence of virus accumulating in peripheral tissues such as the lymph nodes and spleen.[27] However, disease phenotypes within genetically diverse POWV lineage II strains, specifically, in mice have not been well studied. Notably, there is limited research on the viral determinants of POWV neuroinvasion and disease. POWV has a positive-sense RNA genome that encodes for three structural proteins (C, prM, E) and seven nonstructural proteins (NS1, NS2A, NS2B, NS3, NS4A, NS4B, NS5).[40] These proteins are important for viral entry into the cell, replication, assembly, and immune evasion, although there are very few studies investigating the role of these proteins in POWV pathogenesis.

This study aimed to understand the relationship between POWV lineage II virus genotype and disease phenotype using an established C57BL/6 mouse model. Several isolates from different geographical regions and a Midwest lineage II infectious clone-derived virus were selected to determine differences in morbidity and mortality in C57BL/6 mice. Two strains from New York had a higher rate of infection within spleen and brain tissues compared to mice infected with the infectious clone. These New York strains share three unique amino acid mutations in E, NS1, and NS5 proteins compared to the other isolates; however, when the mutations are engineered into an infectious clone, they only recapitulate the early neuroinvasion phenotype and not spleen tropism. Overall, our results demonstrate the complexity of genotypic differences impacting variation within POWV lineage II disease phenotypes in mice.

3.2 Results

Selected POWV lineage II strains. As previously demonstrated by our group, POWV lineage II strains group phylogenetically based on their geographic location (**Figure 3.1A**).[140] Lineage II strains were selected to represent the geographic range and genetic diversity within lineage II (**Figure 3.1B, Table 3.1**).

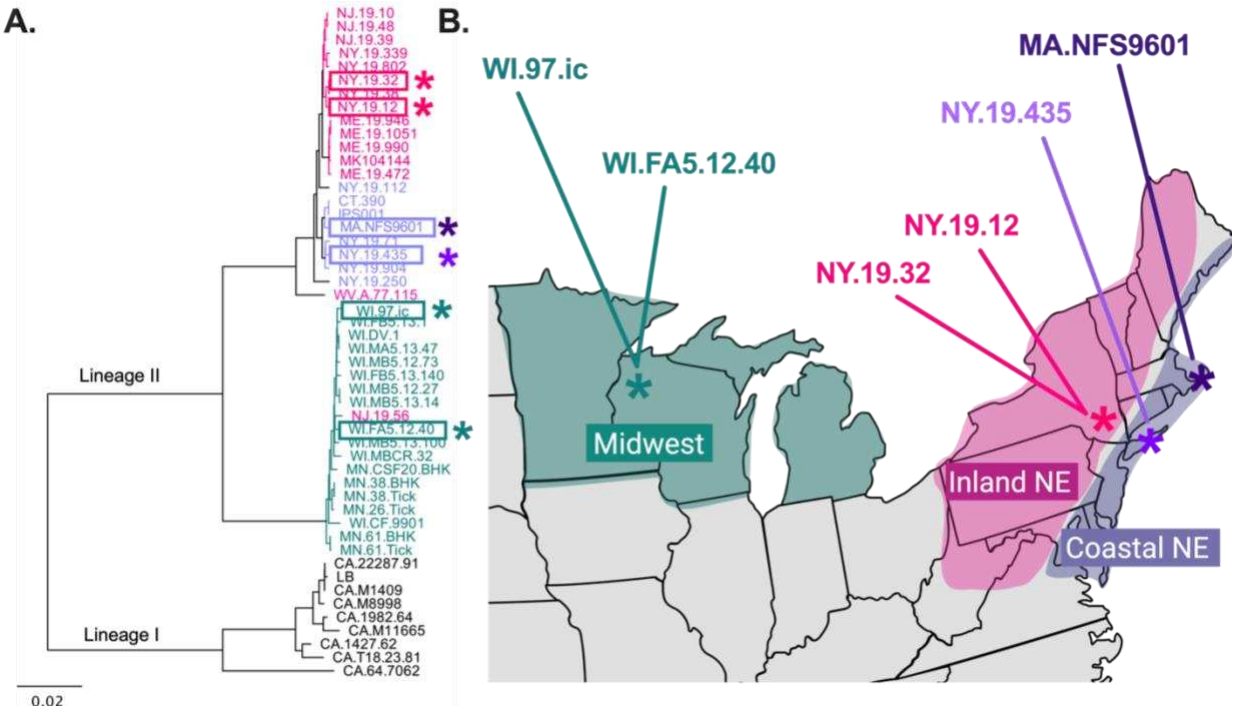

Figure 3.1. POWV lineage II strains selected based on geography. A) A rooted neighbor-joining phylogenetic tree of full genome amino acid sequences of POWV lineage I and II sequences generated in Geneious Prime ® 2023.0.1 (black = lineage I; purple = lineage II, coastal Northeast; pink = lineage II, inland Northeast; teal = lineage II, Midwest). Viruses used in subsequent studies are boxed. **B)** United States map showing location where each lineage II POWV strain was originally collected, color-coded as described in A (asterisks correspond to selected strains in the phylogenetic tree).

POWV morbidity and mortality in mice. Differences in morbidity and mortality in C57BL/6 mice using genetically diverse strains were assessed. Survival of mice infected with MA.NFS9601, NY.19.435, WI. FA5.12.40, or WI.97.ic ranged from 30-75% over 14 days (**Figure 3.2A**). Conversely, by seven days post-infection, 75% and 100%

of NY.19.32 and NY.19.12 infected mice, respectively, had succumbed to disease (**Figure 3.2A**).

Table 3.1. Selected POWV lineage II strain characteristics.

Strain	Location	Year	Origin	Passage History	Accession number
MA.NFS9601	Nantucket, MA	1996	*I. scapularis*	SM1B2	HM440559
NY.19.435	Connetquot, NY	2019	*I. scapularis*	B2	OP823469
WI.FA5.12.40	Spooner, WI	2008	*I. scapularis*	B2	OP823475
WI.97.ic	Spooner, WI	1997	*I. scapularis*	B3	OP823482*
NY.19.32	Saratoga Spa, NY	2019	*I. scapularis*	B2	OP823462
NY.19.12	Saratoga Spa, NY	2019	*I. scapularis*	B2	OP823461

SM = suckling mice, B = BHK cells, *WI.97.ic is a recombinant virus derived from this GenBank accession number sequence

Survival was significantly lower in NY.19.12 infected mice compared with WI.97.ic mice ($p<0.0001$). By day three post-infection, NY.19.12 and NY.19.32 infected mice displayed mild clinical signs, and by day seven post-infection, 78% had succumbed to disease, compared to only 22% of mice infected with other POWV strains (**Figure 3.2B**). By day six post-infection, all NY.19.12 infected mice were exhibiting signs of forelimb weakness (**Figure 3.2C**). Additionally, most NY.19.12 and NY.19.32 infected mice rapidly lost weight within seven days of infection (**Figure 3.2D**), whereas weight loss for other groups varied, with many mice recovering following initial weight loss (**Figure 3.2D**).

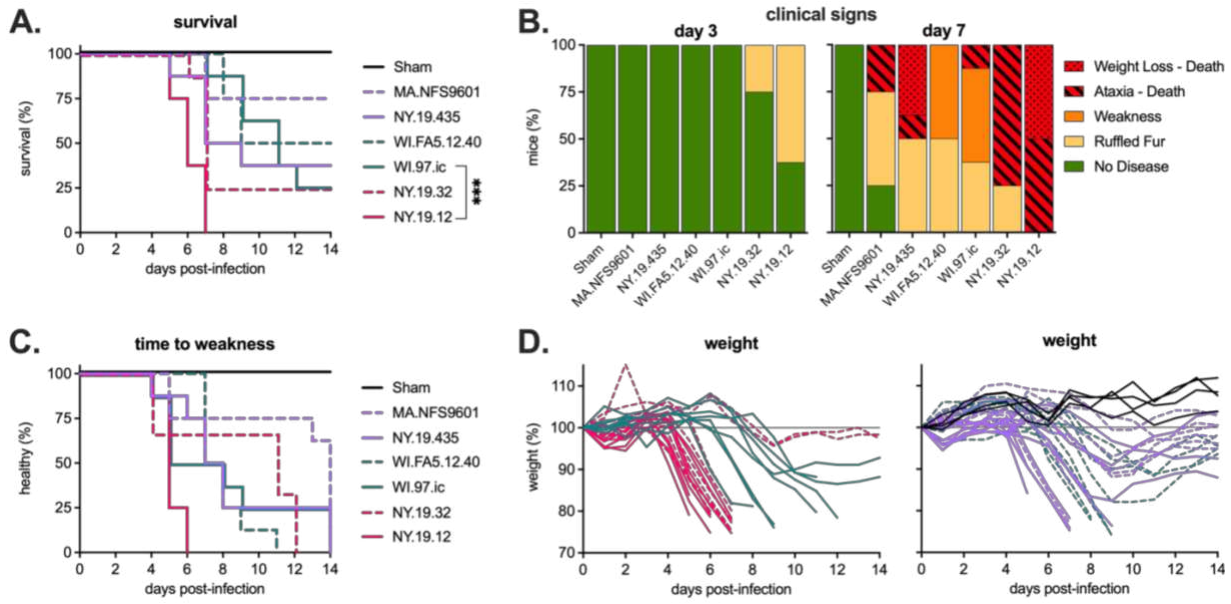

Figure 3.2. NY.19.12 and NY.19.32 cause increased morbidity and mortality in mice. Mice were infected with POWV (MA.NFS9601, NY.19.435, WI.FA5.12.40, WI.97.ic, NY.19.32, NY.19.12) or sham, and monitored daily for 14 days (n = 8 per strain). **A)** Kaplan-Meier survival curves. Survival of each virus was compared to WI.97.ic, with log-rank (Mantel-Cox) test, *** p<0.0001. **B)** Clinical signs on days 3 and 7 post-infection. **C)** The amount of time for mice to exhibit forelimb weakness. No comparisons between each virus and WI.97.ic was significant using log-rank (Mantel-Cox) test, p>0.05. **D)** Percent weight change from starting weight of NY.19.12, NY.19.32, and WI.97.ic infected mice, and MA.NFS9601, NY.19.435, WI.FA5.12.40, and sham infected mice.

Viral tissue tropism in mice. To determine POWV infection kinetics and tissue tropism for NY.19 isolates and WI.97.ic, infected C57BL/6 mice were sampled over ten days. For mice sacrificed between one to six days post-infection, there was no weight loss (**Figure 3.3A**). Of the remaining cohorts, at seven days post-infection, only NY.19.12 and NY.19.32 mice lost weight (**Figure 3.3A**), and 15% of those mice succumbed to disease, compared to WI.97.ic infected mice which only displayed mild to moderate clinical signs (**Figure 3.3B**). Viremia was detected more frequently in NY.19.12 and NY.19.32 infected mice compared to WI.97.ic, most notably between one

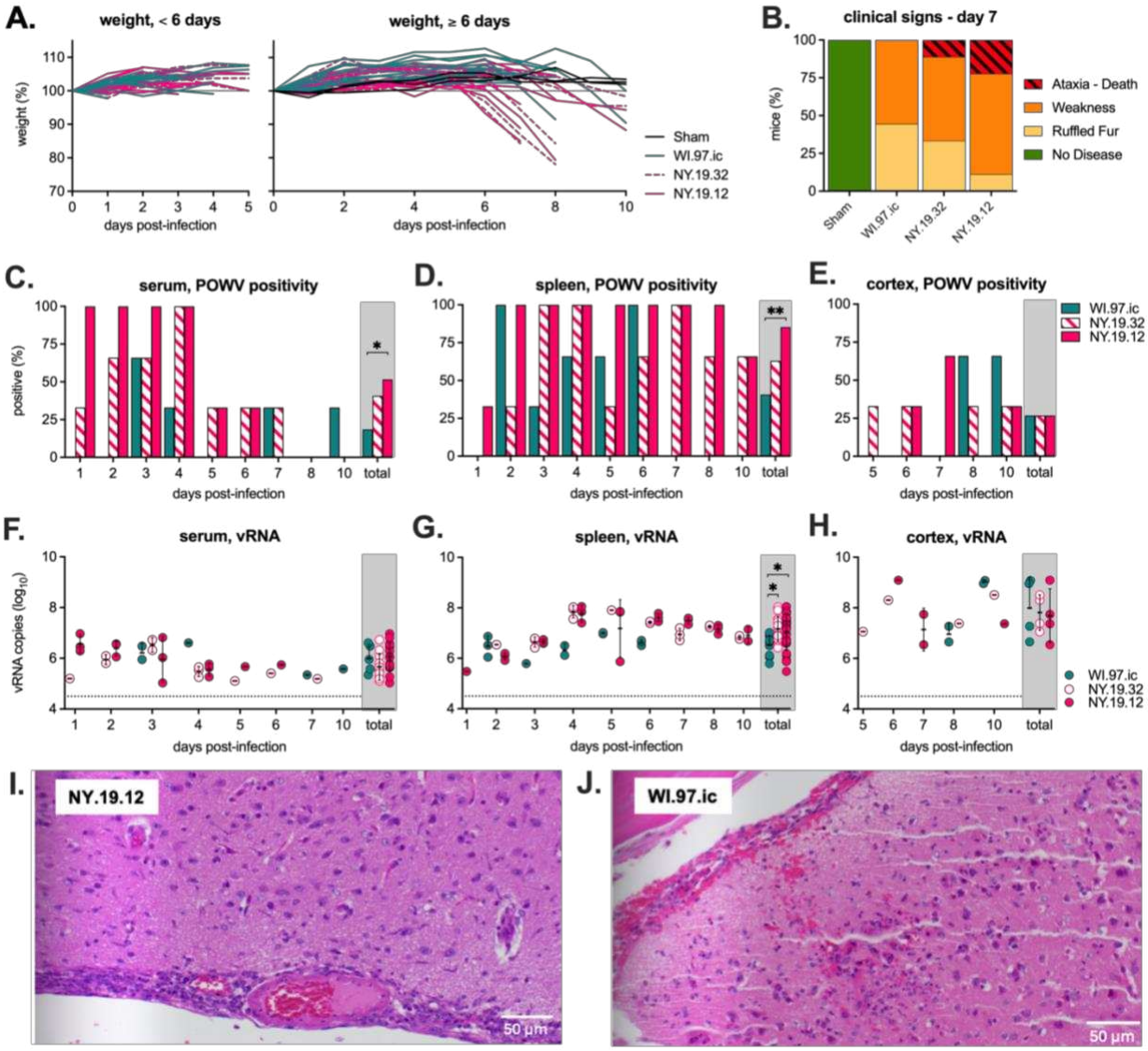

Figure 3.3. NY.19.12 and NY.19.32 mice succumb to disease earlier and have higher rates of tissue infection. Mice were infected with POWV (NY.19.12, NY.19.32, WI.97.ic) or sham, sacrificed, and sampled over a ten-day course of infection (n = 27 per infection cohort, 3 mice sacrificed per time point). **A)** Percent weight change from starting weight for mice sacrificed days 1 through 5 post-infection (n = 15) and those sacrificed post-day six (n = 12). **B)** Clinical signs seven days post-infection (n = 9). Positive POWV (%) **C)** serum, **D)** spleen and **E)** cortex per day and overall (Fisher's exact test, * $p<0.05$, ** $p<0.01$). vRNA copies per **F)** milliliter of serum, and gram of **G)** spleen, and **H)** cortex per day post-infection (mean ± standard deviation). The dotted line shows the limit of detection. For each sample type, one-way ANOVA Kruskal Wallis test on total samples (* $p<0.05$). Histopathology of **I)** NY.19.12 infected mouse brain and **J)** WI.97.ic infected mouse brain.

to four days post-infection, and significantly more frequently across all timepoints combined ($p<0.05$) (**Figure 3.3C**). In addition, NY.19.12 vRNA was detected significantly more frequently than WI.97.ic in spleens throughout the course of infection ($p<0.01$) (**Figure 3.3D**) and in the cortex at earlier time points (days five and six) compared to WI.97.ic (day eight) (**Figure 3.3E**). Despite lower rates of viremia and later rates of neuroinvasion in WI.97.ic infected mice, levels of vRNA were similar to NY.19.12 and NY.19.32 infected mice (**Figure 3.3F/H**). In the spleen, however, average vRNA was significantly higher in NY.19.12 and NY.19.32 infected mice compared to WI.97.ic ($p<0.05$) (**Figure 3.3G**). The brain (right half) from mice that succumbed to disease by day ten were compared using histopathology. Overall, lesions between viruses were similar, with lymphohistiocytic meningitis of the cerebrum with gliosis, neuronal degeneration, and necrosis in all infected brains (**Figure 3.3I/J)**.

Viral RNA in distinct brain regions. It has been demonstrated that POWV lineage I and other tick-borne flaviviruses infect distinct brain regions; however, this has not been well characterized for POWV lineage II.[59,64] A pilot study was conducted to determine any potential differences in viral distribution in the brain at six days post-infection (i.e., disease onset) between NY.19.12 and WI.97.ic by measuring virus in four distinct brain regions (olfactory bulbs, cortex, cerebellum, and brainstem) (**Figure 3.4A**). No mice succumbed to disease or lost weight by six days post-infection (**Figure 3.4B/C**). However, at day six post-infection 100% of NY.19.12 infected mice exhibited neurological signs (i.e., forelimb weakness), compared to 33% of WI.97.ic infected mice (**Figure 3.4D**), and NY.19.12-infected mice displayed weakness earlier than those infected with WI.97.ic (**Figure 3.4E)**. In all NY.19.12 and WI.97.ic infected mice, vRNA

was detected in the brainstem, cortex, and olfactory bulbs (**Figure 3.4F**), but NY.19.12 had higher rates of virus detection in the cerebellum and the spleen (**Figure 3.4F**). However, even in tissues where virus was detected at different rates (spleen, cerebellum), levels of vRNA within tissues were similar across strains (**Figure 3.4G**).

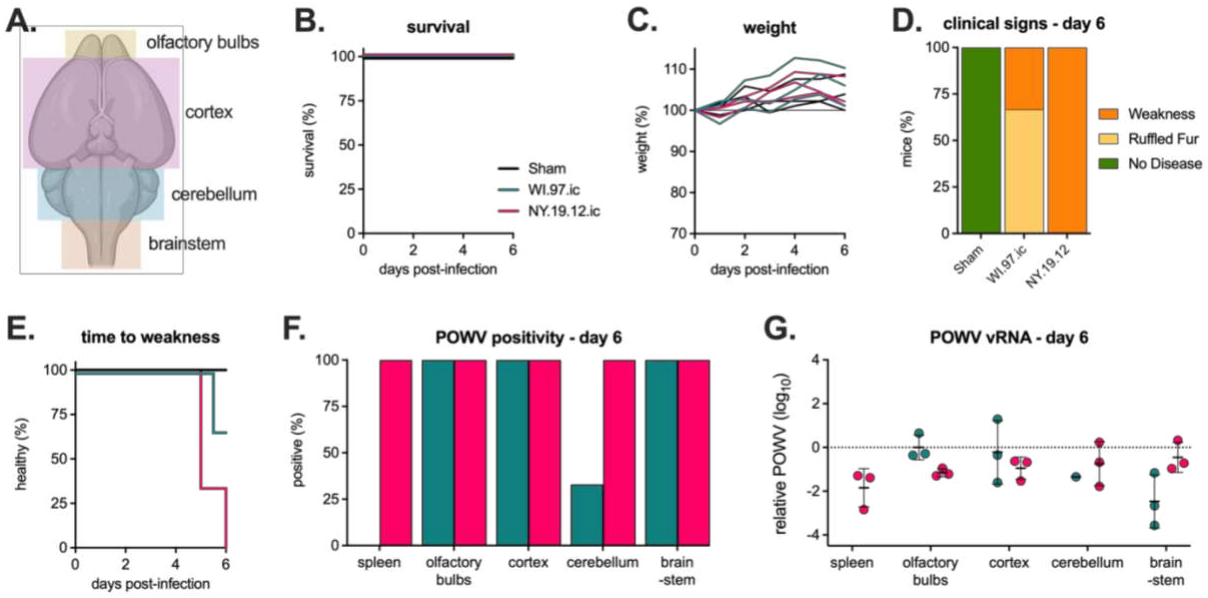

Figure 3.4. NY.19.12 infected mice display early neurological signs and vRNA appears more frequently in cerebellum and spleen. Mice were infected with POWV (NY.19.12, WI.97.ic) or sham and sacrificed at six days post infection (n = 3 per cohort). **A)** Brain regions that were harvested (olfactory bulbs, cortex, cerebellum, and brainstem). **B)** Kaplan-Meier survival curve. **C)** Percent weight change from starting weight. **D)** Clinical signs six days post-infection. **E)** The amount of time for mice to exhibit forelimb weakness. Comparison of WI.97.ic and NY.19.12 was not significant using log-rank (Mantel-Cox) test, $p>0.05$. **F)** Positive POWV (%) samples from spleen, olfactory bulbs, cortex, cerebellum, and brainstem (no significant differences by Fisher's exact test). **G)** Relative POWV RNA normalized to GAPDH and WI.97.ic olfactory bulbs, from spleen, olfactory bulbs, cortex, cerebellum, and brainstem. No significant differences within sample type by Mann Whitney t-test ($p>0.05$).

To further understand NY.19.12 neuropathology and immune cell involvement, mice were infected with NY.19.12 and sacrificed at day six post-infection, where half of each mouse brain was stained for POWV, NeuN (neurons), and GFAP (astrocytes) and imaged. There was colocalization of POWV with neuronal cells, which strongly suggests

that POWV specifically infects neurons (**Figure 3.5A**) compared to an uninfected mouse (**Figure 3.5B**). Conversely, there is minimal colocalization of POWV with astrocytes (**Figure 3.5C/D**).

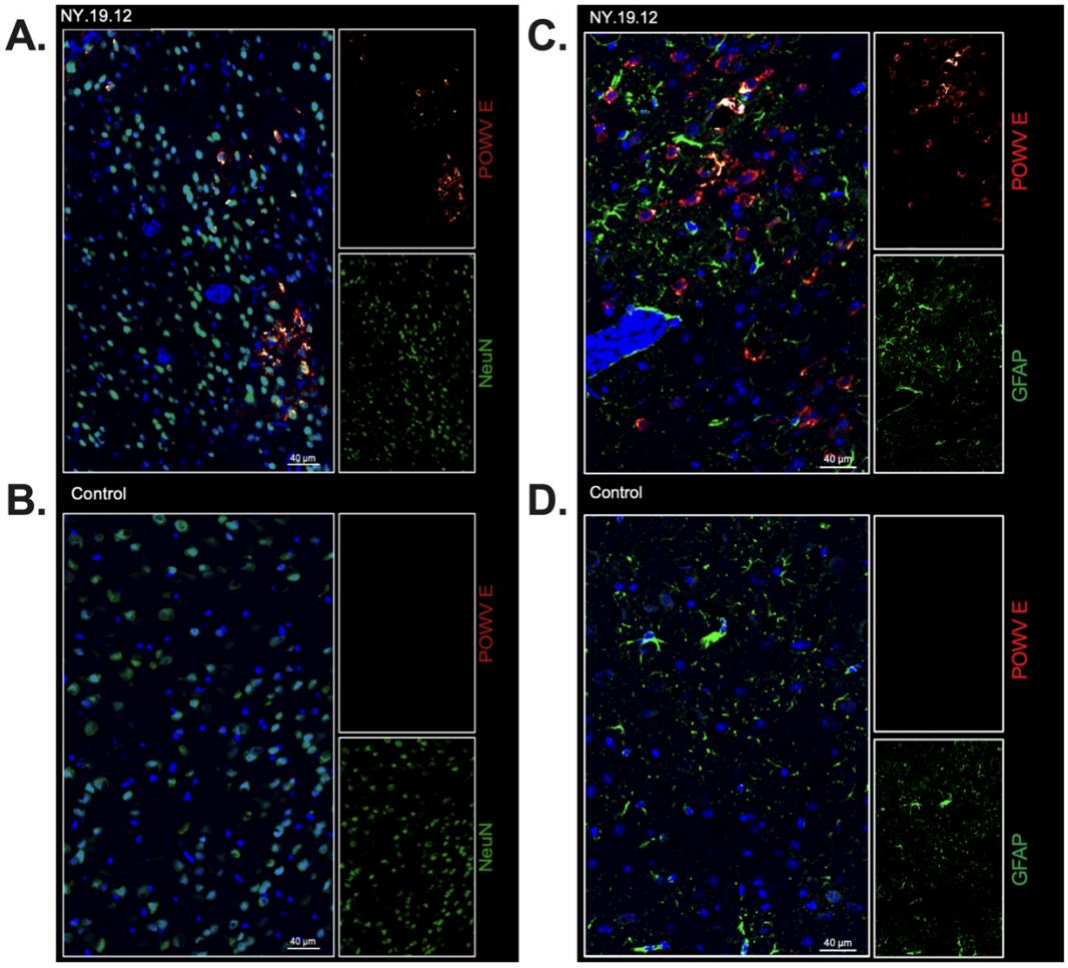

Figure 3.5. NY.19.12 specifically infects neurons with minimal astrocyte recruitment. Mice were infected with NY.19.12 and sacrificed at six days post infection, where infected brains were processed for IFA. Axial images of **A)** an NY.19.12 infected mouse brain with POWV in red and neurons (NeuN) in green, **B)** an uninfected control brain for NeuN, as well as **C)** astrocytes (GFAP) in green and **D)** an uninfected control brain for GFAP.

Genetic differences between strains. To identify genetic differences between virus strains, the amino acid sequences of all POWV strains used in the morbidity and mortality study were aligned (see **Table 3.1**). NY.19.12 and NY.19.32 share three unique

amino acid mutations in envelope, NS1 and NS5 (**Figure 3.6A**). These residues (env 205, NS1 178, NS5 649) were compared across 50 lineage I and lineage II POWV strains. The envelope and NS1 mutations were only detected in lineage II viruses, predominantly those from the inland Northeast (**Figure 3.6B**). While the NS5 mutation

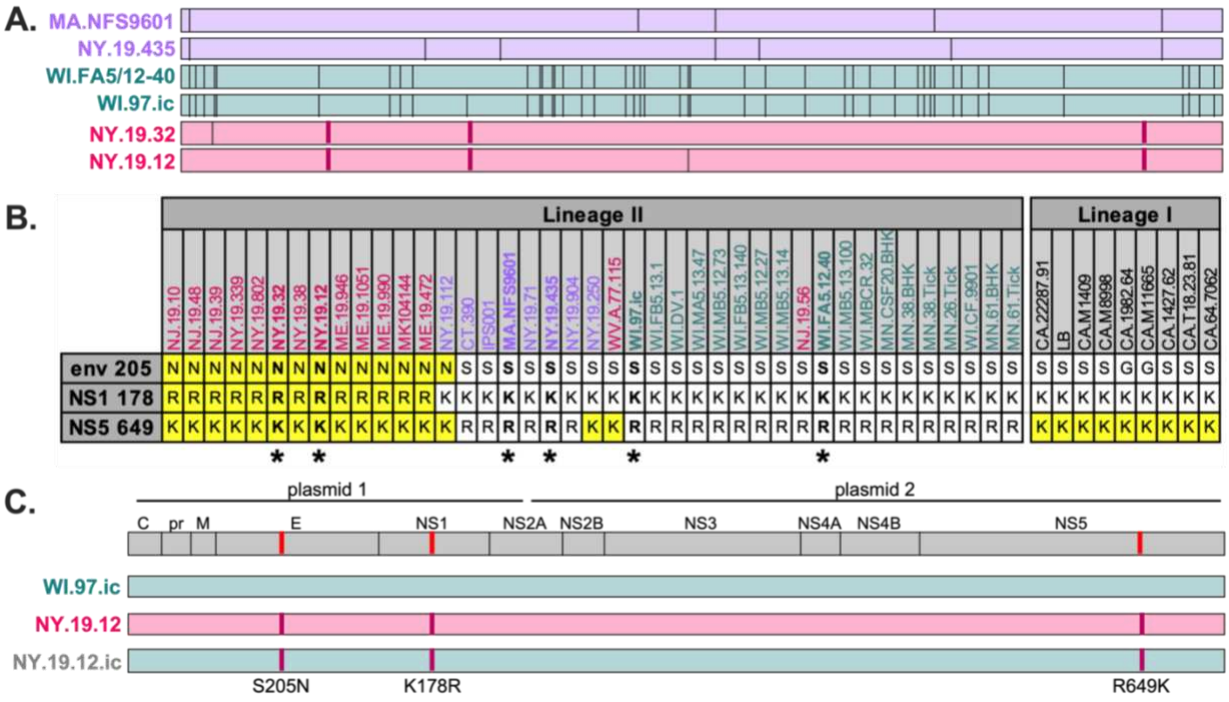

Figure 3.6. NY.19.32 and NY.19.12 share three amino acid mutations. A) Amino acid alignment of MA.NFS9601, NY.19.435, WI.FA5.12.40, WI.97.ic, NY.19.32, and NY.19.12. Amino acid differences between strains shown as lines. Three amino acids shared by NY.19.32 and NY.19.12 shown in dark pink. **B)** Amino acid residues at env-205, NS1-178, and NS5-649 among POWV lineage I and lineage II strains. Strains are ordered and colored based on the phylogenetic tree (see **Figure 3.1A**). Highlighted residues indicate the presence of the mutation (E-S205N, NS1-K178R, NS5-R649K). Strains labeled with * are viruses used in the morbidity and mortality study (see **Table 3.1**). **C)** E-S205N, NS1-K178R, NS5-R649K mutations were engineered into the WI.97.ic two-plasmid backbone, producing a new infectious clone (NY.19.12.ic).

was detected in those viruses, it was also detected in all lineage I strains. To determine if these mutations were maintained post-neuroinvasion, POWV was sequenced from cortex samples from WI.97.ic, NY.19.32, and NY.19.12 mice that had succumbed to disease (**Figure 3.3E/H**). All three mutations were maintained in NY.19.32 and NY.19.12

infected cortexes, and WI.97.ic did not gain the mutations post-neuroinvasion (**Table 3.2**). To investigate the role of these mutations, they were engineered into a WI.97.ic infectious clone backbone, designated NY.19.12.ic (**Figure 3.6C**).

Table 3.2. Sequence of POWV in cortex.

		env		NS1		NS5	
virus	**sample days**	**S205**	**N205**	**K178**	**R178**	**R649**	**K649**
WI.97.ic	8, 8, 10, 10	100% (4/4)	0% (0/4)	100% (4/4)	0% (0/4)	100% (4/4)	0% (0/4)
NY.19.32	5, 6, 10, 10	0% (0/4)	100% (4/4)	0% (0/4)	100% (4/4)	0% (0/4)	100% (4/4)
NY.19.12	6, 7, 10, 10	0% (0/4)	100% (4/4)	0% (0/4)	100% (4/4)	0% (0/4)	100% (4/4)

NY.19.12.ic intermediate disease phenotype. To further characterize vRNA in distinct brain regions and spleen at both early and late disease, NY.19.12.ic was designed to investigate the role of residues S205N, K178R, and R649K. Morbidity, mortality, and tissue tropism within the brain and spleen at six days post-infection and endpoint were assessed for NY.19.12.ic compared to NY.19.12 and WI.97.ic. Consistent with previous experiments, there was minimal weight loss by day six, but by day 12 post-infection, mice in all cohorts had either lost weight and succumbed to disease, or recovered (**Figure 3.7A**). There were no significant differences in survival between strains (**Figure 3.7B**), but at day four post-infection, ~70% of NY.19.12.ic and NY.19.12 infected mice displayed mild clinical signs, whereas over 80% of WI.97.ic-infected mice were still healthy (**Figure 3.7C**). By day six post-infection, there were higher levels of moderate disease in NY.19.12 and NY.19.12.ic infected mice (**Figure 3.7C**). Additionally,

there was significantly more forelimb weakness in NY.19.12 and NY.19.12.ic cohorts compared to WI.97.ic infected mice ($p<0.05$) (**Figure 3.7D**).

There were higher rates and average levels of vRNA in the blood at two days post-infection in NY.19.12 infected mice compared to both WI.97.ic and NY.19.12.ic (**Figure 3.7E/F).** By day six post-infection, vRNA was detected at comparable rates in the olfactory bulbs across strains. Interestingly, NY.19.12.ic displayed an intermediate infection phenotype between NY.19.12 and WI.97.ic, where there were trends of higher rates of infection in the cortex, cerebellum, and brainstem compared to WI.97.ic (**Figure 3.7G**). Levels of virus within each tissue were comparable across strains (**Figure 3.7H**). By endpoint, vRNA was detected at similar frequencies and levels in the olfactory bulbs, cortex, cerebellum, and brainstem samples across infection cohorts (**Figure 3.7I/J**). Notably, compared to both WI.97.ic and NY.19.12.ic, vRNA was detected at significantly higher frequencies ($p<0.01$) in the spleen of NY.19.12 infected mice at both day six and endpoint, and had significantly higher levels of vRNA by disease end point (**Figure 3.7G/I/J**). Infected mice brains were sliced and processed for immunofluorescence and stained for POWV (**Figure 3.8A-D**). Notably, NY.19.12 and NY.19.12.ic were both detected in the olfactory bulbs (**Figure 3.8F/G**), whereas WI.97.ic was not (**Figure 3.8H)**. In addition, NY.19.12 was detected in the somatosensory areas of the cortex (**Figure 3.8J**) compared to NY.19.12.ic and WI.97.ic (**Figure 3.8K/L**). All infection groups shared POWV distribution patterns in regions such as the fiber tracts around the pons compared to an uninfected control (**Figure 3.8M-P**).

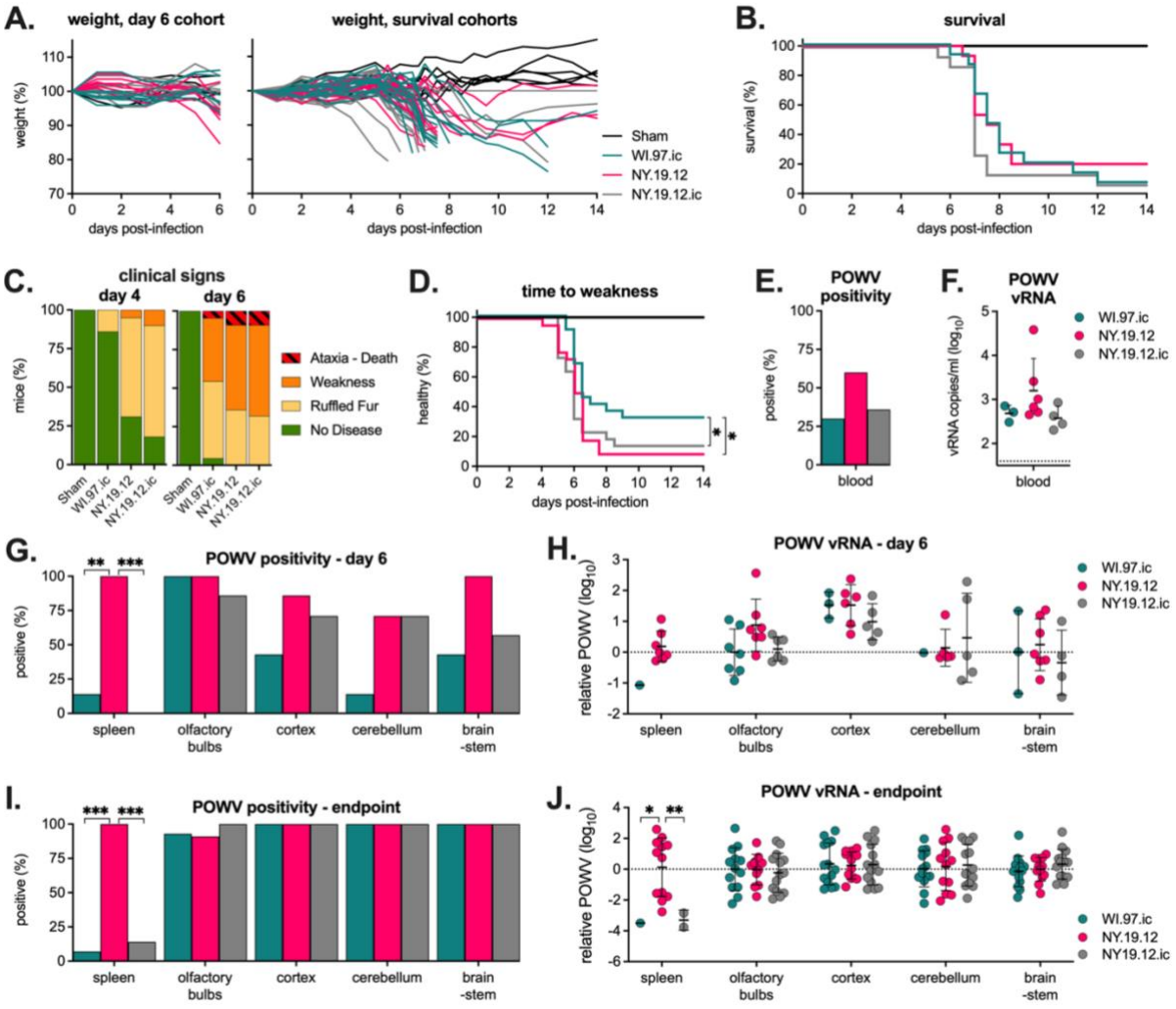

Figure 3.7. NY.19.12.ic infected mice display varying trends in disease progression and virus distribution in the brain at six days post-infection and at endpoint. Mice were infected with POWV (NY.19.12.ic, NY.19.12, and WI.97.ic) or sham and sacrificed at either day six post-infection (n = 7 per virus) or at endpoint (n = 15 total, two independent experiments, n = 8 and n = 7 per virus). **A)** Percent weight change from starting weight for day six cohort and endpoint cohorts. **B)** Kaplan-Meier survival curves for endpoint cohorts, no significant differences between viruses with log-rank (Mantel-Cox) test ($p>0.05$). **C)** Clinical signs four and six days post-infection for all cohorts combined (n = 22 per virus). **D)** The amount of time for mice to exhibit forelimb weakness. Viruses were compared using log-rank (Mantel-Cox) test, * $p<0.05$. **E)** POWV positive (%) blood samples and **F)** vRNA levels from day two post-infection (day six cohort, one endpoint cohort, n = 14 per virus). The dotted line shows the limit of detection. Positive POWV (%) of **G)** day six and **I)** endpoint cohort spleen, olfactory bulbs, cortex, cerebellum, and brainstem (Fisher's exact test, ** $p<0.01$, *** $p<0.001$). **H/J)** Relative POWV vRNA normalized to GAPDH and WI.97.ic olfactory bulbs, from spleen, olfactory bulbs, cortex, cerebellum, and brainstem for **H)** day six cohort and **J)** endpoint cohorts. Within each sample type, two-way ANOVA with Tukey's multiple comparisons test (* $p<0.05$, ** $p<0.01$).

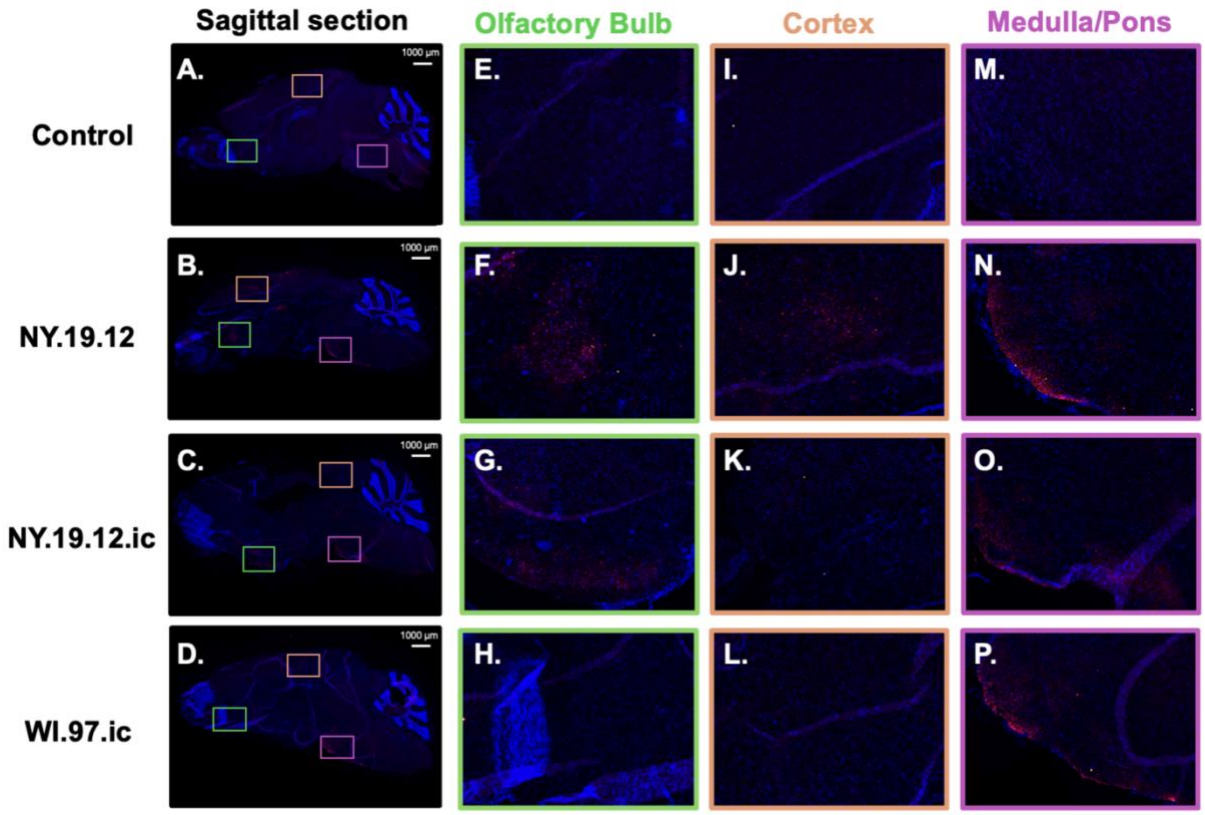

Figure 3.8. POWV viral distribution in the brain of NY.19.12, NY.19.12.ic, and WI.97.ic infected mice. Mice were infected with POWV (NY.19.12.ic, NY.19.12, and WI.97.ic) or sham and sacrificed at day six post-infection (n = 7 per virus). Brains were sliced sagittally and processed for IFA for A) an uninfected control mouse, B) a NY.19.12 infected mouse, C) a NY.19.12.ic infected mouse, and D) a WI.97.ic infected mouse with zoomed in images of **E-H)** the olfactory bulb region (green), **I-L)** the cortex region (orange), and **M-P)** the medulla and pons region (pink) for each.

3.3 Discussion

While it has been previously demonstrated that host genetics impact POWV pathogenesis in mouse models[33], this study investigated genotypic differences of several POWV lineage II strains from New York, Massachusetts, and Wisconsin to determine the role of viral genetics on disease outcomes. Between these strains, there are varying trends in morbidity, mortality, and presence of viral RNA (vRNA) in the blood, spleen and brain. These observations align with previous research on POWV

infection in mice, which typically results in severe neurological disease within 14 days of infection and persistence of virus in the spleen.[28] Our results underscore important differences in tissue infection and virus distribution in the brain within POWV lineage II strains in a mouse model.

The selected lineage II strains from the Northeast and Midwest U.S. showed variation in morbidity and mortality in mice. Although this has been documented among POWV lineage I strains and has been compared between lineages, this study provides robust evidence that POWV lineage II also causes a range of disease phenotypes in mice.[26–28,30] Our data suggests that, regardless of strain, 1) weight loss occurs once neurological disease onset begins and 2) C57BL/6 succumb to disease within 7-14 days but rates of survival vary greatly by strain. Histopathology of NY.19.12 and WI.97.ic mice that succumbed to disease showed similar neuroinflammation patterns in the brain. However, when comparing tissue infection and brain distribution, there are distinct differences between lineage II strains. NY.19.12 and NY.19.32 caused more severe disease (weight loss, clinical signs), earlier vRNA detection in the serum and brain, and persistent vRNA detection in the spleen throughout the course of infection compared to WI.97.ic. Additionally, NY.19.12 was detected in the cerebellum more frequently than WI.97.ic. These data demonstrate that there is variability in pathogenesis and neurotropism within lineage II strains. High-resolution IFA imaging revealed that NY.19.12 primarily targets neurons, with limited astrocyte recruitment. These findings are consistent with current POWV literature and contribute to the growing understanding of POWV infection within the CNS.[27,59,167]

Genetic analysis revealed three unique amino acid mutations shared by NY.19.12 and NY.19.32 in the envelope, NS1, and NS5 proteins. These mutations were also found in a subset of lineage II strains, indicating they likely provide some fitness advantage causing them to be maintained. Although genetically restricted infectious clone viruses are often attenuated relative to naturally isolated strains composed of genetically diverse quasispecies[168,169], they are an important tool allowing us to make direct genetic comparisons between mutants. In our study, the NY.19.12 infectious clone exhibited comparable early viral RNA levels in the cerebellum and disease onset as the natural isolate. Microscopy further showed similarities in neurotropism and viral distribution within the brain. However, some phenotypic differences were not fully recapitulated, suggesting that additional viral or host factors may influence pathogenesis.

Although there have been some studies characterizing POWV neuropathology and immune involvement in the CNS[167], the field remains relatively understudied, and the mechanisms underlying neurotropism and host immune response are not well defined. It is still unclear how the host response shapes viral distribution within the brain. Therefore, further high-resolution imaging of NY.19.12.ic in the brain is warranted to assess neuronal infection and astrocyte recruitment in comparison to NY.19.12. These studies will help elucidate the genetic determinants of cell type specific responses and viral tropism, drawing on insights from whole-brain imaging techniques used in other tick-borne flavivirus models, such as those by Anna Överby's group[64], to better define regional neuroinvasion and pathogenesis.

Interestingly, NY.19.12 infected the spleen at higher rates compared to both NY.19.12.ic and WI.97.ic, indicating something other than these three mutations contributes to this phenotype. Although spleen tropism in flaviviruses is not well understood, it was found that POWV lineage I infected C57BL/6 mice had prominent infection of splenic macrophages.[27] Similarly, studies on dengue virus have demonstrated the spleen can serve as a site for viral replication and contribute to disease severity.[170] Moreover, our group has shown that some Northeast and Midwest lineage II isolates have 100% infection of the spleen throughout early time points.[57] This indicates that enhanced spleen infection may not be unique to NY.19 strains. One explanation could be the absence of quasispecies diversity of infectious clone-derived virus–how this impacts spleen tropism is unclear; however, studies among tick-borne flaviviruses have shown that infectious clones often have weaker neurovirulence because they lack population diversity.[169,171] Other factors that may impact spleen tropism include single nucleotide polymorphisms within a strain or related strains, sfRNA production, or other mechanisms of immune evasion.[172–174] Nonetheless, more studies will need to be done to further understand the importance of the spleen in POWV infection.

While the impact of POWV single nucleotide polymorphisms (SNPs) on disease phenotypes remains largely unknown, recent studies have begun to elucidate the role of SNPs in flavivirus pathogenesis. In Japanese encephalitis virus (JEV), a single envelope amino acid change was linked to increased neurovirulence.[174] Research on tick-borne encephalitis virus (TBEV) found four amino acids in NS5 led to increased neurovirulence.[175] For many flaviviruses, glycosylation mutations in the envelope can

impact virulence and pathogenesis; however, env-205 is not associated with any glycosylation sites.[176] These studies suggest there are likely multiple genetic determinants that contribute to POWV disease and neuroinvasion. Importantly, non-coding genetic variants–such as those affecting regulatory regions, microRNAs, or splicing elements–may also play a critical role in modulating host susceptibility and viral pathogenesis.[177] Future studies incorporating transcriptomic and epigenomic analyses could help clarify these contributions. While our results indicate that SNPs may contribute to certain disease phenotypes, the mechanisms of POWV neuroinvasion remain poorly understood. Overall, this study provides valuable insights into the genetic factors that may impact POWV lineage II disease progression and tissue infection.

3.4 Methods

Cells and viruses. BHK-21 (ATCC CCL-10) and HEK293T (ATCC CRL-3216) cells were grown in DMEM supplemented with 10% fetal bovine serum (FBS), 10 units/mL penicillin, 10 µg/mL streptomycin at 37°C and 5% CO_2. Viruses (described in **Table 3.1**) were passaged on BHK cells, supernatant harvested 3-6 days post-infection, and frozen at -80°C prior to use. Virus inoculum for mouse studies was backtitered via plaque assays to validate virus concentration.

Plaque assays. Standard plaque assays were used to determine infectious virus concentrations. BHK cells were seeded one day prior to infection to be confluent the following day. Virus samples were thawed, serially diluted in infection media (standard growth media with 2% FBS), added to cells and incubated at room temperature for 1 hour on a plate rocker. Cells were overlaid with semi-solid 0.6% tragacanth media and

incubated at 37°C for five days. Cells were fixed and stained with 20% ethanol (EtOH) and 0.1% crystal violet. Plaques were counted manually to calculate titer.

POWV mouse infections. Female C57BL/6 mice (strain #000664) were obtained from Jackson Laboratories. Approval for animal protocols was obtained by the Colorado State University Institutional Animal Care and Use Committee (protocol #5074). All animal infections were conducted in Colorado State University ABSL-3 containment. 8-week-old female mice were inoculated subcutaneously (S.C.) with 10^3 PFU POWV in 100uL or sham infected with 100uL DMEM. Mice were weighed and clinical scores were recorded unblinded by the same individual throughout the course of the studies. Drastic weight loss was observed in the first mouse study (see **Figure 3.1**) due to food access - the pellets in the feeder are difficult to reach for the mice once clinical sign onset (ruffled fur, hunched posture) begins. For subsequent studies, food pellets were placed in the bottom of the cage once clinical sign onset was observed. Clinical scores were assigned following the criteria in **Table 3.3**. Euthanasia criteria were met at a clinical score of 3 or 20% weight loss.

Table 3.3. Clinical sign criteria for POWV infected mice

Clinical signs
Healthy
Hunched posture, ruffled fur
Forelimb weakness
Ataxia

Mouse necropsies and sample processing. Submandibular blood collection was performed with 4 mm lancets and blood was stored in BD Microtainer tubes with serum

separator additive (serum) or EDTA (whole blood). For necropsies, mice were euthanized via 5% isoflurane and cervical dislocation, and blood was collected via cardiac puncture. Cortex and spleens were harvested. For brain region analysis using immunofluorescence, mice were deeply anesthetized with 5% isoflurane and perfused with 30 mL of PBS then 30 mL of freshly prepared 4% paraformaldehyde, and brain regions were harvested. For brain region analysis via qRT-PCR, mice were deeply anesthetized with 5% isoflurane and perfused with 30 mL of PBS and brain regions were harvested. In the time course study (see **Figure 3.3**), samples were placed into 2 mL snap cap tubes with a metal bead, and 10% of each tissue weight was added in volume with DMEM and frozen at -80°C until homogenization. For subsequent studies, samples were placed into 2 mL snap cap tubes with 1 mL of 1X DMEM and a metal bead and frozen at -80°C until homogenization. Mouse tissues were rapidly thawed and homogenized at 30 Hz/s for 2 minutes, then centrifuged at maximum speed for 10 minutes to pellet cellular debris.

Nucleic acid extraction and qRT-PCR. Viral nucleic acid was extracted from 50 µL of serum, whole blood or homogenized mouse tissue using the Omega Viral DNA/RNA Extraction Kit on the KingFisher Flex instrument following manufacturer's instructions. Samples were either normalized for qRT-PCR via 10% weight/volume per sample before homogenization (see **Figure 3.3**) or to total RNA concentration and GAPDH level (see **Figure 3.4/6**). Quantitative real-time PCR (qRT-PCR) was performed using the EXPRESS One-Step qRT-PCR kit and POWV primer-probes targeting the NS5 coding region (blood, spleen, olfactory bulbs, cortex, cerebellum, brainstem), or EXPRESS One-Step SYBR GreenER Kit with mouse GAPDH primers (spleen, olfactory bulbs,

cortex, cerebellum, brainstem), in duplicate (**Table 3.4**).[178] Viral RNA copies were determined using a POWV RNA standard covering the NS5 gene as previously described (**Figure 3.3** and blood/serum samples) or normalized using the delta delta CT method (normalized to GAPDH and WI.97.ic olfactory bulbs) (**Figure 3.4/6**). Details provided in figure legends.

Table 3.4. Primer-probe sequences for qRT-PCR assays.

Primer	**sequence (5' ➔ 3')**
POWV forward	GGCCATGACAGACACAACA
POWV reverse	AGCCAGGCACCAGGGTGATCAT
POWV probe	CACATCCTCACCCTGGCTC (FAM)
Mouse GAPDH forward	TGTGTCCGTCGTGGATCTGA
Mouse GAPDH reverse	CCTGCTTCACCACCTTCTTGA

Sanger sequencing of mutations. vRNA was extracted as described above, and reverse transcription and PCR performed using QIAGEN OneStep RT-PCR Kit following manufacturer's protocol and primers to amplify regions containing each of the mutations (env, NS1 and NS5) (**Table 3.5**). PCR products were gel purified and cleaned up using MACHERRY-NAGEL NucleoSpin Gel and PCR Clean-up kit, then Sanger sequenced.

Table 3.5. **Primer sequences for Sanger sequencing.**

Primer	**sequence (5' ➔ 3')**
env forward	CTGCAAATGAGACCAATGAGAAC
env reverse	CTCCACAAGTTTCTCCACACT
NS1 forward	TTGTGGAGTGTGCCTGAAA
NS1 reverse	AGTGAGAATGAGCTCCTGAATG

NS5 forward	TGGAAGGTGAGGGAGTCAT
NS5 reverse	CCACATCCTTACGGGTCTTT

Generation of NY.19.12 infectious clone. The POWV lineage II two-plasmid cDNA infectious clone was obtained from Aaron Brault, CDC and was rescued and propagated as previously described.[60] Envelope and NS1 mutations were engineered into plasmid 1 via NEBuilder HiFi DNA Assembly Cloning Kit, and the NS5 mutation was engineered into plasmid 2 via NEB Q5® Site-Directed Mutagenesis Kit, using primers designed via NEBuilder Assembly Tool. NY.19.12 infectious clone (NY.19.12.ic) plasmids were transformed into Stbl3 *E. coli* and grown on ampicillin-treated agar plates at 37°C overnight. Individual colonies were isolated and grown overnight in liquid culture and isolated and purified via QIAprep Spin Miniprep Kit. Whole plasmids were sequence verified using Plasmidsaurus. Plasmids 1 and 2 were linearized with BstZ171 and ligated together at a 1:3 ratio with T4 DNA ligase. The ligated product was linearized with NotI, and RNA transcribed via mMESSAGE mMACHINE™ T7 Transcription Kit. Full-length NY.19.12.ic RNA was transfected into HEK293T cells using Lipofectamine 3000. Supernatant was collected at approximately 4-5 days post transfection once cells reached ~50% cytopathic effect. Viral stocks were passaged on BHK-21 cells, concentrated via centrifugation, and titered by plaque assay. Virus sequence at each mutation site (E, NS1, and NS5) was confirmed via Sanger sequencing as described above.

Histopathology. Mouse heads were incubated in nitric acid decalcifier for 24-48 hours. Skulls were cut into sagittal sections using size 60 scalpel blades. Sections were placed in tissue cassettes and sent to the Experimental Pathology Facility at the

Veterinary Diagnostic Laboratory to be embedded in paraffin blocks, cut into thin layers, placed on slides, and examined by a pathologist for inflammation patterns.

Immunofluorescence. The right hemisphere from brains of infected mice were dehydrated in 30% sucrose frozen in OCT Embedding matrix (VWR Chemicals, 361603E) and sectioned (sagittal and axial sections) at 10 µm thickness using CryoStar NX50 cryostat (Thermo Scientific, Waltham, MA, USA) according to manufacturer's instructions at -20°C. Slides were thawed at 37°C for 5 minutes, hydrated in PBS followed by permeabilization and blocking using PBS, 0.2% TritonX (VWR Chemicals, 28817.295), 10% goat serum (Nordic BioSite, CL1200-100) and 0.1% NaN3 (Thermo Fisher Scientific, 26628-22-8). Sections were stained with primary antibodies against POWV E protein (GeneTex, GTX640340, 1:1000), astrocyte marker GFAP (Abcam, ab4674, 1:500) and secondary antibodies donkey anti-rabbit A488 (Invitrogen, A21206, 1:500), donkey anti-rabbit A647 (Invitrogen, A31573, 1:500), DAPI (Sigma, 1:1000) and neuronal marker NeuN-A647 (Abcam ab190565, 1:200). Slides were mounted and imaged at 20x by Pannoramic 250 Flash III digital slide scanner (3DHISTECH Ltd., Budapest, Hungary) (sagittal sections) or Leica SP8 confocal microscope (axial sections). Images were created using Imaris software (version 10.1.1, Bitplane, Zürich, Switzerland).

Data analysis and statistics. All data were analyzed using GraphPad Prism Version 9.5.0. Statistical tests are described in figure legends. Sequences were analyzed in Geneious Prime ® 2023.0.1.

CHAPTER 4: UNDERSTANDING DISEASE CHARACTERISTICS IN C57BL/6 AND MAVS KNOCKOUT MICE FOR NEUROTROPIC FLAVIVIRUSES

4.1 Introduction

Neurotropic flaviviruses such as Powassan virus (POWV) and West Nile virus (WNV) and are significant public health threats due to their ability to invade the central nervous system (CNS) and cause severe neurologic diseases, including encephalitis and long-term neurological sequelae.[73,179,180] POWV, transmitted by ticks, includes two lineages with enzootic cycles in mammalian hosts with humans as dead-end hosts, whereas WNV is mosquito-borne and circulates in an enzootic cycle between mosquitoes and birds with humans and horses as dead-end hosts. Mouse models have been proven indispensable for investigating the pathogenesis of human infections, as they replicate key features of human disease such as age-related susceptibility[34], viral persistence in the CNS[32], and immune-mediated neuroinflammation.[35,69] These models enable controlled studies of viral transmission[50,57,] spread within the brain[26], and host immune responses[35,62,94] which are ultimately critical for informing vaccine development and therapeutic strategies.[29,31,36,61,62,99,100]

The route of viral inoculation can shape disease kinetics and tissue tropism. Peripheral inoculation routes such as subcutaneous (S.C.) or intraperitoneal (I.P.) mimic natural transmission and allow investigation of peripheral tissues and subsequent infection of the CNS. For example, S.C. inoculation of WNV leads to prolonged viral RNA detection in both the brain and spinal cord, highlighting the ability of the virus to persist and spread throughout the CNS.[181] POWV, similarly, demonstrates robust CNS invasion following peripheral inoculation[59], with enhanced disease severity and

persistence in older mice.[32] In contrast, intracranial (I.C.) inoculation bypasses the blood-brain barrier and permits direct assessment of viral replication and immune responses within the brain, thus causing a much faster disease progression.[30]

Histopathological analysis of POWV-infected mouse brains shows marked microglial activation, T-cell infiltration, and region-specific cytokine responses that correlate with clinical severity and age-related vulnerability.[27,32,72] Advanced imaging techniques have greatly enhanced our ability to map viral distribution and neuropathology. Whole-brain imaging enables three-dimensional visualization of viral spread across specific brain regions, where infected brains are imaged via optical projection tomography (OPT) coregistered to ex vivo MRI.[64,182,183] Such approaches have started to uncover the spatiotemporal dynamics of neuroinvasion and neuroinflammation that underlie flavivirus pathogenesis in mice.

Genetic knockout models allow for dissection of specific antiviral pathways in the context of flavivirus neuroinvasion. Mitochondrial antiviral-signaling protein (MAVS) is a signaling pathway critical for type I interferon (IFN-I) induction following viral RNA recognition.[184,185] Mice lacking MAVS exhibit impaired IFN-I responses, making them a valuable tool for probing the early host response to POWV and WNV infection.

In our studies, we investigated the role of MAVS and the IFN-I response during flavivirus infection and how it may shape the distribution of virus in the brain. We developed an ABSL-3 workflow using S.C., I.P., and I.C. inoculation routes in wildtype (C57BL/6) and MAVS knockout mice using POWV lineages I and II and WNV (**Table 4.1**). In addition, to explore whether a chimeric Kunjin virus (ChKUNV) could serve as a lower-containment model for WNV, we included it in our *in vivo* studies. ChKUNV,

designed by Anna Överby's group, is a chimeric virus comprising the WNV backbone and the premembrane and envelope genes from Kunjin virus, an attenuated WNV strain endemic to Australia.[179] For all studies, weight loss and survival were monitored to evaluate disease progression, and brain tissues were collected for imaging. IFA and whole-brain imaging will provide detailed maps of viral distribution in distinct brain regions and immune cell infiltration. Whole-brain images are still being processed and are not included in this report. Together, these models offer complementary insights into peripheral versus direct CNS infection routes, advancing our understanding of how neurotropic flaviviruses invade, persist, and cause neurologic disease and the subsequent host innate immune response.

Table 4.1 Overview of mouse studies.

Study Date	Mouse Strain	Mouse Sex	Virus Strain	Dose (PFU)	Route	Timepoint
25-Mar-24	C57BL/6	Female	POWV NY.19.12, POWV WI.97.ic	10^3	S.C.	6 dpi
25-Mar-24	C57BL/6	Female	POWV NY.19.12	10^4	S.C.	Endpoint
24-Apr-24	MAVS knockout and C57BL/6	Males and females	POWV M11665	10^3	S.C.	Endpoint
1-May-24	MAVS knockout and C57BL/6	Males and females	POWV NY.19.12	10^3	S.C.	Endpoint
31-May-24	C57BL/6	Females	POWV NY.19.12	10^3	I.C.	Endpoint
23-May-24	C57BL/6	Females	WNV NY99, ChKUNV	10^4, 10^5	S.C	Endpoint
24-May-24	C57BL/6	Females	WNV NY99, ChKUNV	10^3, 10^4	I.C.	Endpoint
14-Jun-24	MAVS knockout	Males and females	WNV, ChKUNV	10^5	I.P.	Endpoint
14-Jun-24	MAVS knockout	Female	POWV NY.19.12	10^3	S.C.	Endpoint

15-Jan-25	C57BL/6	Females	POWV NY.19.12.ic, NY.19.12, WI.97.ic	10^3	S.C.	6 dpi, endpoint

ChKUNV, chimeric Kunjin virus; dpi, days post-infection; I.C., intracranial; I.P., intraperitoneal; MAVS, mitochondrial antiviral-signaling protein; PFU, plaque forming units; S.C., subcutaneous; WNV, West Nile virus

4.2 Results

POWV lineage II subcutaneous infection in C57BL/6 mice. To investigate differences in pathogenesis within POWV lineage II viruses and establish a streamlined ABSL-3 workflow for future studies, female C57BL/6 mice were S.C. inoculated with 10^3 PFU of NY.19.12 or WI.97.ic, two POWV lineage II isolates (n=3 per virus). Mice were sacrificed and brain tissues were harvested to determine any potential differences in viral distribution in the brain at six days post-infection (dpi) (i.e., disease onset) by measuring virus in four distinct brain regions (olfactory bulbs, cortex, cerebellum, and brainstem) (**Figure 4.1A**). No mice succumbed to disease or lost weight by six dpi (**Figure 4.1B/C**). However, at day six post-infection 100% of NY.19.12 infected mice exhibited neurological signs (i.e., forelimb weakness), compared to 33% of WI.97.ic infected mice (**Figure 4.1D**), and NY.19.12-infected mice displayed weakness earlier than those infected with WI.97.ic (**Figure 4.1E**). A subsequent study with female mice S.C. inoculated with 10^4 PFU of POWV NY.19.12 was performed to validate and optimize a perfusion protocol by incubating infected mouse brains in paraformaldehyde for either 24 or 96 hours. It was determined that incubating the brain for 24 hours in PFA was sufficient to inactivate infectious virus (data not shown), and an SOP was written and submitted to the CSU biosafety officer.

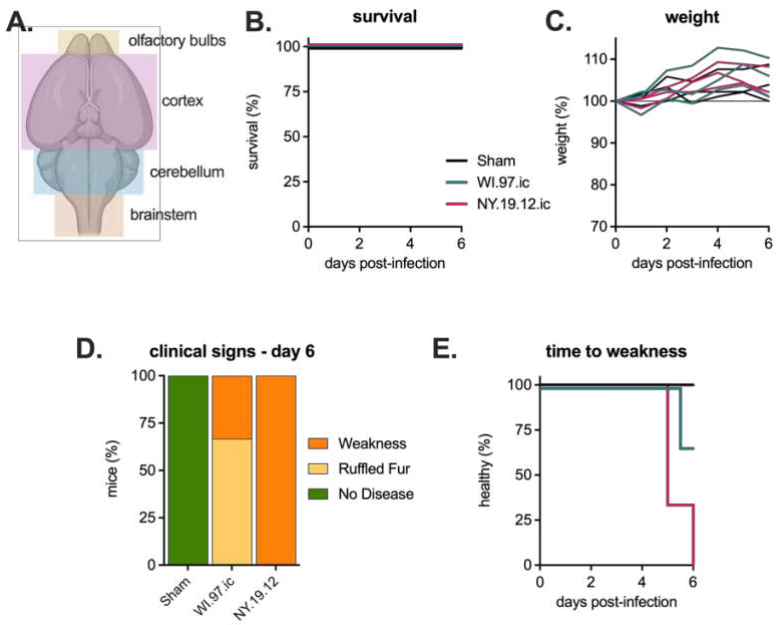

Figure 4.1. POWV lineage II survival in C57BL/6 mice. Mice were S.C. inoculated with 10^3 PFU POWV (NY.19.12, WI.97.ic) or sham and sacrificed at six days post infection (n = 3 per cohort). **A)** Brain regions that were harvested (olfactory bulbs, cortex, cerebellum, and brainstem). **B)** Kaplan-Meier survival curve. **C)** Percent weight change from starting weight. **D)** Clinical signs six days post-infection. **E)** The amount of time for mice to exhibit forelimb weakness. Comparison of WI.97.ic and NY.19.12 was not significant using log-rank (Mantel-Cox) test, $p>0.05$.

POWV lineage I and II subcutaneous infection in MAVS knockout mice. MAVS is a key adaptor in IFN-I response to flaviviruses.[185] POWV M11665, a lineage I strain, was used to assess the role of MAVS-mediated immunity in POWV neurotropism. Male and female MAVS knockout and wildtype C57BL/6 mice were S.C. inoculated with 10^3 PFU of POWV M11665 (n=8 per virus) and weight loss and survival were recorded daily. For all studies, mice were sacrificed when the first mouse from each mouse strain (MAVS, C57BL/6) succumbed to disease. Therefore, all mice were sacrificed at five dpi. By five dpi, 50% of the MAVS knockout mice had succumbed to infection, whereas only 12% of wildtype mice had succumbed to disease (**Figure 4.2A**).

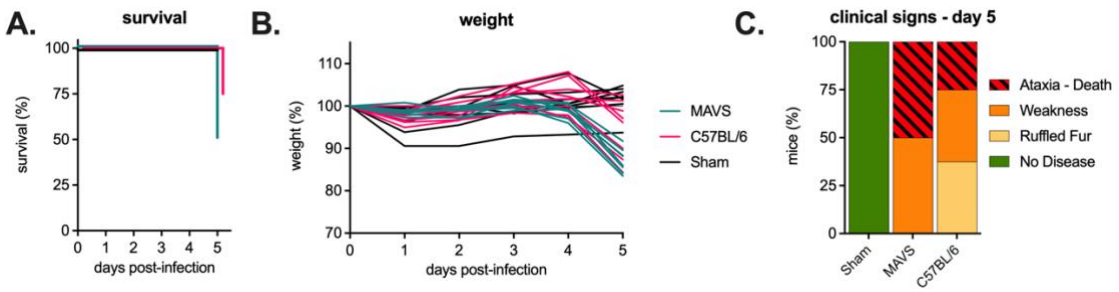

Figure 4.2. POWV lineage I survival in MAVS knockout and C57BL/6 mice. MAVS knockout and wildtype C57BL/6 mice were S.C. inoculated with 10^3 PFU of POWV M11665 or sham (n=8 per virus, 4 males and 4 females) and sacrificed when the first mouse from each strain succumbed to disease. **A)** Kaplan-Meier survival curve. **B)** Percent weight change from starting weight. **C)** Clinical signs five days post-infection.

MAVS knockout mice had also lost ~10% of their weight, whereas only half of infected wildtype mice had lost 10% of their weight (**Figure 4.2B**). Of MAVS knockout mice that did not succumb to disease by five dpi, all displayed moderate clinical signs of weakness, whereas 25% of wildtype mice had succumbed to disease, 37.5% of mice displayed moderate clinical signs, and 37.5% of mice displayed mild clinical signs of ruffled fur (**Figure 4.2C**).

To investigate any lineage specific differences, MAVS knockout and wildtype C57BL/6 mice were S.C. inoculated with 10^3 PFU of POWV NY.19.12, a lineage II POWV strain (n=8, males and females). Mice were sacrificed at six dpi. By six dpi, MAVS knockout mice had lost ~10% of their starting weight and all had displayed moderate clinical signs of weakness, whereas wildtype mice had not lost weight and displayed mild clinical signs (**Figure 4.3A/B**). Comparing lineage I and lineage II in MAVS knockout mice (**Figures 4.2/3**), lineage I caused a slightly faster rate of disease progression by five dpi compared to lineage II, where mice only displayed moderate

clinical signs by six dpi. This aligns with previous studies where lineage I and II have varying clinical presentation and patterns of infection in the CNS.[59]

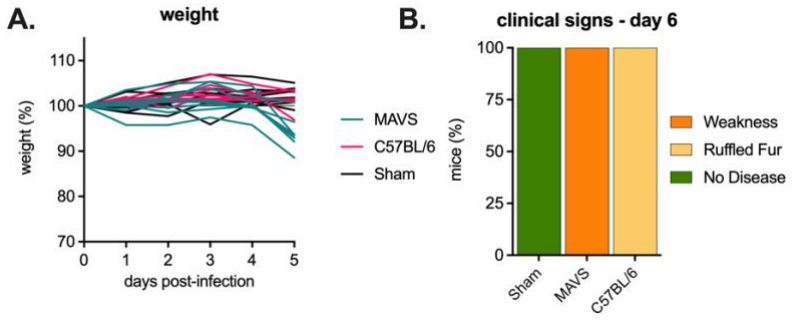

Figure 4.3. POWV lineage II survival in MAVS knockout and C57BL/6 mice. MAVS knockout and wildtype C57BL/6 mice were S.C. inoculated with 10^3 PFU of POWV NY.19.12 or sham (n=8 per virus, 4 males and 4 females) and sacrificed at 6 dpi (when the first mouse succumbed to disease). **A)** Percent weight change from starting weight. **B)** Clinical signs six days post-infection.

POWV NY.19.12 intracranial infection in C57BL/6 mice. I.C. inoculation directly introduces virus into the CNS, bypassing the blood-brain barrier, thus serving as a model to directly study neurotropism and viral distribution among brain regions. Female wildtype C57BL/6 mice were I.C. inoculated with 10^3 PFU of POWV NY.19.12 (n=10). Mice were observed for clinical signs and weight loss. Mice were sacrificed at four dpi, when mice displaying moderate clinical signs had lost more than 10% of their starting

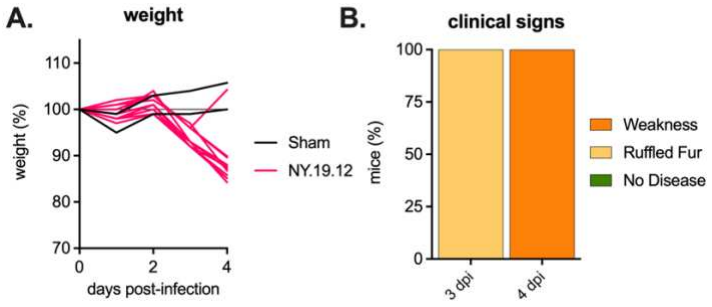

Figure 4.4. POWV lineage II I.C. infection in C57BL/6 mice. Female wildtype C57BL/6 mice were I.C. inoculated with 10^3 PFU of POWV NY.19.12 (n=10) and sacrificed at four dpi (when the first mouse succumbed to disease). **A)** Percent weight change from starting weight. **B)** Clinical signs at three- and four-days post-infection.

weight (**Figure 4.4A**). By three dpi, mice displayed moderate clinical signs of ruffled fur, and by four dpi mice displayed moderate clinical signs of weakness (**Figure 4.4B**).

WNV and chimeric Kunjin Virus subcutaneous infection in C57BL/6 mice. We sought to assess whether ChKUNV is less pathogenic than WNV in mice, which would support its use under BSL-2 conditions. Our goal was to compare the pathogenicity between ChKUNV and WNV using S.C. infection and to evaluate if the prM and E protein of WNV is mediating a more virulent neuroinvasion.

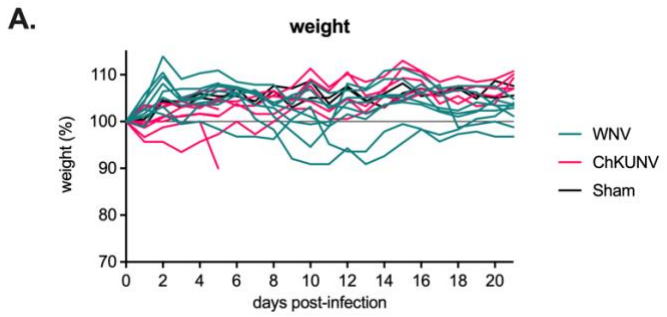

Figure 4.5. WNV and ChKUNV survival in C57BL/6 mice. Female wildtype mice were S.C. inoculated with 10^4 PFU of WNV NY99 (n=8) or 10^5 PFU of ChKUNV (n=5) and monitored for survival. **A)** Percent weight change from starting weight.

Female wildtype mice were S.C. inoculated with 10^4 PFU of WNV NY99 (n=8) or 10^5 PFU of ChKUNV (n=5). Mice were observed for clinical signs and weight loss for 21 days. Mice did not lose weight nor succumb to disease so brains were not harvested (**Figure 4.5A**).

WNV and ChKUNV intracranial infection in C57BL/6 mice. To investigate WNV and ChKUNV pathogenicity in the brain, female wildtype mice were I.C. inoculated with 10^4 PFU of WNV NY99 (n=12) or 10^3 PFU ChKUNV (n=8). Mice were observed for clinical signs and weight loss. 100% of WNV infected mice succumbed to disease at five

dpi (**Figure 4.6A**). WNV infected mice had lost around 10% of their weight at endpoint and 50% of ChKUNV infected mice had lost around 5% of their body weight by six dpi (**Figure 4.6B**). By six dpi, 100% of WNV infected mice had succumbed to disease, whereas only 12.5% of ChKUNV had succumbed to disease and 50% displayed moderate clinical signs of weakness (**Figure 4.6C**).

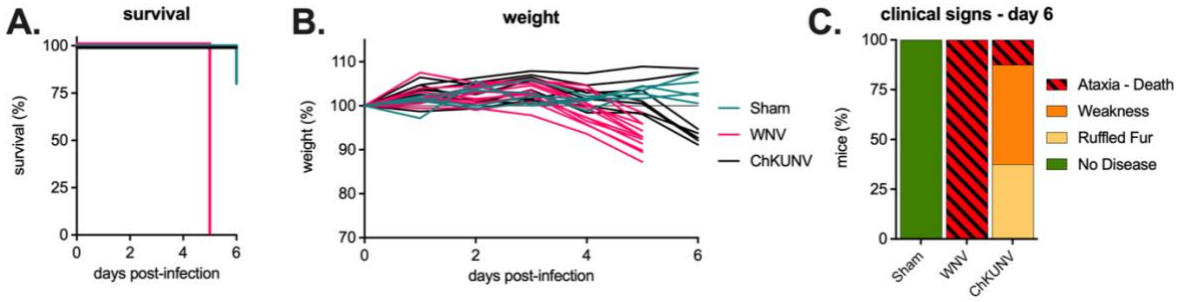

Figure 4.6. WNV and ChKUNV I.C. infection in C57BL/6 mice. Female wildtype mice were I.C. inoculated with 10^4 PFU of WNV NY99 (n=12) or 10^3 PFU ChKUNV (n=8) and sacrificed at endpoint. **A)** Kaplan-Meier survival curve. **B)** Percent weight change from starting weight. **C)** Clinical signs six days post-infection.

WNV and ChKUNV intraperitoneal infection in MAVS knockout mice. To model systemic flavivirus infection and investigate IFN-I responses, male and female MAVS knockout mice were intraperitoneally (I.P.) inoculated with 10^5 PFU of WNV or ChKUNV (n=5 per virus). Unlike the previous studies, individual mice were taken when they succumbed to disease (rather than taking the whole infection group once the first mouse displayed moderate clinical signs). Mice were observed for clinical signs and weight loss. 100% of WNV infected mice succumbed to disease by six dpi (**Figure 4.7A**). All infected mice lost ~15% of their weight (**Figure 4.7B).** By seven dpi, only 37.5% of ChKUNV infected mice displayed mild clinical signs (**Figure 4.7C**). These results suggest a clear phenotype between WNV and ChKUNV infected mice.

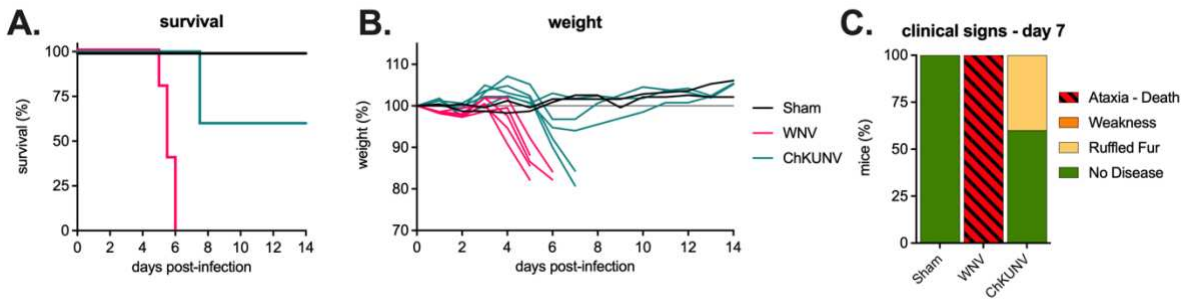

Figure 4.7. WNV and ChKUNV peripheral infection in C57BL/6 mice. Male and female MAVS knockout mice were I.P. inoculated with 10^5 PFU of WNV or ChKUNV (n=5 per virus) and sacrificed at endpoint. **A)** Kaplan-Meier survival curve. **B)** Percent weight change from starting weight. **C)** Clinical signs seven days post-infection.

OPT imaging optimization of POWV infection in MAVS knockout mice. This study aimed to optimize OPT protocols for POWV infected mice. To refine imaging techniques for studying viral CNS infection, female MAVS knockout mice were S.C. inoculated with 10^3 PFU of POWV NY.19.12 (n=6) and weight loss and survival were monitored. All mice had succumbed to disease by six dpi (**Figure 4.8A**). Upon neurological disease onset, mice lost around ~20% of their weight (**Figure 4.8B**). By five dpi, 50% of mice had succumbed to disease and 50% displayed signs of weakness (**Figure 4.8C**).

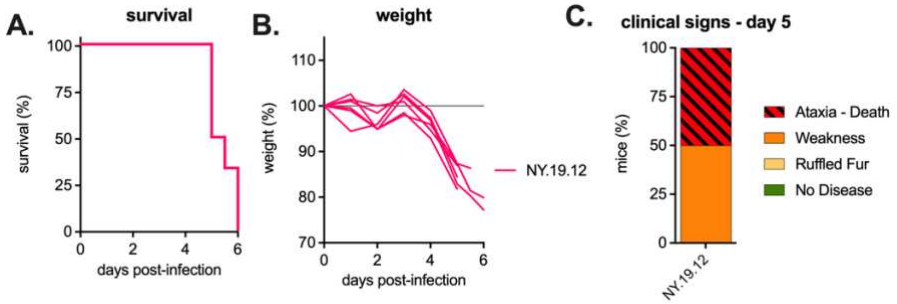

Figure 4.8. POWV lineage II survival in MAVS knockout mice. Female MAVS knockout mice were S.C. inoculated with 10^3 PFU of POWV NY.19.12 (n=6) and sacrificed at endpoint (when the first mouse succumbed to disease). **A)** Kaplan-Meier survival curve. **B)** Percent weight change from starting weight. **C)** Clinical signs five days post-infection.

NY.19.12 infectious clone subcutaneous infection in C57BL/6 mice. NY.19.12.ic was used to investigate the role of residues S205N, K178R, and R649K present in

NY.19.12. Mice were infected with POWV (NY.19.12.ic, NY.19.12, and WI.97.ic) or sham and sacrificed at either day six post-infection (n = 7 per virus) or at endpoint (n = 15 total, two independent experiments, n = 8 and n = 7 per virus). Morbidity and mortality at six dpi and endpoint were assessed for NY.19.12.ic compared to NY.19.12 and WI.97.ic. There were no significant differences in survival between strains (**Figure 4.9A**). There was minimal weight loss by day six, but by day 12 post-infection, mice in all cohorts had either lost weight and succumbed to disease, or recovered (**Figure 4.9B**). At day 4 post-infection, ~70% of NY.19.12.ic and NY.19.12 infected mice displayed mild clinical signs, whereas over 80% of WI.97.ic-infected mice were still healthy. By day 4 post-infection,

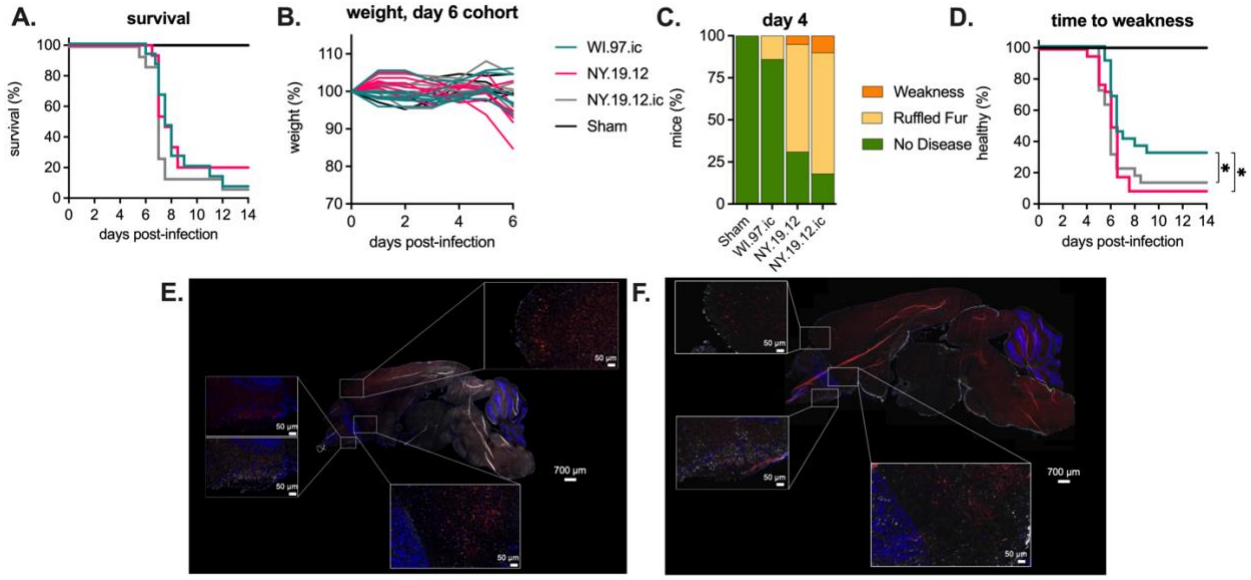

Figure 4.9. NY.19.12 infectious clone in C57BL/6 mice at 6dpi and endpoint. Mice were S.C. inoculated with 10^3 PFU POWV (NY.19.12.ic, NY.19.12, and WI.97.ic) or sham and sacrificed at either day six post-infection (n = 7 per virus) or at endpoint (n = 15 total, two independent experiments, n = 8 and n = 7 per virus). **A)** Percent weight change from starting weight for day six cohort and endpoint cohorts. **B)** Kaplan-Meier survival curves for endpoint cohorts, no significant differences between viruses with log-rank (Mantel-Cox) test ($p>0.05$). **C)** Clinical signs four- and six-days post-infection for all cohorts combined (n = 22 per virus). **D)** The amount of time for mice to exhibit forelimb weakness. Viruses were compared using log-rank (Mantel-Cox) test, * $p<0.05$. As representatives of IFA imaging, a NY.19.12 infected mouse brain was sliced sagittally and stained for POWV envelope protein (red) and a microglial marker Iba1 in gray (**E**) and an astrocyte marker GFAP in gray **(F)**.

there were higher levels of moderate disease in NY.19.12 and NY.19.12.ic infected mice (**Figure 4.9C**). Additionally, there was significantly more forelimb weakness in NY.19.12 and NY.19.12.ic cohorts compared to WI.97.ic infected mice ($p<0.05$) (**Figure 4.9D**). As a representative image of POWV infection, an NY.19.12 infected mouse brain was sliced sagittally and stained for POWV in red, and Iba1 in gray (microglial cells) (**Figure 4.9E)** and GFAP in gray (astrocytes) (**Figure 4.9F**), where NY.19.12 infection is shown to occur in the olfactory bulbs and cortex with minor association with microglia and astrocytes.

4.3 Discussion

We developed a comprehensive workflow and detailed protocol for studying neurotropic flavivirus infection in mouse models. These studies build on the work of Överby and colleagues, who demonstrated that innate immune signaling through IPS-1, also known as MAVS, influences viral tropism and immune activation within the brain during tick-borne flavivirus infection. Their findings revealed that loss of IPS-1 leads to broader viral dissemination, particularly in regions such as the olfactory bulb and brainstem, highlighting the importance of host antiviral pathways in shaping neuropathogenesis.[185]

A major outcome of this work is the development of a flexible model system for studying POWV and related flaviviruses *in vivo*. By leveraging distinct mouse phenotypes, viral strains, and routes of inoculation, we established conditions that can be tailored to specific experimental questions. C57BL/6 mice provide a tractable system for comparative studies of intracranial versus peripheral inoculation routes and allow for

differentiation between mechanisms of direct CNS entry and natural neuroinvasion. This offers insight into how viral strain and host background shape neuropathogenesis. In addition, our results show that MAVS-deficient mice are particularly valuable for understanding innate immune contributions to viral control and dissemination, as they display enhanced susceptibility to both POWV lineage I and II. Together, these models underscore that our studies do not simply define viral outcomes, but rather provide a framework that can be adapted depending on the scientific question, whether to probe immune signaling, viral tropism, or cellular mechanisms of neuroinvasion.

Several limitations of these approaches must be acknowledged. The use of MAVS knockout mice, while critical for dissecting the role of innate immunity, does not fully recapitulate the complexity of viral pathogenesis in immunocompetent hosts and may exaggerate susceptibility phenotypes. C57BL/6 mice, though widely used, also represent only a single genetic background and may not capture the spectrum of host responses relevant to natural infections in humans or wildlife reservoirs. Additionally, while our work provides a proof-of-concept for combining whole-brain imaging with established markers of glial activation, these approaches remain correlative until paired with higher-resolution tools such as single-cell transcriptomics or region-specific functional assays.

Despite advances in understanding flavivirus neuropathogenesis, several unknowns remain regarding how these flaviviruses disseminate from peripheral sites to the brain, the cellular mechanisms that facilitate neuroinvasion, and the host immune factors that determine disease severity.[186–188] In our studies, we found that MAVS mice are more susceptible to both POWV lineage I and II compared to wildtype mice, as seen

in survival, clinical signs, and weight loss trends, highlighting the important role of IFN-I response to POWV infection. In addition, we determined that ChKUNV is less pathogenic than its WNV counterpart in wildtype mice, allowing for future studies on WNV neurotropism at a lower biosafety level.

Furthermore, our imaging efforts will characterize how IFN-I may shape POWV neurotropism and pathogenesis overall. Although imaging results are still in progress, the use of whole-brain imaging and IFA with established markers for astrocytes (GFAP) and microglia (Iba1) will enable detailed spatial mapping of viral antigen and host immune responses throughout the brain. This level of resolution is critical for identifying region-specific infection patterns and immune activation that may not be evident from survival or weight loss data alone. By characterizing and comparing viral strains, host genetic backgrounds, and routes of neuroinvasion, this work establishes a platform for investigating the determinants of flavivirus neuropathogenesis. The resulting data will contribute to a deeper understanding of how innate immune signaling modulates viral distribution and inflammation in the CNS and will help inform future strategies for intervention, vaccine design, and containment classification.

4.4 Methods

Mice. Eight-week-old male and female C57BL/6 mice (Jackson Laboratories, Bar Harbor, ME) were used in experiments. Animals were housed and maintained under specific pathogen-free conditions, and all procedures were performed in accordance with institutional guidelines. Prior to initiating studies, sufficient personal protective equipment (PAPR hoods, Tyvek suits), anesthetics (isoflurane), sharps, and labeling supplies were

ensured to be available. Animal ordering, cage management, and work orders were conducted through the Laboratory Animal Resources. MAVS$^{-/-}$ knockout mice were bred on a C57BL/6 background by NIH Rocky Mountain Laboratories.

Virus preparation and mouse inoculation. Virus stocks were diluted in Dulbecco's Modified Eagle Medium (DMEM) to a final concentration as described in **Table 4.1** prior to inoculation. Virus dilutions were prepared in a biosafety cabinet (BSC) within the BSL-2 laboratory, kept on ice, and transferred into the BSL-3 facility following disinfection with 70% ethanol. Mice were weighed and individually identified using colored Sharpie tail markings on day 0. For S.C. or I.P. inoculation, mice were anesthetized with 2% isoflurane administered via a SomnoFlow anesthesia system. Subsequently, mice were either inoculated S.C. in the inguinal region or I.P. with 100 µL of diluted virus or 100 µL of 1X DMEM for sham controls. For I.C. inoculations, mice were anesthetized with 4% isoflurane and transferred to a nose cone for inoculation. Following infection, mice were monitored daily for weight loss and clinical signs, including ruffled fur, facial edema, forelimb weakness, and ataxia. Mice were euthanized upon reaching humane endpoints defined as ≥20% weight loss or the development of ataxia.

Perfusion and tissue collection. At the experimental endpoint, mice were deeply anesthetized with 5% isoflurane and secured onto a Styrofoam board wrapped with biohazard bags and absorbent materials. A midline incision was made to expose the thoracic cavity. Perfusion was performed by puncturing the left ventricle with a butterfly needle connected to a syringe containing 15 mL of cold PBS, while the right atrium was snipped to allow efflux. Following PBS perfusion, an additional 15 mL of freshly prepared

4% paraformaldehyde (PFA) was perfused in the same manner. This was performed with a detailed workflow to minimize aerosols in the animal BSL-3 space as described below.

Figure 4.10. ABSL-3 workflow of perfusion and necropsies. Left) Biosafety cabinet workflow, Middle) Perfusion with waste collection, and Right) Whole brain necropsy.

Brains were harvested by careful dissection, ensuring minimal damage to olfactory bulbs and the flocculus. Brains were placed into 15 mL conical tubes containing 5 mL of 4% PFA and incubated at 4°C for 24 hours. Subsequently, brains were washed three times with PBS and stored in 1X PBS containing 0.01% sodium azide for downstream whole-brain imaging. Other organs were collected by opening the abdominal cavity and placed into 2 mL snap-cap tubes containing 1 mL of 1X DMEM.

Virus quantification by plaque assay. Collected tissues were homogenized in 2 mL snap-cap tubes containing a homogenization bead using a tissue homogenizer operating at 30 Hz for 2 minutes within the BSL-3 BSC. Homogenates were centrifuged at 10,000 × g for 5 minutes. Supernatants were carefully transferred into new tubes for analysis. For plaque assays, supernatants were serially diluted 10-fold (typically 10^{-2} to 10^{-7}) in DMEM supplemented with 2% fetal bovine serum (FBS) and 1% Penicillin-Streptomycin (PenStrep). Diluted samples were adsorbed onto BHK-21 cell monolayers seeded in 12-well plates and incubated at room temperature with gentle rocking for 1 hour. After

incubation, a 2 mL overlay of tragacanth gum solution was added to each well. Plates were incubated at 37°C for five days, then fixed and stained with crystal violet. Plaques were enumerated to calculate viral titers.

RNA extraction. For viral RNA quantification, an aliquot of tissue homogenate was mixed with TRIzol reagent at a 1:3 sample-to-reagent ratio. Tubes were decontaminated with 70% ethanol and transferred to the Material Transfer Area before proceeding with RNA extraction under BSL-2 conditions following the manufacturer's protocol.

Immunohistochemistry. The right hemisphere from brains of infected mice were dehydrated in 30% sucrose frozen in OCT Embedding matrix (VWR Chemicals, 361603E) and sectioned (sagittal sections) at 10 µm thickness using CryoStar NX50 cryostat (Thermo Scientific, Waltham, MA, USA) according to manufacturer's instructions at -20°C. Slides were thawed at 37°C for 5 minutes, hydrated in PBS followed by permeabilization and blocking using PBS, 0.2% TritonX (VWR Chemicals, 28817.295), 10% goat serum (Nordic BioSite, CL1200-100) and 0.1% NaN3 (Thermo Fischer Scientific, 26628-22-8). Sections were stained with primary antibodies against POWV E protein (GeneTex, GTX640340, 1:1000), astrocyte marker GFAP (Abcam, ab4674, 1:500) and secondary antibodies donkey anti-rabbit A488 (Invitrogen, A21206, 1:500), donkey anti-rabbit A647 (Invitrogen, A31573, 1:500), DAPI (Sigma, 1:1000) and neuronal marker NeuN-A647 (Abcam ab190565, 1:200). Slides were mounted and imaged at 20x by Pannoramic 250 Flash III digital slide scanner (3DHISTECH Ltd., Budapest, Hungary) (sagittal sections) or Leica SP8 confocal microscope (axial sections). Images were created using Imaris software (version 10.1.1, Bitplane, Zürich, Switzerland).

CHAPTER 5: SUMMARY AND FUTURE CONSIDERATIONS

Powassan virus (POWV) is an emerging tick-borne flavivirus that causes severe neurologic disease in humans.[73,111] Despite its clinical importance, significant gaps remain in our understanding of POWV biology, especially in the context of molecular evolution, pathogenesis, and neuroinvasion.[53,111,189] This body of work addresses several of these knowledge gaps by examining viral recombination, comparing understudied lineage II strains i*n vivo*, and characterizing neurotropic flaviviruses in different mouse models.

A molecular focus of this dissertation was to explore whether recombination plays a role in POWV replication. Using ClickSeq and ViReMa, we identified a consistent pattern of defective viral RNA that arose in field-collected ticks.[8,14,149,159] This included deletion patterns in the methyltransferase and protease domains, suggesting that these sites may be hotspots for polymerase stalling or template switching.[190] The frequency and reproducibility of these deletions across replicates support the idea that POWV, like other RNA viruses, uses recombination to generate genetic diversity or modulate fitness during replication.[191,192] Although recombination has been historically considered rare among flaviviruses, accumulating evidence from related viruses, along with our data, challenges this assumption. Our findings raise important questions about how defective RNAs and structural variants may influence host immune responses, viral persistence, or adaptation in different hosts, and suggest that the role of recombination in POWV evolution and pathogenesis deserves further investigation.

POWV lineage II is increasingly associated with human cases but remain less characterized than lineage I.[4,56] In addition, most research on lineage II focuses on the Spooner isolate from 1997, while other strains are often overlooked.[4,58,140] Here, we characterized and compared POWV lineage II pathogenesis in mice, and our findings highlight that lineage II strains from various U.S. regions exhibit nuanced differences in disease severity, replication kinetics, and spleen tropism. By comparing multiple strains and validating findings with an infectious clone system, we began to define phenotypes associated with lineage II strains in mice. Importantly, while there is existing literature on POWV neurotropism for LB (prototypic lineage I) and Spooner strains[59], our study indicates strain-specific differences in the rate of neuroinvasion and systemic spread. Thus, rather than focusing on where the virus goes in the brain, we should be asking how efficiently it gets there, and what host responses are activated in the process.

This work also compared POWV morbidity and mortality in wildtype and MAVS mouse models. Our results show that MAVS mice are more susceptible to both subcutaneous and intracranial POWV infection, therefore confirming that the type-I interferon response is crucial for protection against POWV. In addition, using immunofluorescence (IFA) and whole-brain imaging[183], we will determine how the type-I interferon response affects neurotropism and viral distribution in the brain.

Taken together, our findings add several key contributions to the field. First, we provide the strongest evidence that POWV can generate defective RNAs through recombination, which may influence viral fitness and immune interactions. Second, we significantly advance our understanding of lineage II strains, offering the first detailed comparative pathogenesis study across multiple lineage II isolates *in vivo*. Third, we

confirm and extend prior assumptions about POWV neurotropism, emphasizing that infection kinetics, not tropism, may drive disease severity. Lastly, we confirm that the type I interferon response is crucial to mounting an antiviral response against POWV.

Despite these advances, several important questions remain. The role of defective RNAs in modulating innate immunity or contributing to viral persistence in neurons is entirely unexplored. Future work using long-read sequencing and functional assays will be critical to understanding these dynamics. In addition, further application of infectious clone systems and site-directed mutagenesis could help link specific mutations to disease outcomes.

Another important facet of POWV disease outcomes to consider is immune modulation at the site of the tick bite. It has been shown that tick saliva manipulates the local immune environment during feeding, and this may play a critical role in the severity of disease.[91,193] Future studies should include single-cell RNA sequencing to dissect the host and viral responses at the site of the tick bite as well as within the brain to understand how tick saliva modulates early host responses in the skin and facilitates POWV neuroinvasion. Ultimately, understanding these early events could be used to discover novel targets for therapeutic or vaccine strategies.

In summary, this study provides an integrated molecular and *in vivo* analysis of POWV, with new findings that reshape how we view recombination, strain diversity, and neuroinvasion. Our use of advanced sequencing methods, comparative infection models, and high-resolution imaging builds a comprehensive framework for future research. As POWV continues to emerge in new regions and tick species[4,45], there is a growing need for data that links molecular genotype to biological outcomes. The work

presented here not only fills key knowledge gaps but also defines a path forward for pathogenesis studies that will deepen our understanding of neurotropic flaviviruses.

REFERENCES

1. Hermance, M. E. & Thangamani, S. Powassan Virus: An Emerging Arbovirus of Public Health Concern in North America. *Vector-Borne and Zoonotic Diseases* vol. 17 453–462 Preprint at https://doi.org/10.1089/vbz.2017.2110 (2017).
2. Kakoullis, L. *et al.* Powassan Virus Infections: A Systematic Review of Published Cases. *Tropical Medicine and Infectious Disease* vol. 8 Preprint at https://doi.org/10.3390/tropicalmed8120508 (2023).
3. Centers for Disease Control and Prevention. Powassan Virus Historic Data (2004-2024). (2025).
4. Vogels, C. B. F. *et al.* Phylogeographic reconstruction of the emergence and spread of Powassan virus in the northeastern United States. *Proc Natl Acad Sci U S A* **120**, (2023).
5. Song, J. *et al.* Recapitulation of the Powassan virus life cycle in cell culture. *mBio* **15**, (2024).
6. Kemenesi, G. & Bányai, K. Tick-borne flaviviruses, with a focus on Powassan virus. *Clin Microbiol Rev* **32**, (2019).
7. Simon-Loriere, E. & Holmes, E. C. Why do RNA viruses recombine? *Nature Reviews Microbiology* vol. 9 617–626 Preprint at https://doi.org/10.1038/nrmicro2614 (2011).
8. Vignuzzi, M. & López, C. B. Defective viral genomes are key drivers of the virus–host interaction. *Nature Microbiology* vol. 4 1075–1087 Preprint at https://doi.org/10.1038/s41564-019-0465-y (2019).
9. García-Arriaza, J., Manrubia, S. C., Toja, M., Domingo, E. & Escarmís, C. Evolutionary Transition toward Defective RNAs That Are Infectious by Complementation. *J Virol* **78**, 11678–11685 (2004).
10. Sukhorukov, G. A. *et al.* The Baikal subtype of tick-borne encephalitis virus is evident of recombination between Siberian and Far-Eastern subtypes. *PLoS Negl Trop Dis* **17**, (2023).
11. Su, M. W., Yuan, H. S. & Chu, W. C. Recombination in the nonstructural gene region in type 2 dengue viruses. *Intervirology* **55**, 225–230 (2012).
12. Jaworski, E. & Routh, A. ClickSeq: Replacing fragmentation and enzymatic ligation with click-chemistry to prevent sequence chimeras. in *Methods in Molecular Biology* vol. 1712 71–85 (Humana Press Inc., 2018).
13. Routh, A., Head, S. R., Ordoukhanian, P. & Johnson, J. E. ClickSeq: Fragmentation-Free Next-Generation Sequencing via Click Ligation of Adaptors to Stochastically Terminated 3′-Azido cDNAs. *J Mol Biol* **427**, 2610–2616 (2015).
14. Jaworski, E. & Routh, A. Parallel ClickSeq and Nanopore sequencing elucidates the rapid evolution of defective-interfering RNAs in Flock House virus. *PLoS Pathog* **13**, (2017).
15. Routh, A. & Johnson, J. E. Discovery of functional genomic motifs in viruses with ViReMa-a virus recombination mapper-for analysis of next-generation sequencing data. *Nucleic Acids Res* **42**, (2014).

16. Langsjoen, R. M. *et al.* Evidence for Powassan virus deletions and defective RNA in field collected ticks. Preprint at https://doi.org/10.1101/2024.09.30.615485 (2024).
17. Huang, K.-J. *et al. Printed in Great Britain Manifestation of Thrombocytopenia in Dengue-2-Virus-Infected Mice*. *Journal of General Virology* vol. 81 (2000).
18. Atrasheuskaya, A., Petzelbauer, P., Fredeking, T. M. & Ignatyev, G. Anti-TNF antibody treatment reduces mortality in experimental dengue virus infection. *FEMS Immunol Med Microbiol* **35**, 33–42 (2003).
19. Weiß, R. *et al.* Immunization with different recombinant West Nile virus envelope proteins induces varying levels of serological cross-reactivity and protection from infection. *Front Cell Infect Microbiol* **13**, (2023).
20. Lazear, H. M. *et al.* A Mouse Model of Zika Virus Pathogenesis. *Cell Host Microbe* **19**, 720–730 (2016).
21. Ruzek, D. Animal models of tick-borne encephalitis for preclinical antiviral research. in *Annual Reports in Medicinal Chemistry* vol. 58 243–256 (Academic Press Inc., 2022).
22. Yu, K. M. & Park, S. J. Tick-borne viruses: Epidemiology, pathogenesis, and animal models. *One Health* vol. 19 Preprint at https://doi.org/10.1016/j.onehlt.2024.100903 (2024).
23. Little, P. B., Thorsen, J., Moore, W. & Weninger, N. *Powassan Viral Encephalitis: A Review and Experimental Studies in the Horse and Rabbit*. *Vet. Pathol* vol. 22 (1985).
24. Frolova, M. P., Isachkova, L. M., Shestopalova, N. M. & Pogodina, V. V. EXPERIMENTAL ENCEPHALITIS IN MONKEYS CAUSED BY THE POWASSAN VIRUS. *Neurosci Behav Physiol* **15**, (1985).
25. Chernesky, M. A. & Whittaker-Haines, P. J. Dose-dependent viremia and the differential immunoglobulin response of hamsters to Powassan. *Can J Microbiol* **18**, 655–661 (1972).
26. Hermance, M. E. *et al.* Development of a small animal model for deer tick virus pathogenesis mimicking human clinical outcome. *PLoS Negl Trop Dis* **14**, 1–23 (2020).
27. Santos, R. I., Hermance, M. E., Gelman, B. B. & Thangamani, S. Spinal cord ventral horns and lymphoid organ involvement in powassan virus infection in a mouse model. *Viruses* **8**, (2016).
28. Scroggs, S. L. P. *et al.* Of Murines and Humans: Modeling Persistent Powassan Disease in C57BL/6 Mice. *mBio* (2023) doi:10.1128/mbio.03606-22.
29. VanBlargan, L. A. *et al.* An mRNA Vaccine Protects Mice against Multiple Tick-Transmitted Flavivirus Infections. *Cell Rep* **25**, 3382-3392.e3 (2018).
30. Mlera, L., Meade-White, K., Saturday, G., Scott, D. & Bloom, M. E. Modeling Powassan virus infection in Peromyscus leucopus, a natural host. *PLoS Negl Trop Dis* **11**, (2017).
31. Cheung, A. M. *et al.* Characterization of Live-Attenuated Powassan Virus Vaccine Candidates Identifies an Efficacious Prime-Boost Strategy for Mitigating Powassan Virus Disease in a Murine Model. *Vaccines (Basel)* **11**, (2023).

32. Mladinich, M. C. *et al.* Age-dependent Powassan virus lethality is linked to glial cell activation and divergent neuroinflammatory cytokine responses in a murine model. *J Virol* **98**, (2024).
33. Jasperse, B. A. *et al.* Neuroinvasive Flavivirus Pathogenesis Is Restricted by Host Genetic Factors in Collaborative Cross Mice, Independently of Oas1b . *J Virol* **97**, (2023).
34. Himmler, G. E. *et al.* Passage-attenuated Powassan virus LI9P protects mice from lethal LI9 challenge and links envelope residue D308 to neurovirulence. *mBio* (2025) doi:10.1128/mbio.00065-25.
35. Hermance, M. E., Santos, R. I., Kelly, B. C., Valbuena, G. & Thangamani, S. Immune cell targets of infection at the tick-skin interface during powassan virus transmission. *PLoS One* **11**, (2016).
36. Malonis, R. J. *et al.* A Powassan virus domain III nanoparticle immunogen elicits neutralizing and protective antibodies in mice. *PLoS Pathog* **18**, (2022).
37. VanBlargan, L. A. *et al.* Broadly neutralizing monoclonal antibodies protect against multiple tick-borne flaviviruses. *Journal of Experimental Medicine* **218**, (2021).
38. El Khoury, M. Y. *et al.* Diagnosis of acute deer tick virus encephalitis. *Clinical Infectious Diseases* **56**, (2013).
39. Klontz, E. H., Chowdhury, N. & Branda, J. A. Laboratory Testing for Powassan Virus: Past, Present, and Future. *Journal of Infectious Diseases* **230**, S70–S75 (2024).
40. Kemenesi, G. & Bányai, K. Tick-borne flaviviruses, with a focus on Powassan virus. *Clin Microbiol Rev* **32**, (2019).
41. McLEAN, D. M. & Donohue, W. L. *POWASSAN VIRUS: ISOLATION OF VIRUS FROM A FATAL CASE OF ENCEPHALITIS*. (1959).
42. Mclean, D. M. *et al.* Powassan Virus: Investigations of Possible Natural Cycles of Infection. *Source: The Journal of Infectious Diseases* **109**, 19–23 (1961).
43. Jordi Casals. Antigenic Relationship Between Powassan and Russian Spring-Summer Encephalitis Viruses. **82**, (1960).
44. Telford, S. R. *et al.* Emerging Infectious Diseases. *Emerging Infectious Disease* **3**, (1997).
45. Hart, C. *et al.* Powassan Virus Lineage I in Field-Collected Dermacentor variabilis Ticks, New York, USA. *Emerg Infect Dis* **29**, 415–417 (2023).
46. Lange, R. E. *et al.* Identification and characterization of novel lineage 1 Powassan virus strains in New York State. *Emerg Microbes Infect* **12**, (2023).
47. Zarnke, R. L. & Yuill, T. M. *POWASSAN VIRUS INFECTION IN SNOWSHOE HARES (Lepus Americanus)*. *Journal of Wildlife Diseases* vol. 17 http://meridian.allenpress.com/jwd/article-pdf/17/2/303/2228701/0090-3558-17_2_303.pdf (1981).
48. Smith, K. *et al.* Powassan virus and other arthropod-borne viruses in wildlife and ticks in Ontario, Canada. *American Journal of Tropical Medicine and Hygiene* **99**, 458–465 (2018).
49. Ebel, G. D. & Kramer, L. D. Short report: Duration of tick attachment required for transmission of Powassan virus by deer ticks. *J Trop Med Hyg* **71**, 268–271 (2004).

50. Obellianne, C., Norman, P. D., Esteves, E. & Hermance, M. E. Interspecies co-feeding transmission of Powassan virus between a native tick, *Ixodes scapularis*, and the invasive East Asian tick, Haemaphysalis longicornis. *Parasit Vectors* **17**, (2024).
51. Goethert, H. K., Mather, T. N., Johnson, R. W. & Telford, S. R. Incrimination of shrews as a reservoir for Powassan virus. *Commun Biol* **4**, (2021).
52. Hassett, E. M. & Thangamani, S. Ecology of Powassan virus in the United States. *Microorganisms* **9**, (2021).
53. Brackney, D. E. & Vogels, C. B. F. The known unknowns of Powassan virus ecology. *J Med Entomol* **60**, 1142–1148 (2023).
54. Krow-Lucal, E. R., Lindsey, N. P., Fischer, M. & Hills, S. L. Powassan Virus Disease in the United States, 2006-2016. *Vector-Borne and Zoonotic Diseases* **18**, 286–290 (2018).
55. Yang, X., Gao, G. F. & Liu, W. J. Powassan virus: A tick borne flavivirus infecting humans. *Biosafety and Health* vol. 4 30–37 Preprint at https://doi.org/10.1016/j.bsheal.2021.12.007 (2022).
56. Ebel, G. D., Foppa, I., Spielman, A. & Telford, S. R. A Focus of Deer Tick Virus Transmission in the Northcentral United States. *Emerg Infect Dis* **5**, (1999).
57. McMinn, R. J., Gallichotte, E. N., Courtney, S., Telford, S. R. & Ebel, G. D. Strain-Dependent Assessment of Powassan Virus Transmission to *Ixodes scapularis* Ticks. *Viruses* **16**, (2024).
58. Lange, R. E. *et al.* Differential Virulence and Host-Specific Fitness of Regionally Distinct Human-Derived Powassan Virus Lineage 2 Strains. *Am J Trop Med Hyg* (2025) doi:10.4269/ajtmh.24-0776.
59. Reynolds, E. S. *et al.* Comparative Pathogenesis of Two Lineages of Powassan Virus Reveals Distinct Clinical Outcome, Neuropathology, and Inflammation. *Viruses* **16**, (2024).
60. Kenney, J. L. *et al.* Generation of a lineage II Powassan virus (deer tick virus) cdna clone: Assessment of flaviviral genetic determinants of tick and mosquito vector competence. *Vector-Borne and Zoonotic Dis* **18**, 371–381 (2018).
61. Cimica, V. *et al.* A virus-like particle-based vaccine candidate against the tick-borne Powassan virus induces neutralizing antibodies in a mouse model. *Pathogens* **10**, (2021).
62. Stone, E. T. *et al.* Balanced T and B cell responses are required for immune protection against Powassan virus in virus-like particle vaccination. *Cell Rep* **38**, (2022).
63. van Leur, S. W., Heunis, T., Munnur, D. & Sanyal, S. Pathogenesis and virulence of flavivirus infections. *Virulence* **12**, 2814–2838 (2021).
64. Chotiwan, N. *et al.* Type I interferon shapes brain distribution and tropism of tick-borne flavivirus. *Nat Commun* **14**, (2023).
65. Noll, K. E., Ferris, M. T. & Heise, M. T. The Collaborative Cross: A Systems Genetics Resource for Studying Host-Pathogen Interactions. *Cell Host and Microbe* vol. 25 484–498 Preprint at https://doi.org/10.1016/j.chom.2019.03.009 (2019).

66. Saul, M. C., Philip, V. M., Reinholdt, L. G. & Chesler, E. J. High-Diversity Mouse Populations for Complex Traits. *Trends in Genetics* vol. 35 501–514 Preprint at https://doi.org/10.1016/j.tig.2019.04.003 (2019).
67. El Khoury, M. Y. *et al.* Potential role of deer tick virus in Powassan encephalitis cases in Lyme disease-endemic areas of New York, U.S.A. *Emerg Infect Dis* **19**, 1926–1933 (2013).
68. Ebel, G. D., Campbell, E. N., Goethert, H. K. & Spielman, A. ENZOOTIC TRANSMISSION OF DEER TICK VIRUS IN NEW ENGLAND AND WISCONSIN SITES. *Am. J. Trop. Med. Hyg* **63**, 36–42 (2000).
69. Izuogu, A. O. *et al.* Interferon signaling in Peromyscus leucopus confers a potent and specific restriction to vector-borne flaviviruses. *PLoS One* **12**, (2017).
70. Holbrook, M. R. *et al. An Animal Model for the Tickborne Flavivirus-Omsk Hemorrhagic Fever Virus*. https://academic.oup.com/jid/article/191/1/100/804092 (2005).
71. Platt, D. J. *et al.* Zika virus-related neurotropic flaviviruses infect human placental explants and cause fetal demise in mice. *Sci Transl Med* **10**, (2018).
72. Carrasco, M. & Horiszny, J. A Fatal Case of Powassan Virus Encephalitis. *Journal of Brown Hospital Medicine* **3**, (2024).
73. Piantadosi, A. & Solomon, I. H. Powassan Virus Encephalitis. *Infectious Disease Clinics of North America* vol. 36 671–688 Preprint at https://doi.org/10.1016/j.idc.2022.03.003 (2022).
74. Shannon E. Dunn, Whitney A. Perry & Sabra L. Klein. Mechanisms and consequences of sex differences in immune responses. *Nat Rev Nephrol* **20**, 37–55 (2023).
75. Sabra L Klein, Andrea Hodgson & Dionne P Robinson. Mechanisms of sex disparities in influenza pathogenesis. *J Leukoc Biol* **92**, 67–73 (2012).
76. Jacobsen, H. & Klein, S. L. Sex Differences in Immunity to Viral Infections. *Frontiers in Immunology* vol. 12 Preprint at https://doi.org/10.3389/fimmu.2021.720952 (2021).
77. S Matsuo, K Morita, K Bundo-Morita & A Igarashi. Differences in susceptibility to peripheral infection with Japanese encephalitis virus among inbred strains of mouse. *Uirusu* **44**, (1994).
78. Hoffman, K. W. *et al.* Sex differences in cytokine production following West Nile virus infection: Implications for symptom manifestation. *Pathog Dis* **77**, (2019).
79. Pujantell, M. & Altfeld, M. Consequences of sex differences in Type I IFN responses for the regulation of antiviral immunity. *Frontiers in Immunology* vol. 13 Preprint at https://doi.org/10.3389/fimmu.2022.986840 (2022).
80. Geurs, T. L., Hill, E. B., Lippold, D. M. & French, A. R. Sex differences in murine susceptibility to systemic viral infections. *J Autoimmun* **38**, (2012).
81. Miorin, L., Maestre, A. M., Fernandez-Sesma, A. & García-Sastre, A. Antagonism of type I interferon by flaviviruses. *Biochem Biophys Res Commun* **492**, 587–596 (2017).
82. Telford, S. R. & Piantadosi, A. L. Powassan virus persistence after acute infection. *mBio* vol. 14 Preprint at https://doi.org/10.1128/mbio.00712-23 (2023).

83. Marín-López, A. *et al.* Mosquito Salivary Proteins and Arbovirus Infection: From Viral Enhancers to Potential Targets for Vaccines. *Pathogens* vol. 12 Preprint at https://doi.org/10.3390/pathogens12030371 (2023).
84. Kazimírová, M. & Štibrániová, I. Tick salivary compounds: Their role in modulation of host defences and pathogen transmission. *Frontiers in Cellular and Infection Microbiology* vol. 4 Preprint at https://doi.org/10.3389/fcimb.2013.00043 (2013).
85. Grubaugh, N. D. *et al.* Transmission bottlenecks and RNAi collectively influence tick-borne flavivirus evolution. *Virus Evol* **2**, (2016).
86. Chmelař, J. *et al.* Sialomes and Mialomes: A Systems-Biology View of Tick Tissues and Tick-Host Interactions. *Trends in Parasitology* vol. 32 242–254 Preprint at https://doi.org/10.1016/j.pt.2015.10.002 (2016).
87. Nuttall, P. A. Tick saliva and its role in pathogen transmission. *Wien Klin Wochenschr* **135**, 165–176 (2023).
88. Blisnick, A. A. *et al.* The immunomodulatory effect of IrSPI, a tick salivary gland serine protease inhibitor involved in *Ixodes ricinus* tick feeding. *Vaccines (Basel)* **7**, (2019).
89. Cavassani, K. A., Aliberti, J. C., Dias, A. R. V., Silva, J. S. & Ferreira, B. R. Tick saliva inhibits differentiation, maturation and function of murine bone-marrow-derived dendritic cells. *Immunology* **114**, 235–245 (2005).
90. Conde, J. N. *et al.* Powassan Viruses Spread Cell to Cell during Direct Isolation from Ixodes Ticks and Persistently Infect Human Brain Endothelial Cells and Pericytes. *Journal of Virology jvi.asm.org* **96**, 1682–1703 (2022).
91. Hermance, M. E. & Thangamani, S. Tick Saliva Enhances Powassan Virus Transmission to the Host, Influencing Its Dissemination and the Course of Disease. *J Virol* **89**, 7852–7860 (2015).
92. Santos, R. I., Hermance, M. E., Reynolds, E. S. & Thangamani, S. Salivary gland extract from the deer tick, *Ixodes scapularis*, facilitates neuroinvasion by Powassan virus in BALB/c mice. *Sci Rep* **11**, (2021).
93. Nemeth, N. M., Root, J. J., Hartwig, A. E., Bowen, R. A. & Bosco-Lauth, A. M. Powassan Virus Experimental Infections in Three Wild Mammal Species. *Am J Trop Med Hyg* **104**, 1048–1054 (2021).
94. Gottschalk, C. G., Peterson, D., Armstrong, J., Knox, K. & Roy, A. Potential molecular mechanisms of chronic fatigue in long haul COVID and other viral diseases. *Infectious Agents and Cancer* vol. 18 Preprint at https://doi.org/10.1186/s13027-023-00485-z (2023).
95. Mlera, L. *et al.* Peromyscus leucopus mouse brain transcriptome response to Powassan virus infection. *J Neurovirol* **24**, 75–87 (2018).
96. Mustafá, Y. M., Meuren, L. M., Coelho, S. V. A. & De Arruda, L. B. Pathways exploited by flaviviruses to counteract the blood-brain barrier and invade the central nervous system. *Frontiers in Microbiology* vol. 10 Preprint at https://doi.org/10.3389/fmicb.2019.00525 (2019).
97. Weber, E. *et al.* Type I Interferon Protects Mice from Fatal Neurotropic Infection with Langat Virus by Systemic and Local Antiviral Responses. *J Virol* **88**, 12202–12212 (2014).

98. Rosendal, E., Lindqvist, R., Chotiwan, N., Henriksson, J. & Överby, A. K. Transcriptional Response to Tick-Borne Flavivirus Infection in Neurons, Astrocytes and Microglia In Vivo and In Vitro. *Viruses* **16**, (2024).
99. Choi, H. *et al.* A novel synthetic dna vaccine elicits protective immune responses against powassan virus. *PLoS Negl Trop Dis* **14**, 1–18 (2020).
100. Ben Said, M. & Kratou, M. Exploring approaches and advancements in the development and evaluation of multi-epitope subunit vaccines against tick-borne viruses. *Veterinary Microbiology* vol. 306 Preprint at https://doi.org/10.1016/j.vetmic.2025.110577 (2025).
101. Nguyen, T. L. & Kim, H. Immunoinformatics and computational approaches driven designing a novel vaccine candidate against Powassan virus. *Sci Rep* **14**, (2024).
102. Agudelo, M. *et al.* Broad and potent neutralizing human antibodies to tick-borne flaviviruses protect mice from disease. *Journal of Experimental Medicine* **218**, (2021).
103. Weiner, L. P., Cole, G. A. & Nathanson, N. *Experimental Encephalitis Following Peripheral Inoculation of West Nile Virus in Mice of Different Ages*. *J. Hyg., Camb* vol. 68 (1970).
104. Price, W. H. & Thind, I. S. IMMUNIZATION OF MICE AGAINST RUSSIAN SPRING-SUMMER VIRUS COMPLEX AND MONKEYS AGAINST POWASSAN VIRUS WITH ATTENUATED LANGAT ES VIRUS DURATION OF PROTECTION. *Am J Trop Med Hyg* **22**, (1973).
105. Woodall, J. P. & Roz, A. Experimental Milk-Borne Transmission of Powassan Virus in the Goat. *Am J Trop Med Hyg* **26**, (1977).
106. Douam, F. & Ploss, A. The use of humanized mice for studies of viral pathogenesis and immunity. *Current Opinion in Virology* vol. 29 62–71 Preprint at https://doi.org/10.1016/j.coviro.2018.03.003 (2018).
107. Wang, Z. *et al.* A mosquito salivary protein-driven influx of myeloid cells facilitates flavivirus transmission. *EMBO Journal* **43**, 1690–1721 (2024).
108. Chiffi, G., Grandgirard, D., Leib, S. L., Chrdle, A. & Růžek, D. Tick-borne encephalitis: A comprehensive review of the epidemiology, virology, and clinical picture. *Reviews in Medical Virology* vol. 33 Preprint at https://doi.org/10.1002/rmv.2470 (2023).
109. Cornelius, A. D. A. *et al.* Langat virus infection affects hippocampal neuron morphology and function in mice without disease signs. *J Neuroinflammation* **17**, (2020).
110. Chotiwan, N. *et al.* Type I interferon shapes the distribution and tropism of tick-borne flavivirus. doi:10.1101/2021.11.16.468804.
111. Ebel, G. D. Update on Powassan virus: Emergence of a North American tick-borne flavivirus. *Annu Rev Entomol* **55**, 95–110 (2010).
112. Goldfield, M., Austin, S. M., Black, H. C., Taylor, B. F. & Altman, R. A NON-FATAL HUMAN CASE OF POW ASSAN VIRUS ENCEPHALITIS. *Am J Trop Med Hyg* **22**, (1973).
113. G N Leonova, L M Isachkova, N I Baranov & S P Krugliak. Role of Powassan virus in the etiological structure of tick-borne encephalitis in the Primorsky Kray. *Vopr Virusol* **2**, 173–176 (1980).

114. Hermance, M. E. & Thangamani, S. Powassan Virus: An Emerging Arbovirus of Public Health Concern in North America. *Vector-Borne and Zoonotic Dis* **17**, 453–462 (2017).
115. Chen, R., Wang, E., Tsetsarkin, K. A. & Weaver, S. C. Chikungunya Virus 3′ Untranslated Region: Adaptation to Mosquitoes and a Population Bottleneck as Major Evolutionary Forces. *PLoS Pathog* **9**, (2013).
116. Holmes, E. C., Worobey, M. & Rambaut, A. Phylogenetic Evidence for Recombination in Dengue Virus. *Mol. Biol. Evol* **16**, 405–409 (1999).
117. S. Susanna Twiddy & Edward C. Holmes. The extent of homologous recombination in members of the genus Flavivirus. *Journal of General Virology* **84**, (2003).
118. Baltimore, D. *Mechanism of RNA Recombination in Liovirus*. *Cell* vol. 47 (1986).
119. N. C. Debnath, R. Tiernery, B. K. Sil, M. R. Wills & A. D. T. Barrett. In vitro homotypic and heterotypic interference by defective interfering particles of West Nile virus. *Journal of General Virology* **72**, (1991).
120. Pesko, K. N. *et al.* Internally deleted WNV genomes isolated from exotic birds in New Mexico: Function in cells, mosquitoes, and mice. *Virology* **427**, 10–17 (2012).
121. Holmes, E. C. Error thresholds and the constraints to RNA virus evolution. *Trends Microbiol* **11**, 543–546 (2003).
122. Collins, R. L. *et al.* A structural variation reference for medical and population genetics. *Nature* **581**, 444–451 (2020).
123. Poirier, E. Z. *et al.* Low-Fidelity Polymerases of Alphaviruses Recombine at Higher Rates To Overproduce Defective Interfering Particles. *J Virol* **90**, 2446–2454 (2016).
124. Sempere, R. N. & Arias, A. Establishment of a cell culture model of persistent flaviviral infection: Usutu virus shows sustained replication during passages and resistance to extinction by antiviral nucleosides. *Viruses* **11**, (2019).
125. Rezelj, V. V. *et al.* Defective viral genomes as therapeutic interfering particles against flavivirus infection in mammalian and mosquito hosts. *Nat Commun* **12**, (2021).
126. Langsjoen, R. M., Muruato, A. E., Kunkel, S. R., Jaworski, E. & Routh, A. Differential alphavirus defective rna diversity between intracellular and extracellular compartments is driven by subgenomic recombination events. *mBio* **11**, 1–20 (2020).
127. Sun, Y. *et al.* Immunostimulatory Defective Viral Genomes from Respiratory Syncytial Virus Promote a Strong Innate Antiviral Response during Infection in Mice and Humans. *PLoS Pathog* **11**, 1–21 (2015).
128. Wang, D. *et al.* The SARS-CoV-2 subgenome landscape and its novel regulatory features. *Mol Cell* **81**, 2135-2147.e5 (2021).
129. Vasilijevic, J. *et al.* Reduced accumulation of defective viral genomes contributes to severe outcome in influenza virus infected patients. *PLoS Pathog* **13**, (2017).
130. Brennan, J. W. & Sun, Y. Defective viral genomes: advances in understanding their generation, function, and impact on infection outcomes. *mBio* vol. 15 Preprint at https://doi.org/10.1128/mbio.00692-24 (2024).

131. Easton, A. J. *et al.* A novel broad-spectrum treatment for respiratory virus infections: Influenza-based defective interfering virus provides protection against pneumovirus infection in vivo. *Vaccine* **29**, 2777–2784 (2011).
132. Mlera, L. *et al.* Development of a model system for tick-borne flavivirus persistence in HEK 293T cells. *mBio* **6**, (2015).
133. Norberg, P., Roth, A. & Bergström, T. Genetic recombination of tick-borne flaviviruses among wild-type strains. *Virology* **440**, 105–116 (2013).
134. Bertrand, Y. J. K., Johansson, M. & Norberg, P. Revisiting recombination signal in the tick-borne encephalitis virus: A simulation approach. *PLoS One* **11**, (2016).
135. Bertrand, Y., Töpel, M., Elväng, A., Melik, W. & Johansson, M. First dating of a recombination event in mammalian tick-borne flaviviruses. *PLoS One* **7**, (2012).
136. Liu, W. J., Sedlak, P. L., Kondratieva, N. & Khromykh, A. A. Complementation Analysis of the Flavivirus Kunjin NS3 and NS5 Proteins Defines the Minimal Regions Essential for Formation of a Replication Complex and Shows a Requirement of NS3 in cis for Virus Assembly . *J Virol* **76**, 10766–10775 (2002).
137. Chin, W. X. *et al.* Flavivirus genome recoding by codon optimisation confers genetically stable in vivo attenuation in both mice and mosquitoes. *PLoS Pathog* **19**, (2023).
138. Nonaka, E., Ebel, G. D. & Wearing, H. J. Persistence of pathogens with short infectious periods in seasonal tick populations: The relative importance of three transmission routes. *PLoS One* **5**, (2010).
139. Costero, A. & Grayson, A. A. Experimental Transmission of Powassan virus (Flaviviriade) By *Ixodes scapularis* Ticks (Acari:Ixodidae). *Am J Trop Med Hyg* **55**, 536–546 (1996).
140. Mcminn, R. J. *et al.* Phylodynamics of deer tick virus in North America. *Virus Evol* **9**, 1–8 (2023).
141. Grzegorz Karbowiak, Beata Biernat, Joanna Werszko & Leszek Rychlik. The transstadial persistence of tick-borne encephalitis virus in Dermacentor reticulatus ticks in natural conditions. *Acta Parasitol* **61**, 201–203 (2016).
142. Raney, W. R., Herslebs, E. J., Langohr, I. M., Stone, M. C. & Hermance, M. E. Horizontal and Vertical Transmission of Powassan Virus by the Invasive Asian Longhorned Tick, Haemaphysalis longicornis, Under Laboratory Conditions. *Front Cell Infect Microbiol* **12**, (2022).
143. Lange, R. E., Prusinski, M. A., Dupuis, A. P. & Ciota, A. T. Direct Evidence of Powassan Virus Vertical Transmission in *Ixodes scapularis* in Nature. *Viruses* **16**, (2024).
144. Aaskov, J., Buzacott, K., Thu, H. M., Lowry, K. & Holmes, E. C. Long-term transmission of defective RNA viruses in humans and Aedes mosquitoes. *Science (1979)* **311**, 236–238 (2006).
145. Lancaster, M. U., Hodgetts, S. I., Mackenzie, J. S. & Urosevic, N. Characterization of Defective Viral RNA Produced during Persistent Infection of Vero Cells with Murray Valley Encephalitis Virus. *J Virol* **72**, 2474–2482 (1998).
146. Yoon, S. W. *et al. Characterization of Homologous Defective Interfering RNA during Persistent Infection of Vero Cells with Japanese Encephalitis Virus*. *Mol. Cells* vol. 21.

147. Lu, G. & Gong, P. Crystal Structure of the Full-Length Japanese Encephalitis Virus NS5 Reveals a Conserved Methyltransferase-Polymerase Interface. *PLoS Pathog* **9**, (2013).
148. Li, D. *et al.* Defective interfering viral particles in acute dengue infections. *PLoS One* **6**, (2011).
149. Routh, A., Head, S. R., Ordoukhanian, P. & Johnson, J. E. ClickSeq: Fragmentation-Free Next-Generation Sequencing via Click Ligation of Adaptors to Stochastically Terminated 3′-Azido cDNAs. *J Mol Biol* **427**, 2610–2616 (2015).
150. Yun, S. M. *et al.* First complete genomic characterization of two tick-borne encephalitis virus isolates obtained from wild rodents in South Korea. *Virus Genes* **42**, 307–316 (2011).
151. Chiramel, A. I. *et al.* TRIM5α Restricts Flavivirus Replication by Targeting the Viral Protease for Proteasomal Degradation. *Cell Rep* **27**, 3269-3283.e6 (2019).
152. Rajsbaum, R., García-Sastre, A. & Versteeg, G. A. TRIMmunity: The roles of the TRIM E3-ubiquitin ligase family in innate antiviral immunity. *Journal of Molecular Biology* vol. 426 1265–1284 Preprint at https://doi.org/10.1016/j.jmb.2013.12.005 (2014).
153. Alnaji, F. G., Reiser, W. K., Rivera-Cardona, J., Te Velthuis, A. J. W. & Brooke, C. B. Influenza A Virus Defective Viral Genomes Are Inefficiently Packaged into Virions Relative to Wild-Type Genomic RNAs. *mBio* (2021).
154. Oxana A. Belova *et al.* Properties of the tick-borne encephalitis virus population during persistent infection of ixodid ticks and tick cell lines. *Ticks Tick Borne Dis* **8**, 895–906 (2017).
155. Robich, R. M. *et al.* Prevalence and genetic characterization of deer tick virus (Powassan Virus, Lineage II) in *Ixodes scapularis* ticks collected in Maine. *Am J Trop Med Hyg* **101**, 467–471 (2019).
156. Chen, S., Zhou, Y., Chen, Y. & Gu, J. Fastp: An ultra-fast all-in-one FASTQ preprocessor. in *Bioinformatics* vol. 34 i884–i890 (Oxford University Press, 2018).
157. Langmead, B. & Salzberg, S. L. Fast gapped-read alignment with Bowtie 2. *Nat Methods* **9**, 357–359 (2012).
158. Walker, B. J. *et al.* Pilon: An integrated tool for comprehensive microbial variant detection and genome assembly improvement. *PLoS One* **9**, (2014).
159. Routh, A. & Johnson, J. E. Discovery of functional genomic motifs in viruses with ViReMa-a virus recombination mapper-for analysis of next-generation sequencing data. *Nucleic Acids Res* **42**, (2014).
160. Guex, N. & Peitsch, M. C. SWISS-MODEL and the Swiss-PdbViewer: An environment for comparative protein modeling. *Electrophoresis* **18**, 2714–2723 (1997).
161. Remmert, M., Biegert, A., Hauser, A. & Söding, J. HHblits: Lightning-fast iterative protein sequence searching by HMM-HMM alignment. *Nat Methods* **9**, 173–175 (2012).
162. Studer, G. *et al.* ProMod3 - A versatile homology modelling toolbox. *PLoS Comput Biol* **17**, (2021).
163. Love, M. I., Huber, W. & Anders, S. Moderated estimation of fold change and dispersion for RNA-seq data with DESeq2. *Genome Biol* **15**, (2014).

164. Eisen, M. B., Spellman, P. T., Brown, P. O. & Botstein, D. *Cluster Analysis and Display of Genome-Wide Expression Patterns*. *Genetics* vol. 95 www.pnas.org. (1998).
165. Piantadosi, A. *et al.* Emerging Cases of Powassan Virus Encephalitis in New England: Clinical Presentation, Imaging, and Review of the Literature. *Clinical Infectious Diseases* **62**, 707–713 (2015).
166. Eisen, L. Pathogen transmission in relation to duration of attachment by I*xodes scapularis* ticks. *Ticks Tick Borne Dis* **9**, 535–542 (2018).
167. Normandin, E. *et al.* Powassan virus neuropathology and genomic diversity in patients with fatal encephalitis. *Open Forum Infect Dis* **7**, (2020).
168. Shi, P.-Y., Tilgner, M., Lo, M. K., Kent, K. A. & Bernard, K. A. Infectious cDNA Clone of the Epidemic West Nile Virus from New York City. *J Virol* **76**, 5847–5856 (2002).
169. Daisuke Hayasaka *et al.* Amino acid changes responsible for attenuation of virus neurovirulence in an infectious cDNA clone of the Oshima strain of Tick-borne encephalitis virus . *Journal of General Virology* **85**, (2004).
170. Khanam, A., Gutiérrez-Barbosa, H., Lyke, K. E. & Chua, J. V. Immune-Mediated Pathogenesis in Dengue Virus Infection. *Viruses* vol. 14 Preprint at https://doi.org/10.3390/v14112575 (2022).
171. Campbell, M. S. & Pletnev, A. G. Infectious cDNA clones of Langat tick-borne flavivirus that differ from their parent in peripheral neurovirulence. *Virology* **269**, 225–237 (2000).
172. Bavia, L., Mosimann, A. L. P., Aoki, M. N. & Duarte Dos Santos, C. N. A glance at subgenomic flavivirus RNAs and microRNAs in flavivirus infections. *Virol J* **13**, (2016).
173. Chen, S., Wu, Z., Wang, M. & Cheng, A. Innate immune evasion mediated by flaviviridae non-structural proteins. *Viruses* vol. 9 Preprint at https://doi.org/10.3390/v9100291 (2017).
174. Wang, X. *et al.* Near-atomic structure of Japanese encephalitis virus reveals critical determinants of virulence and stability. *Nat Commun* **8**, (2017).
175. Yoshii, K. *et al.* A Critical Determinant of Neurological Disease Associated with Highly Pathogenic Tick-Borne Flavivirus in Mice. *J Virol* **88**, 5406–5420 (2014).
176. Carbaugh, D. L. & Lazear, H. M. Flavivirus Envelope Protein Glycosylation: Impacts on Viral Infection and Pathogenesis. *J Virol* **94**, (2020).
177. Ward, L. D. & Kellis, M. Interpreting noncoding genetic variation in complex traits and human disease. *Nature Biotechnology* vol. 30 1095–1106 Preprint at https://doi.org/10.1038/nbt.2422 (2012).
178. Ren, S. *et al. Selection of Housekeeping Genes for Use in Quantitative Reverse Transcription PCR Assays on the Murine Cornea*. http://www.molvis.org/molvis/v16/a120 (2010).
179. Rossi, S. L., Ross, T. M. & Evans, J. D. West nile virus. *Clinics in Laboratory Medicine* vol. 30 47–65 Preprint at https://doi.org/10.1016/j.cll.2009.10.006 (2010).
180. Cody, S. G., Adam, A., Siniavin, A., Kang, S. S. & Wang, T. Flaviviruses—Induced Neurological Sequelae. *Pathogens* vol. 14 Preprint at https://doi.org/10.3390/pathogens14010022 (2025).

181. Appler, K. K. *et al.* Persistence of west Nile virus in the central nervous system and periphery of mice. *PLoS One* **5**, (2010).
182. Eriksson, A. U. *et al.* Near infrared optical projection tomography for assessments of β-cell mass distribution in diabetes research. *J Vis Exp* (2013) doi:10.3791/50238.
183. Willekens, S. M. A. *et al.* An MR-based brain template and atlas for optical projection tomography and light sheet fluorescence microscopy in neuroscience. *Front Neurosci* **18**, (2024).
184. Saurabh Losarwar, Bhaskaranand Pancholi, Raja Babu & Debapriya Garabadu. Mitochondria-dependent innate immunity: A potential therapeutic target in flavivirus infection. *Int Immunopharmacol* **154**, (2025).
185. Kurhade, C. *et al.* Type I Interferon response in olfactory bulb, the site of tick-borne flavivirus accumulation, is primarily regulated by IPS-1. *J Neuroinflammation* **13**, (2016).
186. Suthar, M. S., Diamond, M. S. & Gale, M. West Nile virus infection and immunity. *Nature Reviews Microbiology* vol. 11 115–128 Preprint at https://doi.org/10.1038/nrmicro2950 (2013).
187. de Vries, L. & Harding, A. T. Mechanisms of Neuroinvasion and Neuropathogenesis by Pathologic Flaviviruses. *Viruses* vol. 15 Preprint at https://doi.org/10.3390/v15020261 (2023).
188. Aurélie Velay *et al.* Tick-borne encephalitis virus: molecular determinants of neuropathogenesis of an emerging pathogen. *Crit Rev Microbiol* **45**, (2019).
189. Srichawla, B. S. *et al.* Neuroinvasion of emerging and re-emerging arboviruses: A scoping review. *SAGE Open Medicine* vol. 12 Preprint at https://doi.org/10.1177/20503121241229847 (2024).
190. Zhou, Y. *et al.* Structure and Function of Flavivirus NS5 Methyltransferase. *J Virol* **81**, 3891–3903 (2007).
191. Caldwell, H. S., Pata, J. D. & Ciota, A. T. The Role of the Flavivirus Replicase in Viral Diversity and Adaptation. *Viruses* vol. 14 Preprint at https://doi.org/10.3390/v14051076 (2022).
192. Wang, H., Cui, X., Cai, X. & An, T. Recombination in Positive-Strand RNA Viruses. *Frontiers in Microbiology* vol. 13 Preprint at https://doi.org/10.3389/fmicb.2022.870759 (2022).
193. Kleissl, L. *et al.* Ticks' tricks: immunomodulatory effects of ixodid tick saliva at the cutaneous tick-host interface. *Frontiers in Immunology* vol. 16 Preprint at https://doi.org/10.3389/fimmu.2025.1520665 (2025).

Table S2.1 RNA metagenomic short-read sequencing information

Collection_Season	Missing	Missing	Missing	Missing	Missing	Missing	Missing	Missing
Collection_Year	2020	2020	2020	2020	2020	2020	2020	2018
Location(State)	MA	MA	MA	MA	MA	MA	MA	MA
Location(City)	Missing	Medfield	SouthGrafton	Harvard	Glenburn	Bowdoinham	WestGray	Missing
Species	Tick	Tick	Tick	Tick	Tick	Tick	Tick	Tick
meanmapq	255	255	255	255	255	255	255	255
meanbaseq	37.4	37.2	34.4	37.2	34.5	36.2	34.8	37.6
meandepth	64.0882	120.98	626.45	951.35	846.829	252.476	4348.88	180.037
coverage	99.4279	99.917	99.6124	99.797	99.8247	99.7416	99.9539	99.8247
covbases	10775	10830	10795	10815	10818	10809	10832	10819
nummapped	4921	9677	48111	71661	71896	20733	356747	13042
endpos	10837	10839	10837	10837	10837	10837	10837	10838
startpos	1	1	1	1	1	1	1	1
#rname	L2A-HM440559.1_p	L2A-HM440559.1_p	L2A-HM440559.1_p	L2A-HM440559.1_p	L2A-HM440559.1_p	L2A-HM440559.1_p	L2A-HM440559.1_p	L2A-HM440559.1_p
numreads	129687	1253400	251909	944722	2258130	2446418	3715969	417258
Library_Prep	Nextera	Nextera	Nextera	Nextera	Nextera	Nextera	Nextera	Nextera
Reference 3	10.3390/v16060830	N/A	N/A	N/A	N/A	N/A	N/A	N/A
Reference 2	10.4269/ajtmh.23-0643	10.4269/ajtmh.23-0643	N/A	N/A	10.4269/ajtmh.23-0643	10.4269/ajtmh.23-0643	N/A	10.4269/ajtmh.23-0643
Reference 1	10.1093/ve/vead008	10.1093/ve/vead008	10.1093/ve/vead008	10.1093/ve/vead008	10.1093/ve/vead008	10.1093/ve/vead008	10.1093/ve/vead008	10.1093/ve/vead008
GenBank_Accession	OP823422	OP823422	OP823411	OP823412	OP823413	OP823414	OP823415	OP823419
SRA_RunID	SRR31643123	SRR31643122	SRR31643111	SRR31643100	SRR31643071	SRR31643060	SRR31643049	SRR31643087
SRA_Library_Name	MA_Ma_SM20.M26_2020_NX1	MA_Me_MSH20.F85_2020_NX1	MA_SG_Deer20.M9_2020_NX1	MA_H_Deer20.M29_2020_NX1	MA_G_Deer20.M52_2020_NX1	MA_B_Deer20.M90_2020_NX1	MA_WG_Deer20.M105_2020_NX1	MA_S_DH18.P61.g2_2018_NX1
Biosample_ID	SAMN37217310	SAMN37217314	SAMN37217330	SAMN37217305	SAMN37217304	SAMN37217296	SAMN37217384	SAMN37217329
Biosample_Name	MA_Ma_SM20.M26_2020	MA_Me_MSH20.F85_2020	MA_SG_Deer20.M9_2020	MA_H_Deer20.M29_2020	MA_G_Deer20.M52_2020	MA_B_Deer20.M90_2020	MA_WG_Deer20.M105_2020	MA_S_DH18.P61.g2_2018
BioProject	PRJNA1011343	PRJNA1011343	PRJNA1011343	PRJNA1011343	PRJNA1011343	PRJNA1011343	PRJNA1011343	PRJNA1011343
Study_ID	POWV_TUF_001A	POWV_TUF_002B	POWV_TUF_009I	POWV_TUF_010J	POWV_TUF_011K	POWV_TUF_012L	POWV_TUF_013M	DH18-P61-g2

Missing	Fall	Fall	Fall	Fall	Fall	Fall	Fall	Fall	Fall	Fall
2018	2020	2020	2020	2020	2020	2020	2020	2020	2020	2020
MA	ME	ME	ME	ME	ME	ME	ME	ME	ME	ME
Missing	Wells	Wells	Wells	Wells	Wells	Wells	Wells	Wells	Wells	Wells
Tick	Tick	Tick	Tick	Tick	Tick	Tick	Tick	Tick	Tick	Tick
255	255	255	255	255	255	255	255	255	255	255
37.6	35.6	35.7	35.6	35.9	35.8	35.8	35.8	35.8	35.9	34.4
119.138	1284.84	1491.45	2481.21	285.791	604.489	2314.82	859.619	427.054	964.823	1177.09
99.2987	99.5755	99.4925	99.7693	99.1234	99.4187	99.8247	99.6032	99.3725	99.7693	99.5663
10761	10791	10782	10812	10742	10774	10818	10794	10769	10812	10790
8579	142590	162256	266836	30067	64666	251505	93514	45146	101417	140819
10837	10837	10837	10837	10837	10837	10837	10837	10837	10837	10837
1	1	1	1	1	1	1	1	1	1	1
L2A-HM440559.1_p	L2A-HM440559.1_p	L2A-HM440559.1_p	L2A-HM440559.1_p	L2A-HM440559.1_p	L2A-HM440559.1_p	L2A-HM440559.1_p	L2A-HM440559.1_p	L2A-HM440559.1_p	L2A-HM440559.1_p	L2A-HM440559.1_p
337270	17808675	14361944	21856272	21290906	17980427	16888393	10531363	15780567	17134628	28606915
Nextera	Nextera	Nextera	Nextera	Nextera	Nextera	Nextera	Nextera	Nextera	Nextera	Nextera
N/A	N/A	N/A	N/A	N/A	N/A	N/A	N/A	N/A	N/A	N/A
10.4269/ajtmh.23-0643	10.4269/ajtmh.23-0643	10.4269/ajtmh.23-0643	10.4269/ajtmh.23-0643	10.4269/ajtmh.23-0643	10.4269/ajtmh.23-0643	10.4269/ajtmh.23-0643	10.4269/ajtmh.23-0643	10.4269/ajtmh.23-0643	N/A	10.4269/ajtmh.23-0643
10.1093/ve/vead008	10.1093/ve/vead008	10.1093/ve/vead008	10.1093/ve/vead008	10.1093/ve/vead008	10.1093/ve/vead008	10.1093/ve/vead008	10.1093/ve/vead008	10.1093/ve/vead008	N/A	10.1093/ve/vead008
OP823417	OP823426	OR340576	OR340583	OR340582	OP823427	OP823428	OP823429	OR340569	N/A	OP823430
SRR31643076	SRR31643074	SRR31643121	SRR31643120	SRR31643119	SRR31643118	SRR31643117	SRR31643116	SRR31643115	SRR31685272	SRR31643114
MA_MV_DH18.D81.A1.A3_2018_NX1	ME_W_299.3_2020_NX1	ME_W_299.GdAD6.2.3_2020_NX1	ME_W_299.GrdAE6.3_2020_NX1	ME_W_337.GdBG5.4_2020_NX1	ME_W_338.GdAC3.1.3_2020_NX1	ME_W_338.GdAC3.2.3_2020_NX1	ME_W_338.GdAC5.3_2020_NX1	ME_W_338.GdAE4.3_2020_NX1	ME_W_338.BB2_2020_NX1	ME_W_422.3A_2020_NX1
SAMN37217311	SAMN37217358	SAMN37217359	SAMN37217361	SAMN37217367	SAMN37217364	SAMN37217365	SAMN37217366	SAMN37217368	SAMN45738111	SAMN37217371
MA_MV_DH18.D81.A1.A3_2018	ME_W_299.3_2020	ME_W_299.GdAD6.2.3_2020	ME_W_299.GrdAE6.3_2020	ME_W_337.GdBG5.4_2020	ME_W_338.GdAC3.1.3_2020	ME_W_338.GdAC3.2.3_2020	ME_W_338.GdAC5.3_2020	ME_W_338.GdAE4.3_2020	ME_W_338.BB2_2020	ME_W_422.3A_2020
PRJNA1011343	PRJNA1011342	PRJNA1011342	PRJNA1011342	PRJNA1011342	PRJNA1011342	PRJNA1011342	PRJNA1011342	PRJNA1011342	PRJNA1011342	PRJNA1011342
DH18-D81-A1-A3	POWV_MMC_001A	POWV_MMC_003C	POWV_MMC_004D	POWV_MMC_005E	POWV_MMC_006F	POWV_MMC_007G	POWV_MMC_008H	POWV_MMC_009I	POWV_MMC_010J	POWV_MMC_011K

Fall	Fall	Fall	Fall	Fall	Fall	Missing	Summer	Summer	Summer	Summer
2020	2020	2020	2020	2020	2020	2019	2019	2019	2019	2019
ME	ME	ME	ME	ME	ME	ME	ME	ME	ME	ME
Wells	Wells	Wells	Wells	Wells	Wells	Missing	Missing	Missing	Missing	Missing
Tick	Tick	Tick	Tick	Tick	Tick	Tick	Tick	Tick	Tick	Tick
255	255	255	255	255	255	255	255	255	255	255
35.8	35.9	35.9	35.7	35.6	35.5	35.7	38.7	38.8	38.7	38.6
1261.65	1126.29	867.306	1172.07	949.548	1943.72	832.243	395.338	247.975	224.507	122.42
99.6493	99.7601	99.9723	99.1511	99.6124	99.5386	99.6678	99.2433	99.1234	99.1326	98.782
10799	10811	10834	10745	10795	10787	10801	10755	10742	10743	10705
135678	118399	96538	127875	104686	214759	90704	44380	27041	25195	13928
10837	10837	10837	10837	10837	10837	10837	10837	10837	10837	10837
1	1	1	1	1	1	1	1	1	1	1
L2A-HM440559.1_p	L2A-HM440559.1_p	L2A-HM440559.1_p	L2A-HM440559.1_p	L2A-HM440559.1_p	L2A-HM440559.1_p	L2A-HM440559.1_p	L2A-HM440559.1_p	L2A-HM440559.1_p	L2A-HM440559.1_p	L2A-HM440559.1_p
17726051	18084247	5528165	23130339	18279299	16517253	71761383	8450880	10867654	8812959	6454394
Nextera	Nextera	Nextera	Nextera	Nextera	Nextera	Nextera	Nextera	Nextera	Nextera	Nextera
N/A	N/A	N/A	N/A	N/A	N/A	N/A	N/A	N/A	N/A	N/A
N/A	10.4269/ajtmh.23-0643	10.4269/ajtmh.23-0643	10.4269/ajtmh.23-0643	10.4269/ajtmh.23-0643	10.4269/ajtmh.23-0643	10.4269/ajtmh.23-0643	10.4269/ajtmh.23-0643	10.4269/ajtmh.23-0643	10.4269/ajtmh.23-0643	10.4269/ajtmh.23-0643
10.1093/ve/vead008	10.1093/ve/vead008	10.1093/ve/vead008	10.1093/ve/vead008	10.1093/ve/vead008	10.1093/ve/vead008	10.1093/ve/vead008	10.1093/ve/vead008	10.1093/ve/vead008	10.1093/ve/vead008	10.1093/ve/vead008
OR340579	OP823431	OR340574	OP823455	OP823456	OR340571	OP823432	OR340578	OP823441	OR340581	OR340568
SRR31643113	SRR31643112	SRR31643110	SRR31643109	SRR31643108	SRR31643107	SRR31643106	SRR31643104	SRR31643103	SRR31643102	SRR31643101
ME_W_422.GdAB2.2.3_2020_NX1	ME_W_422.3D_2020_NX1	ME_W_154.1.2020_NX1	ME_W_189.4_2020_NX1	ME_W_231.2_2020_NX1	ME_W_268.8.2020_NX1	ME_R_472_2019_NX1	ME_W_068.F_2019_NX1	ME_W_344.9_2019_NX1	ME_W_369.4_2019_NX1	ME_W_018.D_2019_NX1
SAMN37217373	SAMN37217372	SAMN37217363	SAMN37217362	SAMN37217369	SAMN37217370	SAMN37217322	SAMN37217345	SAMN37217346	SAMN37217347	SAMN37217348
ME_W_422.GdAB2.2.3_2020	ME_W_422.3D_2020	ME_W_154.1.2020	ME_W_189.4_2020	ME_W_231.2_2020	ME_W_268.8.2020	ME_R_472_2019	ME_W_068.F_2019	ME_W_344.9_2019	ME_W_369.4_2019	ME_W_018.D_2019
PRJNA1011343	PRJNA1011343	PRJNA1011343	PRJNA1011343	PRJNA1011343	PRJNA1011343	PRJNA1011343	PRJNA1011343	PRJNA1011343	PRJNA1011343	PRJNA1011343
POWV_MMC_012L	POWV_MMC_014N	POWV_MMC_015O	POWV_MMC_016P	POWV_MMC_017Q	POWV_MMC_018R	POWV_ME19-472_tick	MMC2	MMC4	MMC5	MMC6

Fall	Fall	Fall	Fall	Fall	Fall	Fall	Fall	Fall	Fall	Fall
2019	2019	2019	2019	2019	2019	2019	2019	2019	2018	2018
ME	ME	ME	ME	ME	ME	ME	ME	ME	ME	ME
Missing	Missing	Missing	Missing	Missing	Missing	Missing	Missing	Missing	Missing	Missing
Tick	Tick	Tick	Tick	Tick	Tick	Tick	Tick	Tick	Tick	Tick
255	255	255	255	255	255	255	255	255	255	255
38.3	38.6	38.5	38.7	38.4	38.3	38.5	38.6	38.6	38.6	38.5
317.689	485.843	397.93	1087.85	676.003	208.628	1241.45	390.545	311.77	6511.69	1047.69
99.2618	99.2433	99.0219	99.3357	99.1972	99.8708	99.5478	99.4094	99.1326	99.4648	99.677
10757	10755	10731	10766	10750	10824	10788	10773	10743	10779	10802
36145	54656	44271	120919	77694	23942	141914	45013	35345	716249	115942
10837	10837	10837	10838	10837	10838	10837	10837	10837	10837	10837
1	1	1	1	1	1	1	1	1	1	1
L2A-HM440559.1_p	L2A-HM440559.1_p	L2A-HM440559.1_p	L2A-HM440559.1_p	L2A-HM440559.1_p	L2A-HM440559.1_p	L2A-HM440559.1_p	L2A-HM440559.1_p	L2A-HM440559.1_p	L2A-HM440559.1_p	L2A-HM440559.1_p
3850868	7096538	6177168	13083943	4131720	6297941	9507456	11477455	13004214	7173267	10377549
Nextera	Nextera	Nextera	Nextera	Nextera	Nextera	Nextera	Nextera	Nextera	Nextera	Nextera
N/A	N/A	N/A	N/A	N/A	N/A	N/A	N/A	N/A	N/A	N/A
10.4269/ajtmh.23-0643	10.4269/ajtmh.23-0643	10.4269/ajtmh.23-0643	10.4269/ajtmh.23-0643	10.4269/ajtmh.23-0643	10.4269/ajtmh.23-0643	10.4269/ajtmh.23-0643	10.4269/ajtmh.23-0643	10.4269/ajtmh.23-0643	10.4269/ajtmh.23-0643	10.4269/ajtmh.23-0643
10.1093/ve/vead008	10.1093/ve/vead008	10.1093/ve/vead008	10.1093/ve/vead008	10.1093/ve/vead008	10.1093/ve/vead008	10.1093/ve/vead008	10.1093/ve/vead008	10.1093/ve/vead008	10.1093/ve/vead008	10.1093/ve/vead008
OP823448	OR340572	OP823449	OP823450	OP823451	OP823452	OP823453	OR340573	OR340575	OP823446	OP823447
SRR31643099	SRR31643098	SRR31643097	SRR31643096	SRR31643095	SRR31643094	SRR31643093	SRR31643075	SRR31643073	SRR31643072	SRR31643070
ME_W_003.4_2019_NX1	ME_W_032.7_2019_NX1	ME_W_087.4F_2019_NX1	ME_W_131.1A_2019_NX1	ME_W_276.10_2019_NX1	ME_W_450.3D_2019_NX1	ME_W_532.7_2019_NX1	ME_W_535.7_2019_NX1	ME_W_173.G_2019_NX1	ME_W_076.1_2018_NX1	ME_W_106.3_2018_NX1
SAMN37217349	SAMN37217350	SAMN37217351	SAMN37217352	SAMN37217353	SAMN37217354	SAMN37217355	SAMN37217356	SAMN37217357	SAMN37217343	SAMN37217344
ME_W_003.4_2019	ME_W_032.7_2019	ME_W_087.4F_2019	ME_W_131.1A_2019	ME_W_276.10_2019	ME_W_450.3D_2019	ME_W_532.7_2019	ME_W_535.7_2019	ME_W_173.G_2019	ME_W_076.1_2018	ME_W_106.3_2018
PRJNA1011343	PRJNA1011343	PRJNA1011343	PRJNA1011343	PRJNA1011343	PRJNA1011343	PRJNA1011343	PRJNA1011343	PRJNA1011343	PRJNA1011343	PRJNA1011343
MMC7	MMC8	MMC9	MMC10	MMC11	MMC12	MMC13	MMC14	MMC15	MMC18	MMC19

Missing	Missing	Missing	Missing	Missing	Missing	Missing	Missing	Missing	Missing	Missing
2018	2019	2019	2019	2019	2019	2019	2019	2019	2019	2019
ME	NJ	NJ	NJ	NY	NY	NY	NY	NY	NY	NY
Missing	Missing	Missing	Missing	Missing	Missing	Missing	Missing	Missing	Missing	Missing
Tick	Tick	Tick	Tick	Tick	Tick	Tick	Tick	Tick	Tick	Tick
255	255	255	255	255	255	255	255	255	255	255
37.5	36.1	36.1	36.1	37.2	37.1	37.4	37.3	37.4	37.2	37.5
491.792	215.915	9690.72	136.524	1117.83	122.129	621.809	234.45	101.228	150.808	770.744
99.2895	99.1972	99.9723	99.3513	99.7324	99.7509	99.7324	99.677	98.8465	99.7139	99.4925
10760	10750	10834	10721	10808	10810	10808	10802	10712	10806	10782
35641	23497	1071997	14953	90864	11579	53485	21018	7789	14668	64502
10837	10837	10837	10791	10837	10837	10837	10837	10837	10837	10837
1	1	1	1	1	1	1	1	1	1	1
L2A-HM440559.1_p	L2A-HM440559.1_p	L2A-HM440559.1_p	L2B-HM440561.1_p	L2A-HM440559.1_p	L2A-HM440559.1_p	L2A-HM440559.1_p	L2A-HM440559.1_p	L2A-HM440559.1_p	L2A-HM440559.1_p	L2A-HM440559.1_p
553537	23880049	24828799	23752933	639604	756885	198952	377139	876971	838438	842139
Nextera	Nextera	Nextera	Nextera	Nextera	Nextera	Nextera	Nextera	Nextera	Nextera	Nextera
N/A	N/A	N/A	10.3390/v16060830	N/A	N/A	N/A	N/A	N/A	N/A	N/A
N/A	N/A	N/A	N/A	N/A	N/A	N/A	N/A	N/A	N/A	N/A
10.1093/ve/vead008	10.1093/ve/vead008	10.1093/ve/vead008	10.1093/ve/vead008	10.1093/ve/vead008	10.1093/ve/vead008	10.1093/ve/vead008	10.1093/ve/vead008	10.1093/ve/vead008	10.1093/ve/vead008	10.1093/ve/vead008
OP823443	OP823458	OP823459	OP823460	OP823466	OP823461	OP823467	OP823462	OP823468	OP823463	OP823469
SRR31643069	SRR31643068	SRR31643067	SRR31643065	SRR31643064	SRR31643062	SRR31643059	SRR31643057	SRR31643055	SRR31643053	SRR31643051
ME_WM192_2018_NX1	NJ_H_10_2019_NX1	NJ_H_48_2019_NX1	NJ_H_56_2019_NX1	NY_C_112_2019_NX1	NY_SS_12_2019_NX1	NY_CP_250_2019_NX1	NY_SS_32_2019_NX1	NY_SS_339_2019_NX1	NY_SS_38_2019_NX1	NY_C_435_2019_NX1
SAMN37217340	SAMN37217316	SAMN37217317	SAMN37217318	SAMN37217300	SAMN37217328	SAMN37217298	SAMN37217324	SAMN37217325	SAMN37217326	SAMN37217301
ME_WM192_2018	NJ_H_10_2019	NJ_H_48_2019	NJ_H_56_2019	NY_C_112_2019	NY_SS_12_2019	NY_CP_250_2019	NY_SS_32_2019	NY_SS_339_2019	NY_SS_38_2019	NY_C_435_2019
PRJNA1011343	PRJNA1011343	PRJNA1011343	PRJNA1011343	PRJNA1011343	PRJNA1011343	PRJNA1011343	PRJNA1011343	PRJNA1011343	PRJNA1011343	PRJNA1011343
ME18-M192	POWV_NJ19-10_tick	POWV_NJ19-48_tick	POWV_NJ19-56_tick	POWV_NY19-112_tick	POWV_NY19-12_tick	POWV_NY19-250_tick	POWV_NY19-32_tick	POWV_NY19-339_tick	POWV_NY19-38_tick	POWV_NY19-435_tick

Missing	Missing	Missing	Missing	Missing	Missing	Missing	Missing	Missing	Missing	Missing
2019	2019	2019	2019	2019	2019	2019	2019	2019	2019	2019
NY	NY	ME	NJ	NJ	NJ	NY	NY	NY	NY	NY
Missing	Missing	Missing	Missing	Missing	Missing	Missing	Missing	Missing	Missing	Missing
Tick	Tick	BHK	BHK	BHK	BHK	BHK	BHK	BHK	BHK	BHK
255	255	255	255	255	255	255	255	255	255	255
37.1	37.4	37.7	37.5	37.7	37.6	37.6	37.7	35.7	35.6	37.7
174.955	930.921	4047.15	2199.15	23254.6	7491.44	9301.04	2493.06	133.527	9898.51	10515.9
99.4833	99.7693	99.8431	99.8431	99.9539	99.9815	99.9354	99.8616	99.7416	99.9262	99.9354
10781	10812	10820	10820	10832	10780	10830	10822	10809	10829	10830
14669	82883	338803	174757	1845538	615179	749716	190538	13282	947855	849688
10837	10837	10837	10837	10837	10782	10837	10837	10837	10837	10837
1	1	1	1	1	1	1	1	1	1	1
L2A-HM440559.1_p	L2A-HM440559.1_p	L2A-HM440559.1_p	L2A-HM440559.1_p	L2A-HM440559.1_p	L2B-HM440561.1_p	L2A-HM440559.1_p	L2A-HM440559.1_p	L2A-HM440559.1_p	L2A-HM440559.1_p	L2A-HM440559.1_p
368180	527611	972630	1153552	2058582	1270258	821136	1203745	79131	1574052	1112417
Nextera	Nextera	Nextera	Nextera	Nextera	Nextera	Nextera	Nextera	Nextera	Nextera	Nextera
N/A	N/A	N/A	N/A	N/A	N/A	N/A	N/A	N/A	N/A	N/A
N/A	N/A	N/A	N/A	N/A	N/A	N/A	N/A	N/A	N/A	N/A
10.1093/ve/vead008	10.1093/ve/vead008	10.1093/ve/vead008	10.1093/ve/vead008	10.1093/ve/vead008	10.1093/ve/vead008	10.1093/ve/vead008	10.1093/ve/vead008	10.1093/ve/vead008	10.1093/ve/vead008	10.1093/ve/vead008
OP823465	OP823470	N/A	N/A	N/A	N/A	N/A	N/A	N/A	N/A	N/A
SRR31643048	SRR31643046	SRR31685277	SRR31685276	SRR31685271	SRR31685270	SRR31685269	SRR31685268	SRR31685267	SRR31685266	SRR31685265
NY_C_71_2019_NX1	NY_SS_802_2019_NX1	ME_R_472_2019_BHK1_NX1	NJ_H_10_2019_BHK1_NX1	NJ_H_48_2019_BHK1_NX1	NJ_H_56_2019_BHK1_NX1	NY_C_112_2019_BHK1_NX1	NY_SS_12_2019_BHK1_NX1	NY_CP_250_2019_BHK1_NX1	NY_SS_32_2019_BHK1_NX1	NY_SS_339_2019_BHK1_NX1
SAMN37217302	SAMN37217327	SAMN45738098	SAMN45738099	SAMN45738100	SAMN45738101	SAMN45738102	SAMN45738103	SAMN45738104	SAMN45738105	SAMN45738106
NY_C_71_2019	NY_SS_802_2019	ME_R_472_2019_BHK1	NJ_H_10_2019_BHK1	NJ_H_48_2019_BHK1	NJ_H_56_2019_BHK1	NY_C_112_2019_BHK1	NY_SS_12_2019_BHK1	NY_CP_250_2019_BHK1	NY_SS_32_2019_BHK1	NY_SS_339_2019_BHK1
PRJNA1011343	PRJNA1011343	PRJNA1011343	PRJNA1011343	PRJNA1011343	PRJNA1011343	PRJNA1011343	PRJNA1011343	PRJNA1011343	PRJNA1011343	PRJNA1011343
POWV_NY19-71_tick	POWV_NY19-802_tick	POWV_ME19-472_BHK	POWV_NJ19-10_BHK	POWV_NJ19-48_BHK	POWV_NJ19-56_BHK	POWV_NY19-112_BHK	POWV_NY19-12_BHK	POWV_NY19-250_BHK	POWV_NY19-32_BHK	POWV_NY19-339_BHK

Missing	Missing	Missing	Missing	Fall	Fall	Fall	Fall	Fall	Fall	Fall
2019	2019	2019	2019	2020	2020	2020	2020	2020	2020	2020
NY	NY	NY	NY	ME	ME	ME	ME	ME	ME	ME
Missing	Missing	Missing	Missing	Wells	Wells	Wells	Wells	Wells	Wells	Wells
BHK	BHK	BHK	BHK	Tick	Tick	Tick	Tick	Tick	Tick	Tick
255	255	255	255	255	255	255	255	255	255	255
37.6	37.6	37.7	37.6	33.1	33.1	33.1	33.1	33.1	33.1	33.1
3401.18	12553	3450.47	4142.14	1674.62	3511.85	3532.21	4578.86	7431.47	2881.89	764.852
99.9354	99.9262	99.797	99.9908	99.594	99.8247	99.7232	99.5848	98.4682	99.5663	99.5294
10830	10829	10815	10836	10793	10818	10807	10792	10671	10790	10786
266909	1006418	292681	324576	105218	216485	229531	289408	458243	178956	47983
10837	10837	10837	10837	10837	10837	10837	10837	10837	10837	10837
1	1	1	1	1	1	1	1	1	1	1
L2A-HM440559.1_p	L2A-HM440559.1_p	L2A-HM440559.1_p	L2A-HM440559.1_p	L2A-HM440559.1_p	L2A-HM440559.1_p	L2A-HM440559.1_p	L2A-HM440559.1_p	L2A-HM440559.1_p	L2A-HM440559.1_p	L2A-HM440559.1_p
1139412	1300504	1351566	873342	6784921	11138672	11142302	9580795	12062358	10749737	6088411
Nextera	Nextera	Nextera	Nextera	ClickSeq	ClickSeq	ClickSeq	ClickSeq	ClickSeq	ClickSeq	ClickSeq
N/A	N/A	N/A	N/A	N/A	N/A	N/A	N/A	N/A	N/A	N/A
N/A	N/A	N/A	N/A	N/A	N/A	N/A	N/A	N/A	N/A	N/A
10.1093/ve/vead008	10.1093/ve/vead008	10.1093/ve/vead008	10.1093/ve/vead008	N/A	N/A	N/A	N/A	N/A	N/A	N/A
N/A	N/A	N/A	N/A	N/A	N/A	N/A	N/A	N/A	N/A	N/A
SRR31685264	SRR31685275	SRR31685274	SRR31685273	SRR31643044	SRR31643092	SRR31643091	SRR31643090	SRR31643089	SRR31643088	SRR31643086
NY_SS_38_2019_BHK1_NX1	NY_C_435_2019_BHK1_NX1	NY_C_71_2019_BHK1_NX1	NY_SS_802_2019_BHK1_NX1	ME_W_299.3_2020_CS1	ME_W_299.GdAD6.2.3_2020_CS1	ME_W_299.GrdAE6.3_2020_CS1	ME_W_338.GdAC3.2.3_2020_CS1	ME_W_338.GdAC5.3_2020_CS1	ME_W_422.GdAB2.2.3_2020_CS1	ME_W_422.3D_2020_CS1
SAMN45738107	SAMN45738108	SAMN45738109	SAMN45738110	SAMN37217358	SAMN37217359	SAMN37217361	SAMN37217365	SAMN37217366	SAMN37217373	SAMN37217372
NY_SS_38_2019_BHK1	NY_C_435_2019_BHK1	NY_C_71_2019_BHK1	NY_SS_802_2019_BHK1	ME_W_299.3_2020	ME_W_299.GdAD6.2.3_2020	ME_W_299.GrdAE6.3_2020	ME_W_338.GdAC3.2.3_2020	ME_W_338.GdAC5.3_2020	ME_W_422.GdAB2.2.3_2020	ME_W_422.3D_2020
PRJNA1011343	PRJNA1011343	PRJNA1011343	PRJNA1011343	PRJNA1011343	PRJNA1011343	PRJNA1011343	PRJNA1011343	PRJNA1011343	PRJNA1011343	PRJNA1011343
POWV_NY19-38_BHK	POWV_NY19-435_BHK	POWV_NY19-71_BHK	POWV_NY19-802_BHK	POWV_MMC_001A	POWV_MMC_003C	POWV_MMC_004D	POWV_MMC_007G	POWV_MMC_008H	POWV_MMC_012L	POWV_MMC_014N

Fall	Fall	Missing	Missing	Missing	Missing	Missing	Missing	Missing
2020	2020	2020	2020	2020	2020	2020	2020	2020
ME	ME	MA	MA	MA	MA	MA	MA	MA
Wells	Wells	Missing	Medfield	SouthGrafton	Harvard	Glenburn	Bowdoinham	WestGray
Tick	Tick	Tick	Tick	Tick	Tick	Tick	Tick	Tick
255	255	255	255	255	255	255	255	255
33.1	33.1	33.1	33.2	35.7	35.8	33.1	33.2	35.7
1780.59	1543.14	2819.21	5176.2	1385.41	7096.84	3053.53	1587.16	13124.7
100	99.5755	99.4925	100	99.594	99.6586	99.5848	99.5848	99.5663
10837	10791	10782	10839	10793	10800	10792	10792	10790
117008	126019	175678	319523	90737	464068	197914	101051	854484
10837	10837	10837	10839	10837	10837	10837	10837	10837
1	1	1	1	1	1	1	1	1
L2A-HM440559.1_p	L2A-HM440559.1_p	L2A-HM440559.1_p	L2A-HM440559.1_p	HM440559_pilon	HM440559_pilon	L2A-HM440559.1_p	L2A-HM440559.1_p	HM440559_pilon
8242632	11974782	3311151	13532214	461307	8102740	9756088	7921774	6016933
ClickSeq	ClickSeq	ClickSeq	ClickSeq	ClickSeq	ClickSeq	ClickSeq	ClickSeq	ClickSeq
N/A	N/A	N/A	N/A	N/A	N/A	N/A	N/A	N/A
N/A	N/A	N/A	N/A	N/A	N/A	N/A	N/A	N/A
N/A	N/A	N/A	N/A	N/A	N/A	N/A	N/A	N/A
N/A	N/A	N/A	N/A	N/A	N/A	N/A	N/A	N/A
SRR31643085	SRR31643084	SRR31643083	SRR31643082	SRR31643081	SRR31643080	SRR31643079	SRR31643078	SRR31643077
ME_W_154.1.2020_CS1	ME_W_268.8.2020_CS1	MA_Ma_SM20.M26_2020_CS1	MA_Me_MSH20.F85_2020_CS1	MA_SG_Deer20.M9_2020_CS1	MA_H_Deer20.M29_2020_CS1	MA_G_Deer20.M52_2020_CS1	MA_B_Deer20.M90_2020_CS1	MA_WG_Deer20.M105_2020_CS1
SAMN37217363	SAMN37217370	SAMN37217310	SAMN37217314	SAMN37217330	SAMN37217305	SAMN37217304	SAMN37217296	SAMN37217384
ME_W_154.1.2020	ME_W_268.8.2020	MA_Ma_SM20.M26_2020	MA_Me_MSH20.F85_2020	MA_SG_Deer20.M9_2020	MA_H_Deer20.M29_2020	MA_G_Deer20.M52_2020	MA_B_Deer20.M90_2020	MA_WG_Deer20.M105_2020
PRJNA1011343	PRJNA1011343	PRJNA1011343	PRJNA1011343	PRJNA1011343	PRJNA1011343	PRJNA1011343	PRJNA1011343	PRJNA1011343
POWV_MMC_015O	POWV_MMC_018R	POWV_TUF_001A	POWV_TUF_002B	POWV_TUF_009I	POWV_TUF_010J	POWV_TUF_011K	POWV_TUF_012L	POWV_TUF_013M

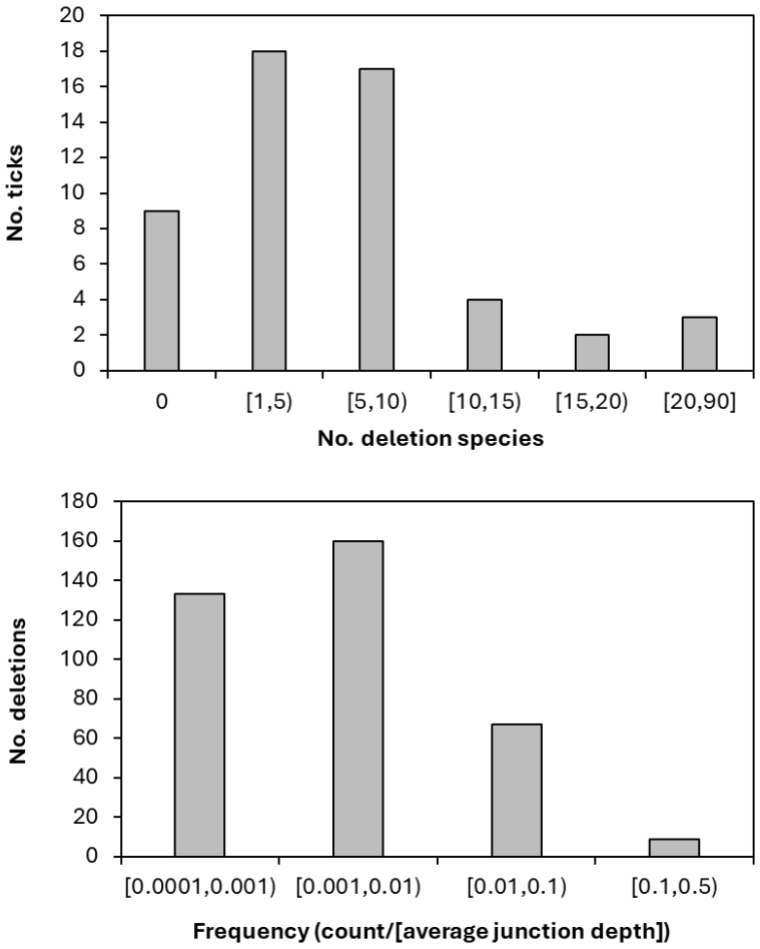

Figure S2.1. Distributions of the number of unique POWV deletions across ticks and the frequency of each unique deletion. RNA from 53 POWV positive ticks was sequenced using a metagenomic approach, and reads were mapped to the POWV genome with a recombination-sensitive mapper. Deletions were extracted and **A)** the distribution of unique deletions across different tick samples was enumerated and; **B)** the per-sample frequency of each unique deletion was calculated by dividing the raw deletion count by the average depth of each breakpoint junction.

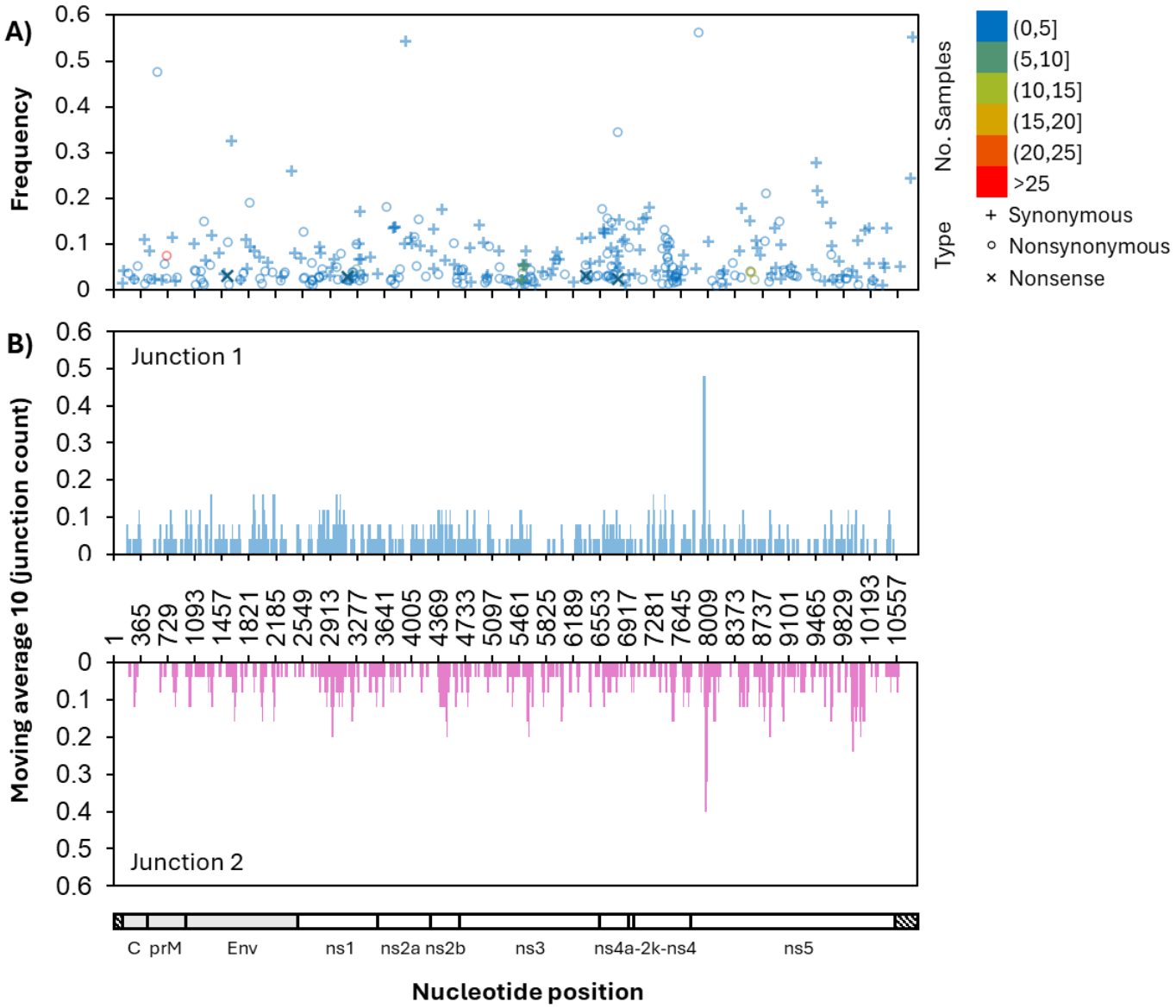

Figure S2.2. Distribution of intrasample single nucleotide variants (iSNVs) and recombination breakpoint junctions across the POWV genome. RNA from 53 POWV-positive ticks was sequenced using a metagenomic approach. **A)** Reads were mapped to the POWV genome using a standard mapping algorithm, and iSNVs were called using ViReMa. Each symbol shows a unique iSNV, the color indicates the number of samples in which that iSNV was identified, and the shape indicates the substitution type (cross, synonymous; open circle, nonsynonymous; and x, nonsense or early-terminating). **B)** Reads were mapped using a recombination-sensitive mapper, deletions were extracted, the number of deletions with a 5' Junction 1 (top) and 3' Junction 2 (bottom) at each nucleotide position was enumerated, and a moving average of 10 was employed to highlight regions with increased recombination activity.

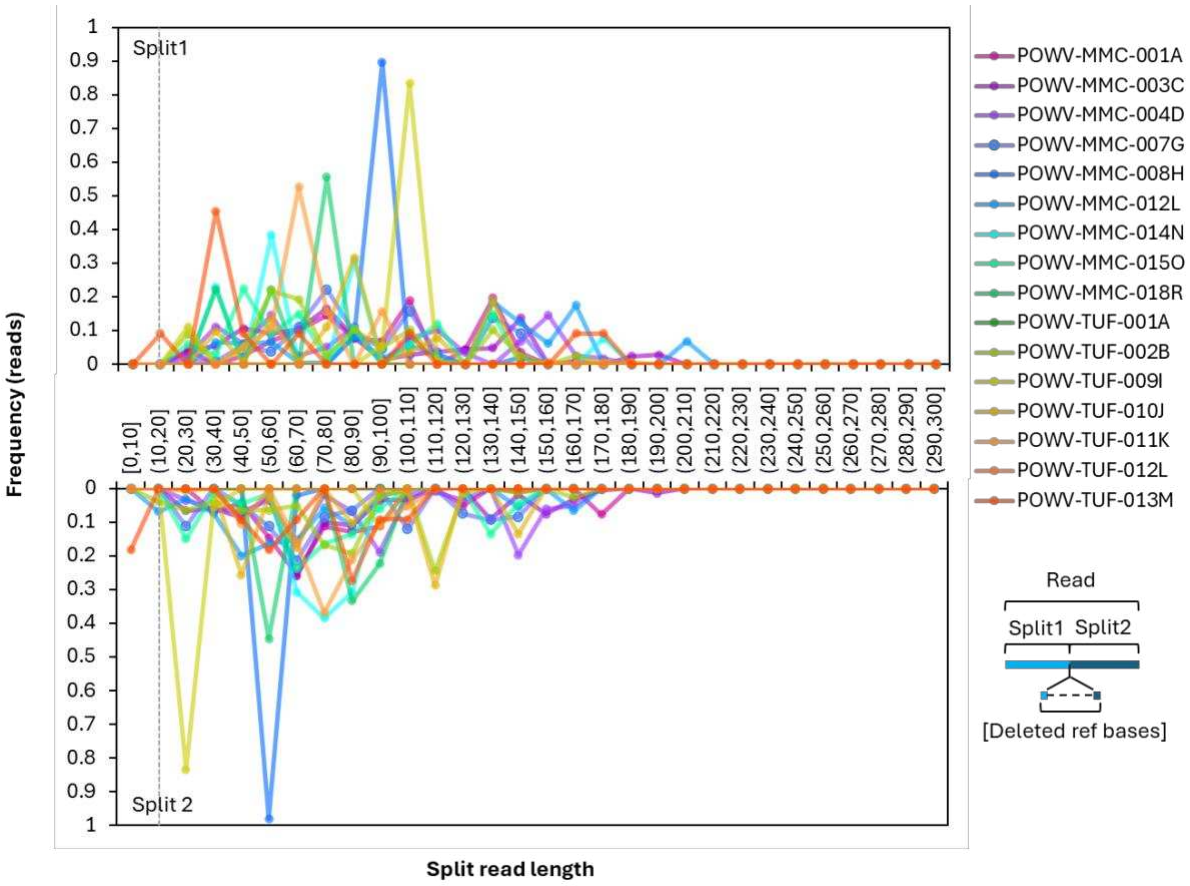

Figure S2.3. Distribution of split read length generated by ClickSeq. RNA from 16 POWV-positive ticks was sequenced using ClickSeq. Then, reads were mapped using a recombination-sensitive mapper, which trims the mismapping end within a recombinant read and maps it as a separate read, creating two split reads per recombinant read. For each library, the length of each split read (split 1, top; split 2, bottom) was enumerated to analyze the distribution of read lengths.